KINGDOM OF SAUDI ARABIA

National Science, Technology and Innovation Plan

Strategic Technology Program

Project title

SEISMIC MICROZONATION AND SITE EFFECT RESPONSE OF DAMMAM AND ALKHOBAR CITIES- EASTERN SAUDI ARABIA

Project No.

08-SPA239-2

Dr. Mohammed S. Fnais (PI)

Prof. Abdullah M. Al-Amri (Co-PI)

Prof. Kamal Abdelrahman (Co-PI)

2012

Abstract

Al-Dammam and Al-Khobar cities affected by distant earthquakes from Zagros fold-fault subduction zone. These earthquakes of magnitude greater than 6.0 could produce great local site effects of the sedimentary layers that significantly affect earthquake ground motions. The evaluation of the site response in these cities is of prime importance for urban developments, safer design of buildings and to the mitigation of the earthquake risks. The earthquake activities around these cities have been collected and precisely analyzed. New ground motion attenuation relation has been predicted for the eastern province of Saudi Arabia through this work.

These cities have been divided into grid of points separated by about 500 m, and then the microtremor measurements have been carried out at 250 sites in Al-Dammam and Al-Khobar cities. These measurements have been acquired with record length of 40 minutes. The measured data has been analyzed using worldwide software to calculate the fundamental frequency peaks and their corresponding amplification factors. The origin of these peaks has been tested to indicate whether of natural or industrial origin.

Based on fundamental frequency (f_0), Al-Dammam city have been classified into four zones; from 0.3 to 3.9 Hz in the 1st zone; from 3.9 to 5.2 Hz in the 2nd zone; from 5.2 to 6.5 in the 3rd zone and from 6.5 to 7.8 Hz for the 4th zone. Whereas Al-Khobar city classified into three zones; from 0.33 to 1.03 Hz for the 1st zone; from 1.03 to 1.23 Hz for the 2nd zone and from 1.23 to 1.73 Hz for the 3rd zone. Accordingly, the eastern zone of these cities have a smaller values of f_0 that reflects greater thickness of soft sediments and maximum amplification while the western zone presents an opposite characteristics. The high-rise buildings in the eastern zone of both cities will affect greatly by low-frequencies originated from the distant earthquakes on western Iran subduction zone. Greater area of Al-Dammam city has f_0 values in the range of 4-8 Hz and could amplify bedrock ground motion as much as 4 times. This indicated that the1-5 story buildings in Al-Dammam city are vulnerable to hazardous resonant shaking from local and near earthquakes.

Geotechnical borehole data in terms of lithology, thickness, Standard Penetration Test (SPT) have been conducted in Al-Dammam and Al-Khobar cities. Average shear-wave velocity (V_{s30})

and site response effects at these boreholes have been estimated according to Boore (2006) approach. The fundamental resonance frequency (f_0) range from 2.9 to 7.0 Hz in Al-Dammam city and from 0.27 to 1.95 Hz in Al-Khobar city that in agreement with that of the Nakamura technique. Based on V_{s30} soil zonation maps for Al-Dammam and Al-Khobar cities have been conducted where V_{s30} ranges from 180 to 500 m/sec in Al-Dammam city and from 106 to 577 m/sec in Al-Khobar city. The soil map of Al-Dammam city correlated with ''C'' and ''D'' soil classes of NEHRP-IBC, while soils of Al-Khobar city fall into ''E'', ''C'' and ''D'' soil classes.

Based on V_{s30} map of Al-Dammam city, the soil profiles of Al_ Dammam city have NEHRP classes C and D characteristics. Class C represented by very dense soil to soft rock with a moderate amplification of earthquake ground motion. Districts of Al-Anud, Al-Khalij; Al-Nakhil, Ibn Khaldun have soil of class C. In addition most of Al-Jallawiyyah, Al-Badiyah, and Madinat Al-Umal districts fall in class C soils. Whereas, Districts of Al-Amamirah; Ar-Rabi; As Suq; Al-Qazzaz, Al-Adamah, Muhammed Ibn Saud fall in class D in addition, the rest areas of Al-Jallawiyyah and Ghinata districts. Class D represented by stiff soil profiles that induced significant

amplification of earthquake ground shaking. While, Al-Khobar city illustrates classes E, D, and C soil profiles constitute the surface soil of Al-Khobar city. Class E is represented by soft soil profiles with a higher amplification of earthquake ground motion. The eastern districts of Al-Khobar as Al-Khobar Al-Shamaliah; Al-Yarmuk; Al-Kornaish; and Al-Bandariyah having class E soil profiles. The soil profiles in the districts of Al-Ulaya; Al-Aqrabiyyah; Madinat Al-Ommal; Al-Khobar Al-Janubiyyah belong to class C. Whereas, the districts of Al-Hada; and Al-Hizan Al-Akhdar districts having soils profiles of class D.

From the seismic hazard point of view, it is noticed that the values of Peak Ground Acceleration (PGA) are not the effective parameter for the damaging effect at these cities. But the fundamental frequencies and periods for the local site and consequently, the low-rise buildings are of valuable effect. This leads to the importance of monitoring and analyzing the ground motion from the distant earthquakes from Zagros belt of Iran and their damaging effects on the high-rise buildings in these cities.

Furthermore, liquefaction potentiality can't be assessed at these cities. It is recommended that, results of this research should

be addressed in a Saudi Building Code and especially in the eastern Saudi Arabia province for anti-earthquakes structures design.

Acknowledgments

Our cordial thanks for the financial support of the National Plan for Strategically Technologies (NPST) at King Saud University, Riyadh, Saudi Arabia. The project was conducted under 08-SPA239-2.

List of Figures

List of Tables

I. INTRODUCTION

Eastern Saudi Arabia gaining great attention due to their affected by the distant earthquake originated from active tectonics of Zagros fold-fault Belt that represents one of the most seismically active belts (Al-Amri et al., 2008). It is well known that, on a world-wide scale, the subduction zone events are quite often the most destructive (Kanamori, 1986). This, in turn, affects the engineering structures such as petrochemical plants, tunnels, bridges and high-rise buildings. Large earthquakes ($M \geq 5$) are quite common along thrust fault belt and have a potential for wide-spread damage. Hence, the ground motion amplification by the topmost soil cover is essential for seismic hazard assessment of these cities due to rapid population growth and new urban communities in the eastern province of Saudi Arabia.

In November 1945, very high magnitude earthquake (M 8.1) along the Makran subduction zone, which significantly affected the eastern province of Saudi Arabia. Furthermore, on June 2nd 1993 an earthquake of magnitude 4.8 occurred in Kuwait near Minagish oil field (southwest of Kuwait). This earthquake has widely been felt and caused panic in the city of Kuwait although of moderate magnitude. The same area was struck again by earthquakes on September 1997 (M 3.9) and December 30, 1997 (M 4.2). Following this, on January 2002 a moderate earthquake (M 5.2) shook

the Musandam Peninsula on the border between Oman and the United Arab Emirates.

The local geology can significantly control the scale and distribution of damages due to strong earthquakes. The amplification of earthquake related ground motion by local site conditions has important implications in urban planning and development. In areas characterized by soft sediments, the amplification of the ground motion is common that lead to enhanced seismic hazard and risk.

Local site response can be evaluated by empirical and theoretical methods. The theoretical method allows detailed analysis of the parameters used in the evaluation; however, it requires a detailed geo-technical information about the materials through which the seismic waves propagate to the surface. The analytical response of plane SV waves impinging on a single layer overlying a half-space is well known and widely used (Lermo and Chávez-García, 1993). Empirical methods are based on seismic records of the sites; thus, dominant frequency and amplification are determined directly. Empirical methods can be separated in two categories: one that use two sites and another that use only one site. Borcherdt (1970) introduced the sediment-to-bedrock ratio (the most common approach) that consists of dividing the spectrum of the measured earthquake motions at a site by that of a nearby reference site (rock site). If the two sites have similar source and path effects, and if the reference site has a negligible site response, then the resulting spectral ratio constitutes an estimate of the site response.

This approach identifies, in most cases, the fundamental resonant frequency and is considered to be the most reliable (Rogers et al., 1984, Singh et al., 1988, Jarpe et al., 1988, Darragh and Shakal 1991, Borcherdt and Glassmoyer 1992, Gutierrez and Singh, 1992, Satoh, et al., 1995; Aguirre and Irikura, 1997; Su, et al., 1998; Beresnev, et al., 1998; Hartzell, 1998; Reinoso and Ordaz, 1999). Many investigators (Tucker and King (1984), McGarr et al. (1991), Field et al. 1992, Jongmans and Campillo (1993), Liu et al. (1992), Zaslavsky et al., (1995), Carver and Hartzell (1996), Hartzell et al. (1996), Zaslavsky et al. (2000) evaluated a site response function from moderate to weak earthquake motions. However, this technique requires a number of earthquake records. In regions with relatively low seismicity, it would be necessary to wait for a significant period of time to obtain a usable data set.

The Borcherdt's approach, in which the ambient seismic noise instead of earthquake is used, has been applied to several studies (Otha et. al., 1978). For frequencies smaller than 0.5 Hz, seismic noise is categorized as microseisms and, for higher frequencies, as microtremors. The main advantage given by this approach is the fact that the spectral characteristics of microtremors have been recognized to be associated with the site conditions (Katz, 1976; Katz and Bellon, 1978; Kagami et al., 1986; Zaslavsky, 1987; Gutierrez and Singh, 1992 and Bard, 2000). It has been shown that with microtremors it is possible to identify the fundamental resonance frequency of the near surface soil deposits.

Nakamura (1989) suggested a method that requires only one recording station. Nakamura hypothesized that site response could be estimated from the horizontal-to-vertical ratio of microtremors. This technique was tested, experimentally and theoretically by different authors (Bard and Tucker, 1985; Lermo and Chavez-Garcia, 1993, 1994; Lachet and Bard, 1994; Field and Jacob, 1995; Zaslavsky et al., 1995, 1998, 2000; Malagnini et al., 1996; Seekins et al., 1996; Gitterman et al., 1996, Teves-Costa et al., 1996; Theodulidis et al., 1996; Safak, 1997; Konno and Ohamachi, 1998; Mucciarelli, 1998; Mucciarell et al, 1998, and Zaslavsky et al., 2003). Results obtained by implementing Nakamura's technique support such use of microtremors measurements for estimating the site response of surface deposits. Lermo and Chávez-García (1993) applied Nakamura's technique to seismic recordings of earthquakes and concluded that this approach is able to reliably estimate the frequency of the fundamental resonant mode and correctly predict the amplification level. Other studies (Field and Jacob, 1993; Wakamatsu and Yasui, 1996; Lachet and Bard, 1994; Coutel and Mora, 1998) indicate that Nakamura method has already proved to be one of the cheapest and most convenient techniques to reliably estimate fundamental frequency, but it needs more work to understand the factors influencing the amplification phenomenon (Bard, 2000). The dynamic characteristics in the frequency domain observed at a certain point include all of the wave motion radiation characteristics at the focal region, the dynamic characteristic of the wave motion propagation route up to the observation point, and the dynamic

characteristics of the surface layers at the observation point as shown in figure (1) (Nakamura, 1996).

The most famous example of the site amplification phenomenon appeared during the occurrence of the earthquake in Mexico City on September 19th, 1985 (Bard, 2007) where more than 10,000 people were killed. Most of the death toll and damages occurred at buildings five to fifteen stories high in downtown Mexico City. This part of the city is built on soft sediments from an ancient lakebed (400 km away from the epicenter), which has the capability of amplifying certain frequencies of ground motion (Fig. 2). The site effects in Mexico City were, perhaps, exceptional, but such factors must always be considered in a thorough seismic hazard assessment since they can exert a very strong influence on the nature of the ground motion and the resulting earthquake loads. The characteristics of the site, including the thickness and nature of soil deposits, can be usually determined with a greater degree of confidence than can the source parameters of future earthquakes. It is therefore recommendable that possible site responses be identified and evaluated separately from the determination of the design bedrock motions.

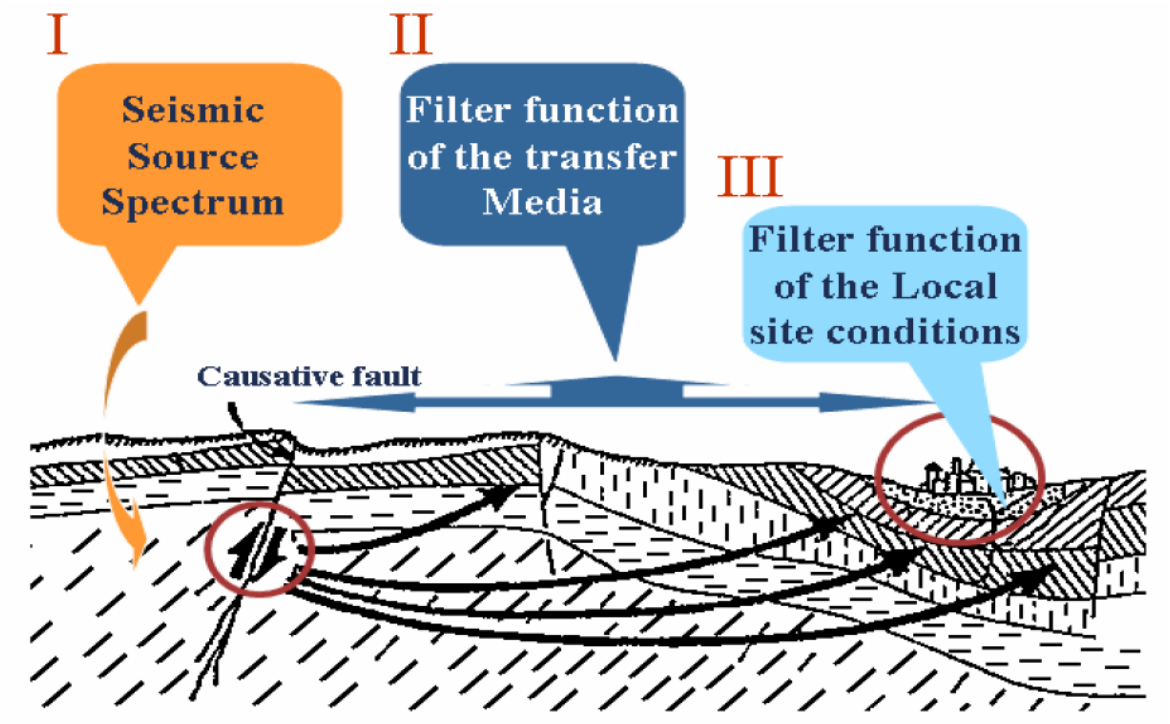

Figure 1: Analysis of the observed ground motion caused by an earthquake (after Nakamura, 1996)

Recently, the average shear wave velocity to a depth of 30 m (Vs30) has become a widely used parameter for classifying sites to predict their potential to amplify seismic shaking and is now adopted in building codes and loss estimation. The site classes estimated from shallow shear wave velocity models are also important in deriving strong motion prediction equations, which can be used for map construction in hazard reduction on a national scale, and in applications of building codes to specific sites. Because of the robustness of the concept underlying Vs30, it has been accepted by the US National Earthquake Hazard Reduction Program (NEHRP) and International Building Code (IBC) as the standards for characterizing soils in seismic hazard analysis.

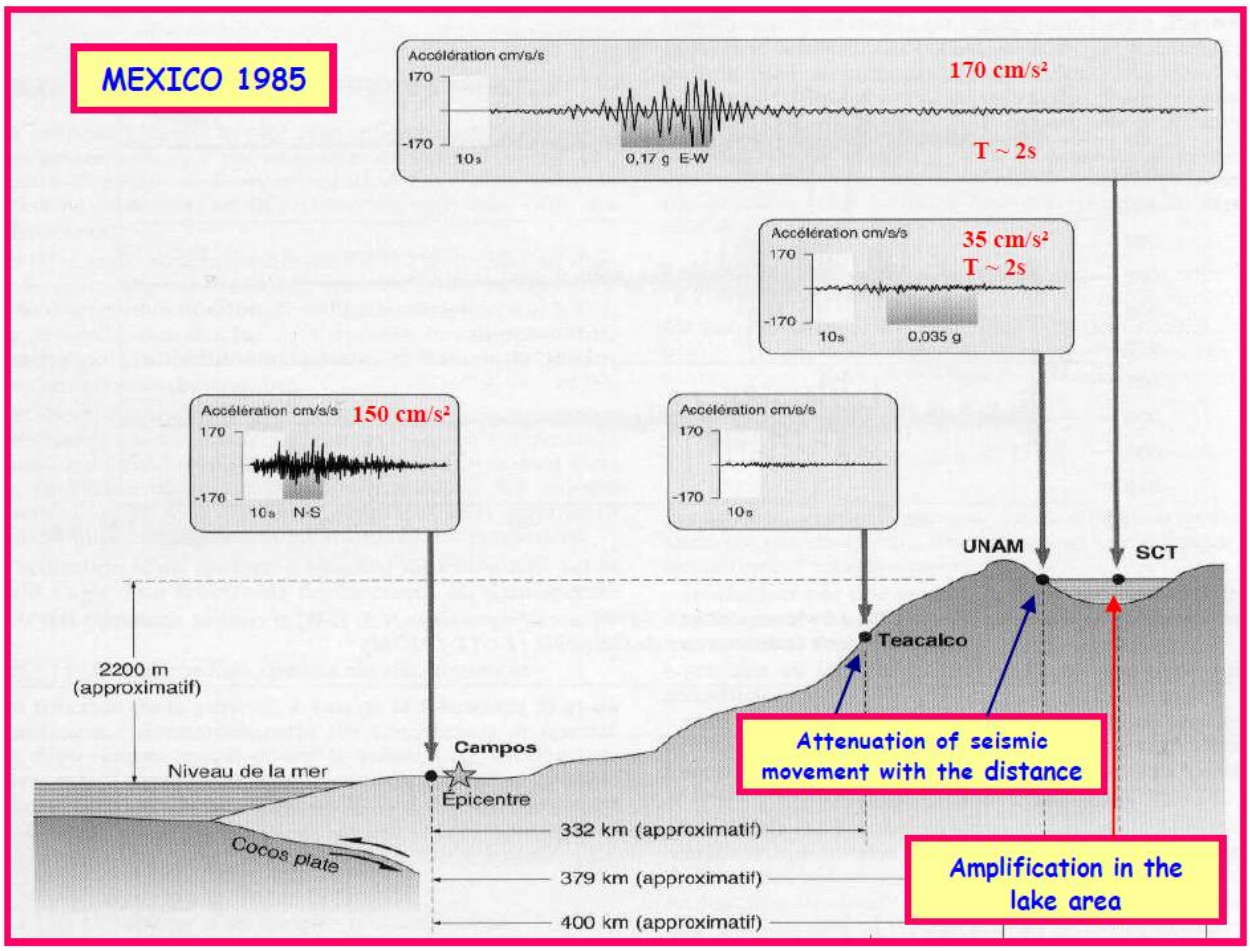

Figure 2: The site effects at Mexico City according to Mexico 85 earthquake (after Bard, 2007)

In 2007, Dubai Municipality conducted seismic microzonation study for Dubai city through the influence of local geotechnical and geological soil conditions on the intensity of ground shaking of Dubai-Sharjah metropolitan area (*Irfan*, 2012). Acceleration-time histories of Dubai and Sharjah were chosen according to spectral shape and similarity in magnitude and distance to a target response spectrum that were obtained from the results of Seismic Hazard Analysis (SHA). Subsurface

geotechnical data of 72 different sites were used. The effect of local site conditions on ground response during earthquake has been evaluated by performing equivalent linear analysis. Dynamic properties of selected soil profiles were evaluated using empirical relations between Standard Penetration Test (STP) N-values and shear wave velocity (Vs). Results indicated that surficial deposits in the area amplified earthquake ground motion. The peak amplification was observed over relatively narrow frequency range of 1.5-5 Hz (0.2-0.8s period) that was found to represent the predominant frequency range of the site classes under consideration.

Fnais et al., (2010) carried out the microzonation study in Yanbu City along the western coast of Saudi Arabia. The local site effects have been estimated in terms of the fundamental frequency and the corresponding amplification factor. Then these results are correlated well with the estimated results from borehole geotechnical data. Accordingly, the results of these studies could be taken into consideration for future urban development and land-use planning.

Seismic risk in areas far from the epicentral zones depends on the local soil conditions. Soft soil deposits attenuate seismic motion at some frequencies and amplify it at others, phenomena known as site effects. An additional factor, not usually included in the definition of site response, is the soil–structure interaction (SSI), whose magnitude will depend on the rigidity contrast between the soil and the structure. The effects of SSI on the dynamic behavior of buildings have been widely

studied. In contrast, the wave radiation from the soil–foundation interface has received comparatively little attention.

The natural frequency of vibration of building is a very important factor that governs all calculations concerning seismic codes for buildings. Most codes are based on knowing the natural frequency of vibration of structure (or equivalently the natural period of vibration T) to know the deformation response of the structure. It became evident that buildings of a certain class or type that is, having a certain natural periods are often damaged from ground shaking when located on geologic conditions having a similar characteristic period. Whereas buildings with different natural periods located on the same geological conditions are not damaged. The natural period of vibration is thus an essential phenomenon that controls the interaction of buildings when the soil is excited by any source of vibration most important of which are earthquakes.

From the engineering point of view, the free-field motion is similar to that recorded at the building base. However, recent studies indicate that SSI effects in densely urbanized areas may modify the free-field motion within distances up to five times the building base dimensions. Two conditions must be met for these effects to be important: the building must be founded on soft soil and the dominant periods of the building and of the soft soil must coincide.

This study aims to estimate the local site response effect for Al-Khobar and Al-Dammam cities, eastern Saudi Arabia (Fig. 3) in terms of fundamental frequency and its corresponding amplification factor. Then, mapping of these values will be constructed using Geographical Information Systems (GIS) approach.

Figure 3: Location map of Al-Dammam and Al-Khobar cities.

II. GEOLOGICAL SETTING

The sedimentary sequence of Saudi Arabia ranges in age from Cambrian to recent where, increasing in thickness when moving from the Arabian Shield in the

west into Arabian Platform in the east. Paleozoic sediments are characterized by its clastic nature, while the Mesozoic and Cenozoic sequences are represented by carbonate rocks. In the central part of Saudi Arabia, both Jurassic and Cretaceous rocks constitute the main surface area, whereas Cenozoic rocks and Quaternary sand dunes are prevailing in the eastern province.

The eastern province is generally constituted by a sequence of continental and shallow marine sediments (Fig. 4). The Paleozoic, Mesozoic, and lower Tertiary strata are exposed in the central part of Saudi Arabia forming a belt bordering the Arabian shield. Along the Arabian Gulf a broad zone of relatively low-relief terrain is located in which the Tertiary and younger deposits effectively mask the older units. The Upper Cretaceous and Eocene rocks consist mainly of limestone and dolomite. The Quaternary stratigraphic sequences mostly consist of non-marine sandstone, sandy marl, and sandy limestone. These sequences dip gently towards the east and northeast under Zagros Mountains (Steineke et al., 1958; Powers et al., 1966; Al-Sayari & Zoetl, 1978; and Vaslet et al., 1991).

The unconsolidated Quaternary deposits comprise great sand deserts and gravel sheets (Powers et al., 1966; A1-Sayari and Zoetl, 1978). Umm er Radhuma Formation of Paleocene and lower Eocene age forms a wide belt extending ~ 1200 km from south to north with a width of 60-120 km. The middle part of the belt is covered with eolian sand. The exposures of this Formation form a gently undulating but rough surface with low isolated hills and benches. This formation consists of a

repetitious series of calcitic and dolomitic limestone (Powers et al., 1966). Outcrops of the Al-Dammam Formation of lower and middle Eocene age are restricted to a number of small but widely scattered patches in the Arabian Gulf coastal region, especially in the vicinity of AL-Khobar City.

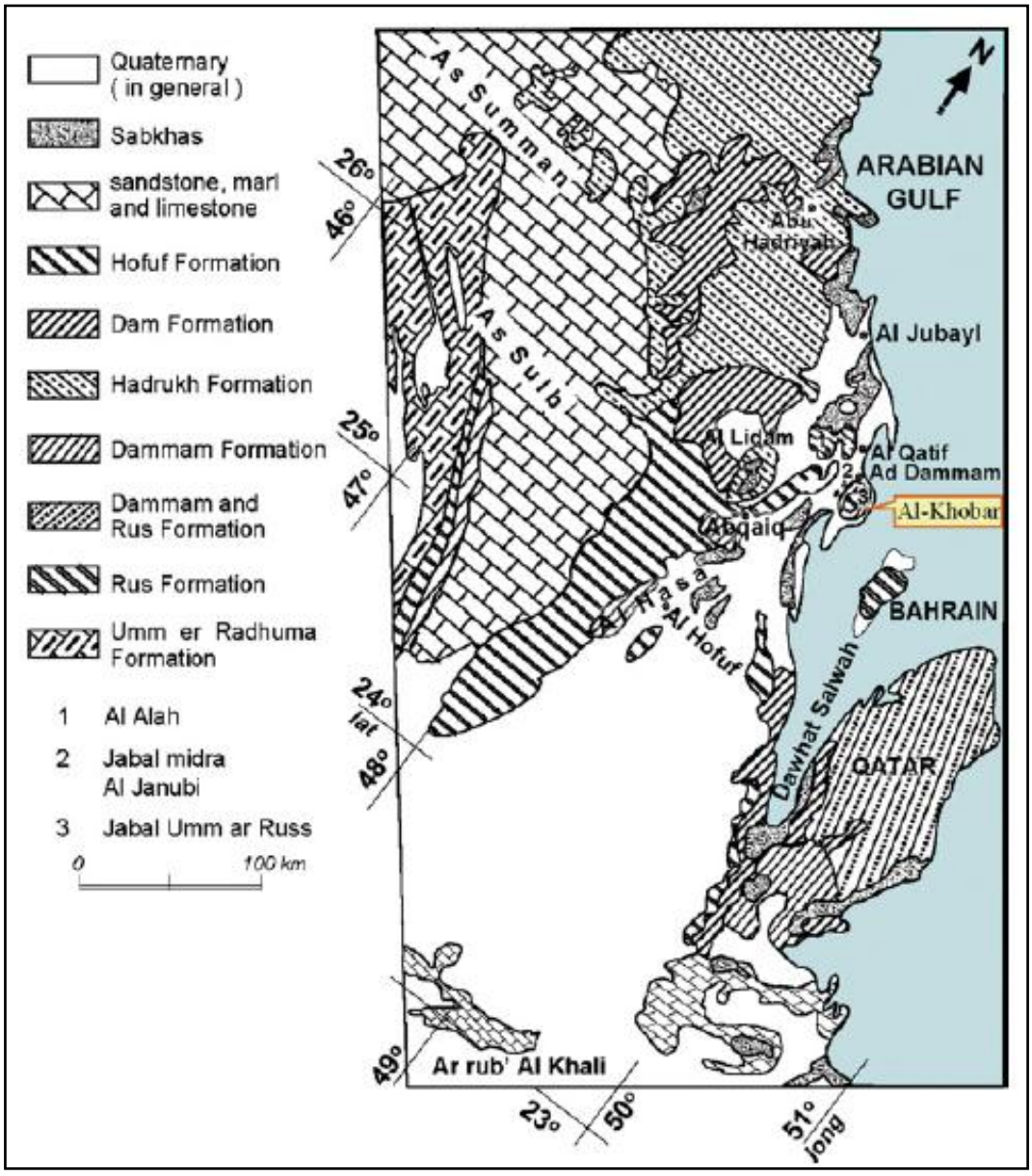

Figure 4: Generalized geologic map of the Arabian Gulf coastal region and its hinterland (After Aiban, 2006).

Tectonically, the Arabian Plate (Fig. 5) underwent through major tectonic events that splits away from the African Plate through two or more episodes of Red Sea floor spreading during pre-early Miocene and post-Miocene times (Coleman, 1971). On the Arabian Gulf side in the east, the tectonic is dominated by collision between the Arabian and Eurasian Plates along the Zagros - Bitlis Thrust Belt.

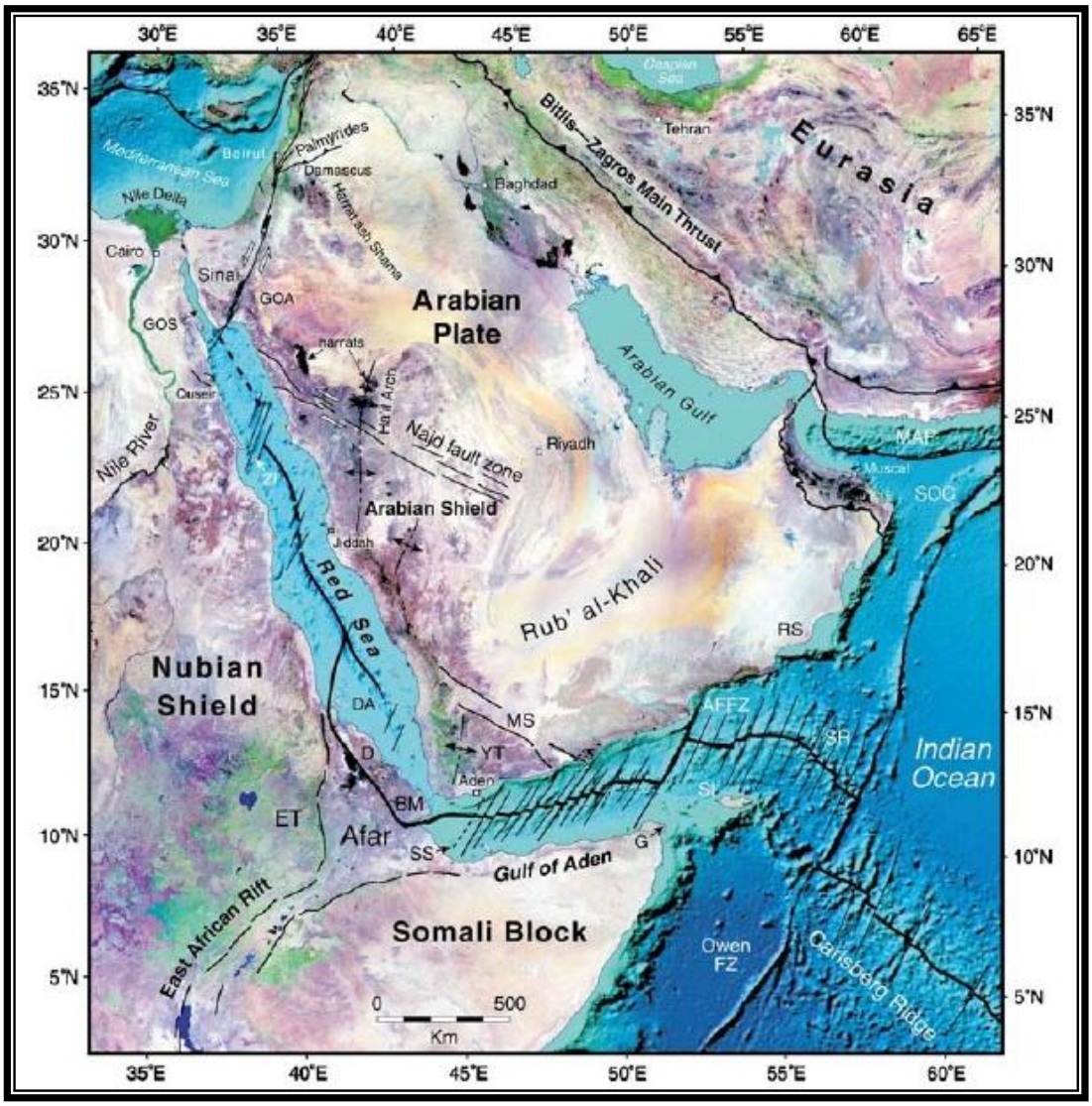

Figure 5: Regional tectonic framework for the Arabian Plate.

According to Sharland et al. (2001), there are five major tectonic episodes that controlled the tectonostratigraphy of the Upper Cambrian and Phanerozoic sedimentary successions in the Arabian Plate. Whereas, during the Precambrian, the basement rocks were subjected to east-west compressive stresses (Schmidt et al., 1979; Ayres et al., 1982 and Al. Husseini, 1989 & 2000). These stresses formed two of the major structural features as follows; 1) N - S trending fault terranes, such as the Summan Platform, Khurais-Burgan trend, Ghawar trend and Qatar Arch trend and b) NW-SE (Najd) and NE-SW (Wadi Al-Batin) oriented fault systems that from a conjugate system (Schmidt et al. 1979). Furthermore, Al-Husseini (2000) illustrated that, Rayn microplate (Fig. 6) constitutes the eastern part of the Arabian Shield. The Amar Collision fused the Rayn micrplate and Afif terrane along the Amar Suture and formed the N-S trending basement controlled fault blocks (Summan, Khurais, Ghawar anticlines and Qatar Arch). These great anticlines are bounded by the orthogonal NE-SW trending (Wadi Batin) and NW-SE trending (Abu Jifan) strike-slip faults.

Eastern Saudi Arabia is part of the Arabian shelf which was subjected to successive transgression and regression cycles of the Gulf waters during the Pleistocene and Holocene ages (El-Naggar, 1988). In general, the surface rocks of the region include both consolidated and unconsolidated sediments (Fig. 7). The consolidated sediments belong to Paleocene to middle Eocene age and Miocene to Pliocene age while the unconsolidated materials contain sediments from Quaternary

age which include shale and claystone. According to Powers et al. (1963); Al- Sayari and Zotl (1978 and Stieneke and et al. (1979), a sequence of continental and shallow marine sediments extends along the Arabian Gulf with relatively low-relief terrain. The Upper Cretaceous and Eocene rocks are represented by limestone and dolomite, while Quaternary sequences are made from sandstone, sandy marl, and sandy limestone of non-marine origin. These sequences dip gently towards the east and northeast under the Zagros thrust belt (Al-Sayari & Zoetl, 1978). The Umm er Radhuma Formation of Paleocene and lower Eocene age forms a wide belt extending ~ 1200 km from south to north with a width of 60-120 km. The exposures of the Umm er Radhuma Formation forms a gently undulating but rough surface with low altitude isolated hills and benches. Outcrops of the Al-Dammam Formation of lower and middle Eocene age are restricted to the Arabian Gulf coastal region.

The following is a brief description of the relevant geological formations (Powers et al., 1963; Johnson, 1978);

Rus Formation *(Tru*) forms the core of Al-Dammam dome, and is typically exposed on Jabal Umm Ar Russ. This formation is Lower Eocene in age and consists mainly of chalky dolomite, chalky limestone and marl. The chalk is white in color and soft, while dolomite is white –pinkish- yellowish in color, micritic to sparry and soft to hard rock. No marine fossils are observed in these rocks during the field observations. This formation is divided into the following three lithologic units:

1. 3.6 m thick white soft chalky porous limestone with calcarenite beds at the top.
2. 31.8 m thick marl and limestone: the material has irregular masses of crystalline gypsum, occasional thin limestone beds and geodal quartz at several levels. The material is highly variable and includes white compact finely crystalline, anhydrite with interbedded green shale and minor amounts of dolomitic limestone. Alternatively, it may include gray marl with coarsely crystalline calcite and interbedded shale and limestone. Such a unit is highly variable both in lithology and thickness.
3. 21.0 m limestone: the material is gray to buff compact commonly partially dolomitized limestone with minor amounts of soft limestone made porous by leaching of small organic remains. Quartz geodes occur rarely in the lower part and are typical of the upper part.

Dammam Formation crops out around the circumference of the Al-Dammam dome and uncomformably overlies the Rus Formation. This formation consists of dolomite, dolomitic limestone, limestone, marl and shale (Tdm). The shale (Tdsh) is yellowish to brown, fossiliferous and thinly laminated. The shale represents the bottom of the formation, while the dolomite, dolomitic limestone and marl represent the topmost of the formation.

This formation is divided into five members:

- 15 m thick Alat limestone and marl: the upper part is light colored chalky and porous, commonly dolomitic limestone. It contains abundant molds of mollusks and other organic remains. The lower part is light colored dolomitic marl.
- 9.3 m thick Khobar limestone and marl: the material is light to dark-brown, in part dolomitic limestone becoming off-white soft marly limestone. The lower part consists of marl.
- 1.0 m thick Alveolina limestone: the material consists of yellowish gray, microcrystalline, partially recrystallized, dolomitized limestone. It contains common specimens of Alveolina elliptica (Sowerby) var. flosculina Silvestri and internal molds of Lucina pharaonis.

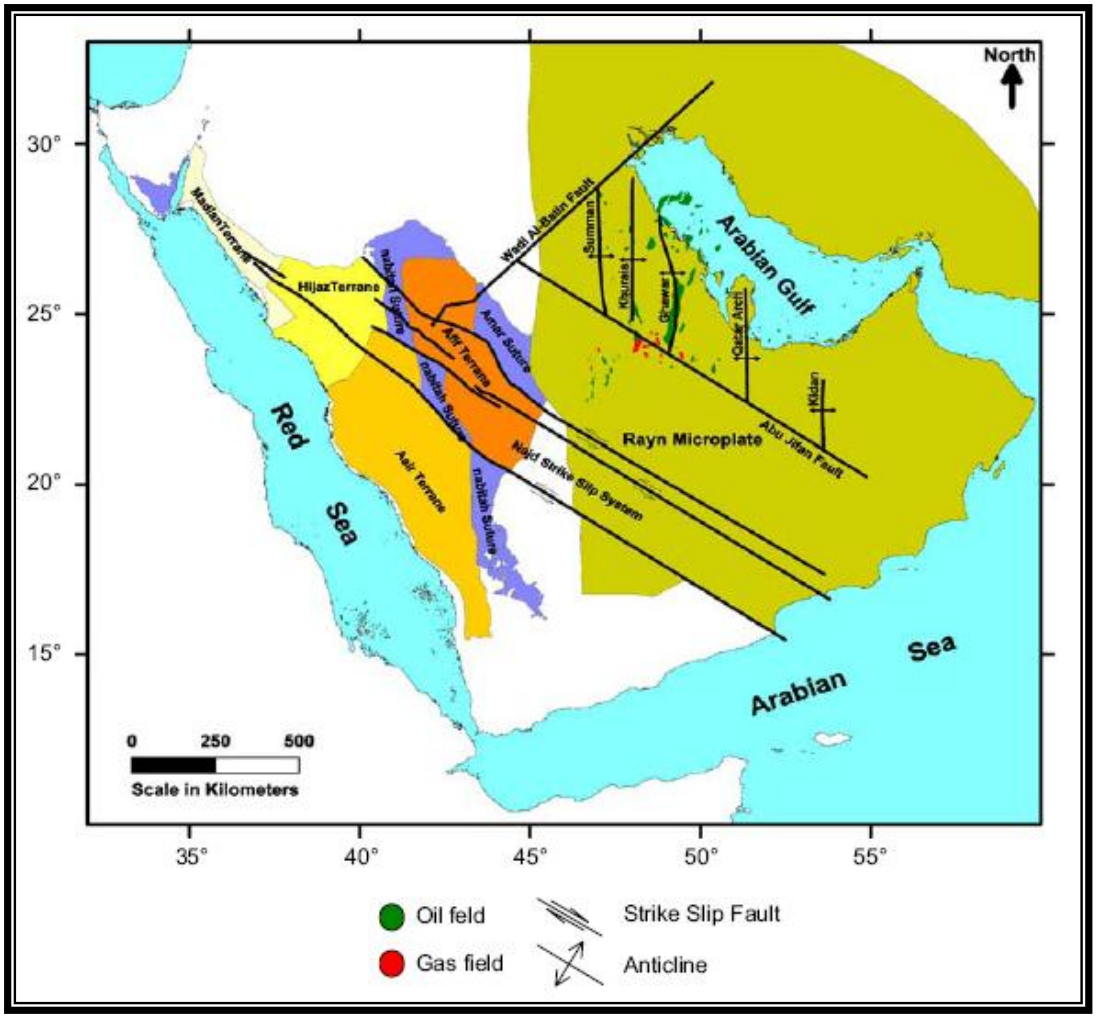

Figure 6: Internal structures of the Arabian Plate (Al-Husseini, 2000).

- 4.2 m thick Saila shale: the member consists of 3.6 m dark brownish-yellow subfissile clay shale underlain by 0.6 m of gray-buff limestone.
- 3.0 m thick Midra shale: the shale member consists of yellowish-brown, fissile, thinly laminated shale, gray marl and impure limestone. It contains scattered fossil shark teeth.

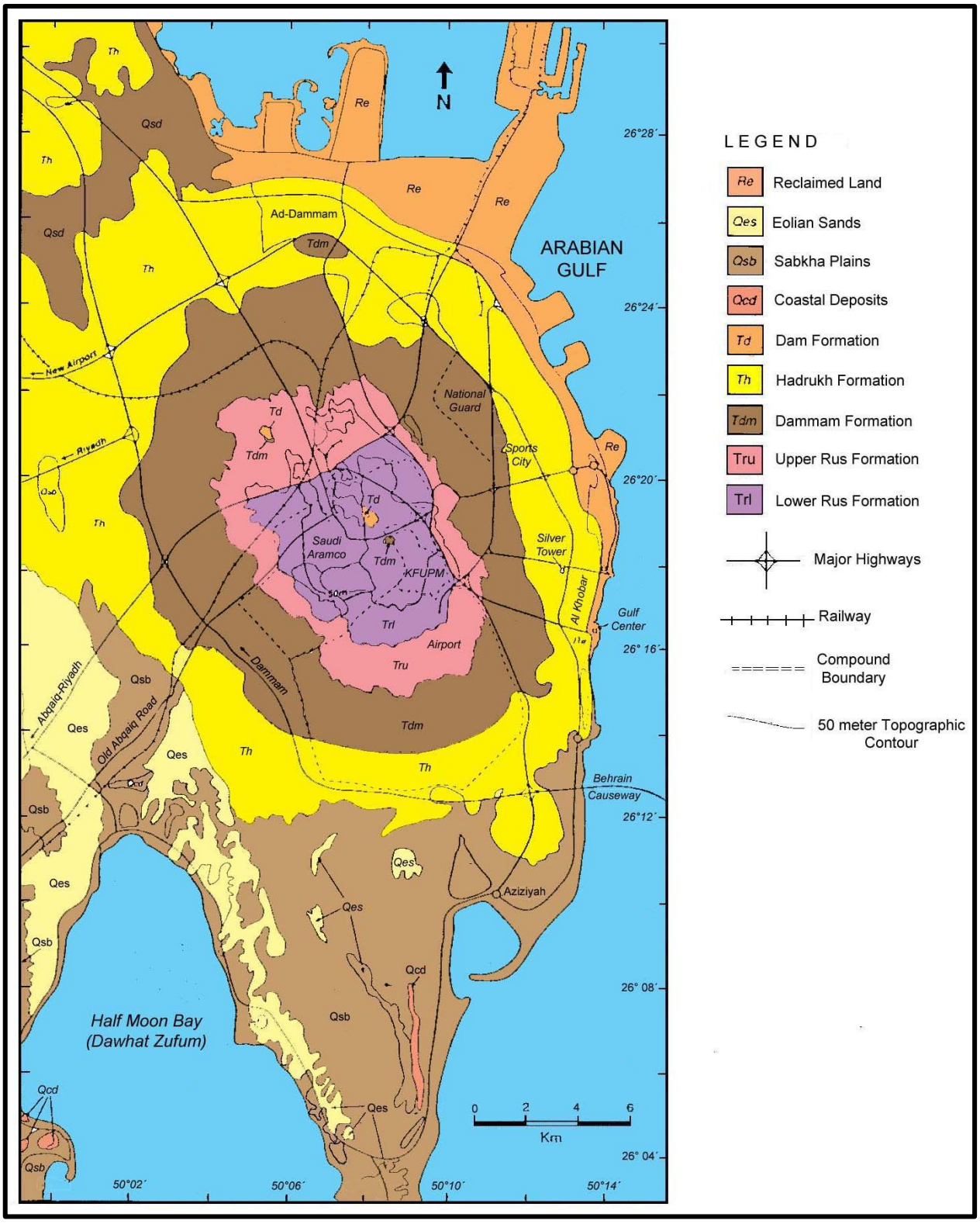

Figure 7: Geological map of Al-Dammam dome (after Weijermars, 1999).

Hadrukh Formation is exposed northwest and west of Al-Dammam dome overlying Al-Dammam Formation. The exposure of this formation is very clear in Al Qatif area. Rocks of this formation are medium grained; mainly green, greenish gray and gray in color and consist of quartoze sandstone, calcareous sandstone, shale and marl. The calcareous sandstone can be observed in the upper part of the formation. The thickness of this formation ranges between 20 m and 90 m and could reach 120 m in some areas. The formation is highly variable and contains shale, sandstone and marl in different colors. Inclusions of gypsum and chert are also present.

Dam Formation is the youngest rocks from Tertiary period in the study area, where it uncomformably overlies the Rus and Al-Dammam formations. Only a part of the formation could be mapped, as its upper part has been eroded away (Al Sayari and Zotl., 1978). The lower part of the formation is exposed at Jabal Midra Al Janubi on the northwestern side of the dome. The Dam formation consists of yellowish gray microcrystalline and sandy limestone. The thickness of this formation varies considerably from 30 m to 100 m. The formation consists mainly of clay with minor marl and limestone in different colors ranging from green to red.

Hufuf Formation reaches 95 m thick and consists of the following four different members:

(1) Gray conglomerate,

(2) Alternating red and white argillaceous sandstone,

(3) Off-white in part impure sandy limestone, and

(4) Red and white conglomerate.

The Quaternary sediments include the sabkhah deposits, coastal deposits, surface carbonate deposits of sand and pebbles, and eolian sand. Most of the marine deposits are 1 to 3 m wide along the shoreline. The surface carbonate deposits are formed in the flat areas as well as in the depressions. The eolian sand exists in the form of sand dunes ranging in height from 5 m to 15 m. The Sabkhah deposits (Qsb) in the area are coastal type, which can mainly be observed in the southern and north-northwestern parts of the area. The distribution of sabkhahs is controlled by topography as they occupy the low lying areas. Some sabkhahs are overlain by a thin layer of eolian sand sheets (2.5 to 5 cm). The sabkhahs sediments are mainly composed of loose to moderately dense sand, silt, clay and salt. The surface carbonate deposits (Qsp) consist of sand and pebble grains derived from the carbonate rocks. These deposits are visible in the flat areas and depressions. They are thin and locally covered by aeolian sand and bounded by the carbonate exposures.

The coastal deposits (Qcd) are restricted to the Arabian Gulf coast. The grains are light beige color and composed mainly of medium grained calcareous sand, oolitic sand and fragments of marine fossils. In some places, the coastal deposits contain evaporites (gypsum) similar to that of Half Moon Bay. The fills in the study area cover different parts with various thicknesses and types. Several coastal sites have been improved by calcareous sand fill that was dredged from the Gulf. The second type is mechanically excavated dunes sand that was transported by trucks to raise the ground surface of the inland sabkhahs.

III. SEISMICITY AND ATTENUATION RELATION OF THE EASTERN PROVINCE

Until recently, the eastern province of Saudi Arabia was considered a stable region with a negligible level of seismicity. However, the lack of seismicity data can also be related to the poor coverage of the region with seismographic stations, which means that smaller events have potentially not been detected. Recently, some of modern seismic stations have been installed in eastern province of Saudi Arabia (Fig. 8). These stations recorded some of low-moderate magnitude events originated from the eastern province of Saudi Arabia.

As mentioned-above, the active tectonics of Zagros Thrust Fault represents the major earthquake prone area affecting the eastern province of Saudi Arabia. Convergence between these plates has lead to the uplift of the Zagros Mountains and Iranian Plateau and makes the region one of the most seismically active in the Middle East (Al-Amri et al., 2008). The boundary is clearly delineated by teleseismic epicentres, although there are fewer epicentres occurred south of Oman. Most earthquakes occur in the crustal part of the Arabian Plate beneath the Zagros belt (Jackson and Fitch, 1981). Large earthquakes ($M \geq 5$) are quite common along this fault and reveal the potential for wide-spread damage from destructive earthquakes. Zagros belt is a prolific source for large magnitude earthquakes with numerous magnitude ($M \geq 7$) events occurring in the last few decades.

Unfortunately, there are few number of seismological studies have been conducted in the eastern province of Saudi Arabia. In spite of this province was subjected to one of large earthquakes ($5.8 \leq Mb \geq 6.2$) based on historical record on 1832 AD (Ambraseys, 1988; Punsalan and Al-Amri, 2003). According to Al-Shaabi (2004), about 69 instrumentally earthquakes ($2.4 < Ml < 5.8$) have been occurred during the period of 1990-1998 around Ghawar reservoir. Some of these events due to the earthquake swarm in June –October 1994. Most of these earthquakes are clustered around the southeastern flank of Al-Ghawar reservoir and this is correlated well with the fault system of Al-Ghawar reservoir.

III.1 Earthquakes Data Resources

For the purposes of characterizing the earthquake activity for Saudi Arabia, a seismically catalogue was compiled throughout gathering the available data from several sources for the Arabian Peninsula and adjacent area. The obtained data covering two of observational periods;

a) Historical period (112-1964 AD), and

b) Instrumental period (1964- Dec. 2009).

In the present study, the earthquake data sources include;

- Two regional catalogues (Ambraseys (1988) ; Ambraseys et al., (1994);
- Seismic Studies Center (SSC) of King Saud University;

- Saudi National Seismographic Network (SNSN) of King Abdull-Aziz City for Science and Technology;
- Saudi Geological Survey (SGS);
- Kuwait National Seismological Network (KNSN);

Then, the collected data were merged and correlated well with the International earthquake data bulletins where these data are precisely reviewed, re-analyzed and refined from duplicated events as;

- International Seismological Center (ISC) on-line bulletin;
- The on-line bulletin of the United States Geological Survey (USGS), which includes information from the Preliminary Determination of Epicenters (PDE) provided by the National Earthquake Information Center (NEIC);
- The on-line bulletin compiled of the European Mediterranean Seismological Center (EMSC).

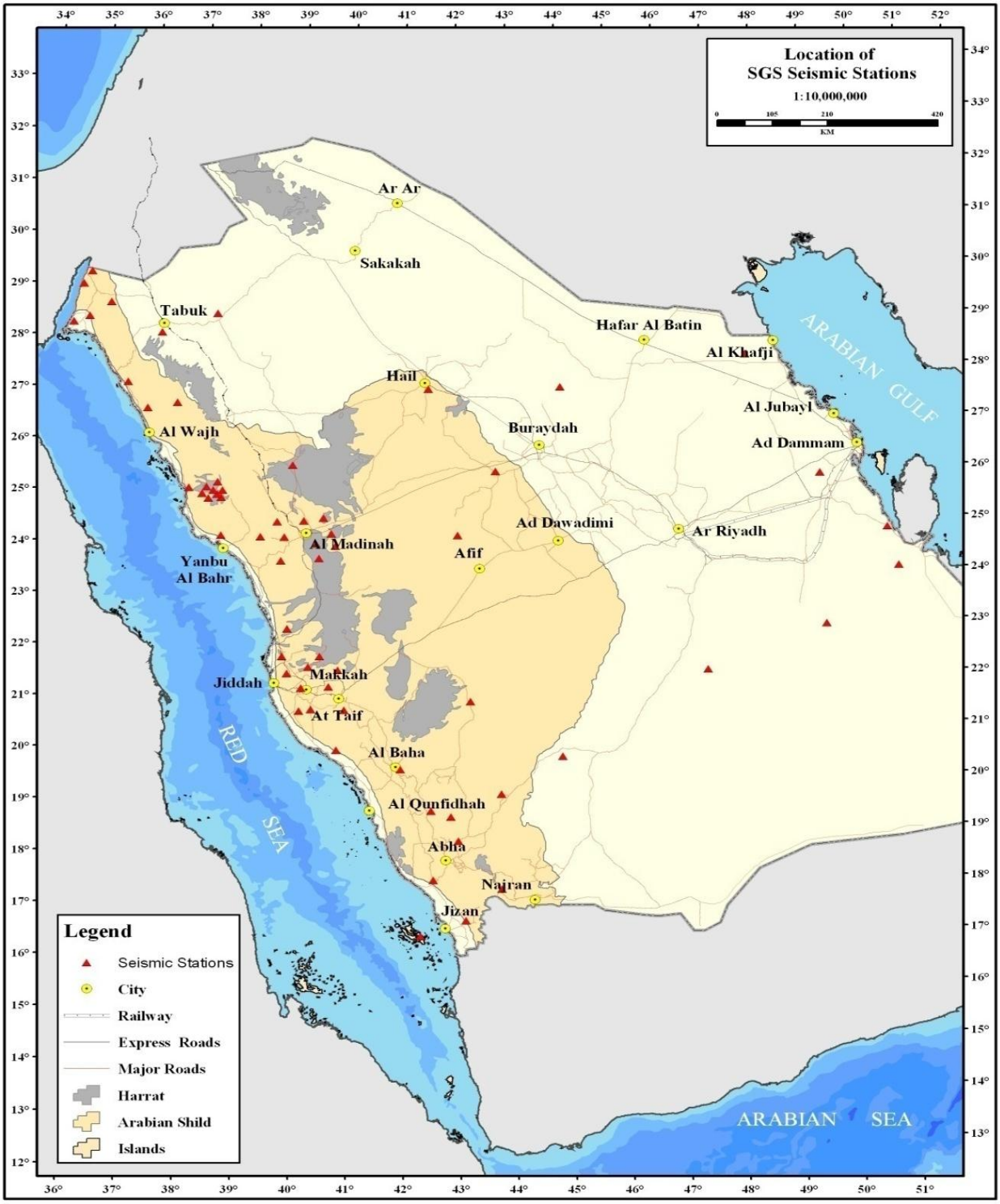

Figure 8: Seismic stations of Saudi Geological Survey.

Some earthquakes have different types of magnitudes were converted and unified into body-wave magnitude (M_b) according to Ambraseys and Bommer (1990); Ambraseys and Free (1997) and Al-Amri et al., (1998). Finally, the spatial distribution of the compiled seismicity catalogue is plotted to construct new seismicity map for the Arabian Plate and adjacent area has been conducted (Fig. 9). The reliability and quality of earthquake data sources have been investigated and considered for the catalogue compilation when conflicting information and duplicates have been encountered. Foreshock and aftershock sequences have been removed from the catalogue using the windowing procedure proposed by Gardner & Knopoff (1974).

III.2 Identification of Seismotectonic source zones

From the definition of Seismic source zone, it should be seismically homogeneous area, in which every point is assumed to have the same probability of being the epicenter of the future earthquake. It is not always possible to compile detailed information of the several criteria required for the ideal delineation of source zones. Hence, a careful consideration of the main tectonic structures and their correlation with the current seismicity can be basis for the delineation of the source zones.

The characteristics of the seismic source may include: Source zone geometry (location and extent, both surface and subsurface), description of Quaternary

displacements (sense of slip on the fault, fault dimensions, age of displacement, estimated displacement per event, estimated magnitudes per offset, rupture length and area, and displacement history or uplift rates of seismogenic folds), Historical and instrumental seismicity associated with each source, Relationship of the fault to other potential seismic sources in the region, Maximum earthquake the source would be capable of producing, and Recurrence model (frequency of earthquake occurrence versus magnitude).

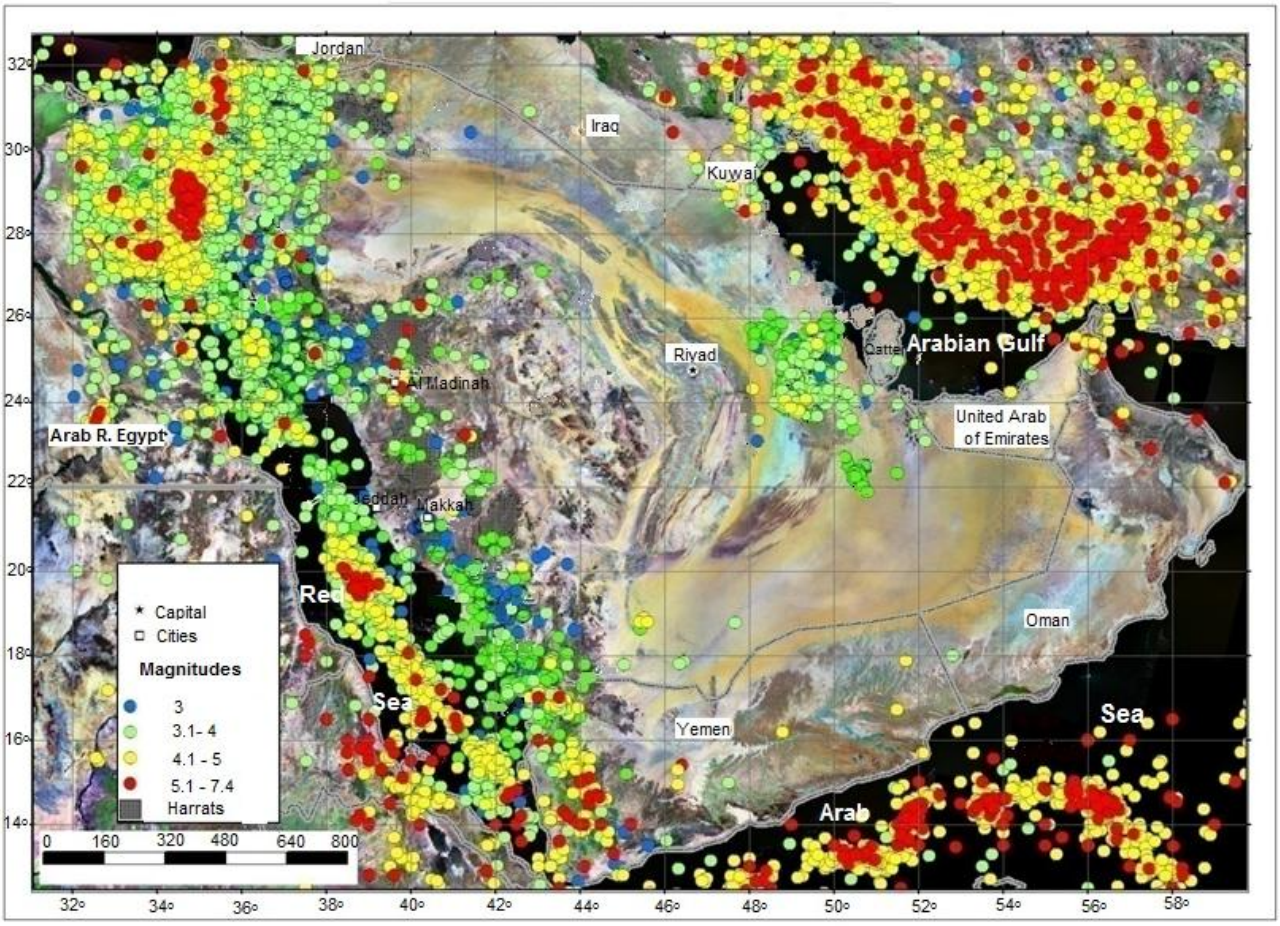

Figure 9: Seismicity map for the Arabian Peninsula (1900 - Dec. 2010).

There are two principal ways are usually used to assess the maximum earthquakes;

1. Estimate the maximum dimensions of future ruptures and relate those dimensions to magnitude. This approach is geared toward characterizing the dimensions of faults. The dimensions of ruptures and/or amount of displacement that might be expected on a fault of interest are estimated from geologic investigations designed to assess what has occurred during past ruptures. As many of the rupture

dimensions as possible should be used to lend stability to the magnitude estimates. Also, the uncertainties in the values of the rupture parameters should be incorporated (Coppersmith and Youngs, 1986 and 1990).

2. Considering the size of historical earthquakes associated with the source and with tectonically-analogous sources. Common acceptable approaches used in assessing maximum earthquakes are: (1) taking the source zone's maximum historical earthquake as the maximum; (2) taking the maximum historical earthquake and add an arbitrary magnitude (or intensity) increment to it; or (3) drawing an analogy to another source zone and use the maximum historical earthquake associated with that source. The maximum earthquakes can also be evaluated based on the opinions provided by a panel of experts with knowledge of the site region (Bernreuter et al., 1989; Coppersmith and Youngs, 1990).

Based on the distribution of earthquakes, geological structures (Al-Husseini, 2000 and Al-Mahmoud et al., 2009) and previous seismotectonic studies (Al-Amri, 2004; Tavakoli, 1996, Abdalla and Al-Homoud, 2004 (a & b); Bou-Rabee and Abdel-Fattah, 2004 and Pascucci et al., 2008), it could be differentiate seven seismogenic source zones (Fig.10) where their characteristics are shown in Table 1.

Table 1: Seismtectonis source zones affecting the eastern Province.

Zone	Source Zone Name	M_{max}	b-values
I	Zagros fold and thrust Belt	7.4	1.00
II	Zagros Foredeep zone	7.2	0.85
III	Zagros Mesopotamian Foredeep	6.9	0.85
IV	Dibba Fault Line zone	6.7	0.8
V	Makran subduction zone	8.5	1.00
VI	Southwest Kuwait (Minagish-Umm Qudair) zone	6.5	0.74
VII	Eastern Province (Al- Ghowar) zone	5.5	0.63

Zagros Fold and Thrust Zone (ZFTZ)

The Zagros mountain belt is a NW-trending fold-and-thrust belt, consisting of a 6-15- km thick sedimentary pile which overlies Precambrian metamorphic basement (McCall et al., 1985; McCall, 1997). The sedimentary cover can be divided into three successive sequences. First, at its base, it is comprised of thick late Precambrian evaporitic deposits (the so-called 'Hormoz Salt') which constitute the main regional décollement for most of the larger folds within the Zagros fold-and-

thrust zone (ZFTZ). This layer is the origin of numerous salt diapers that have pierced the overlying sedimentary cover and risen to the surface.

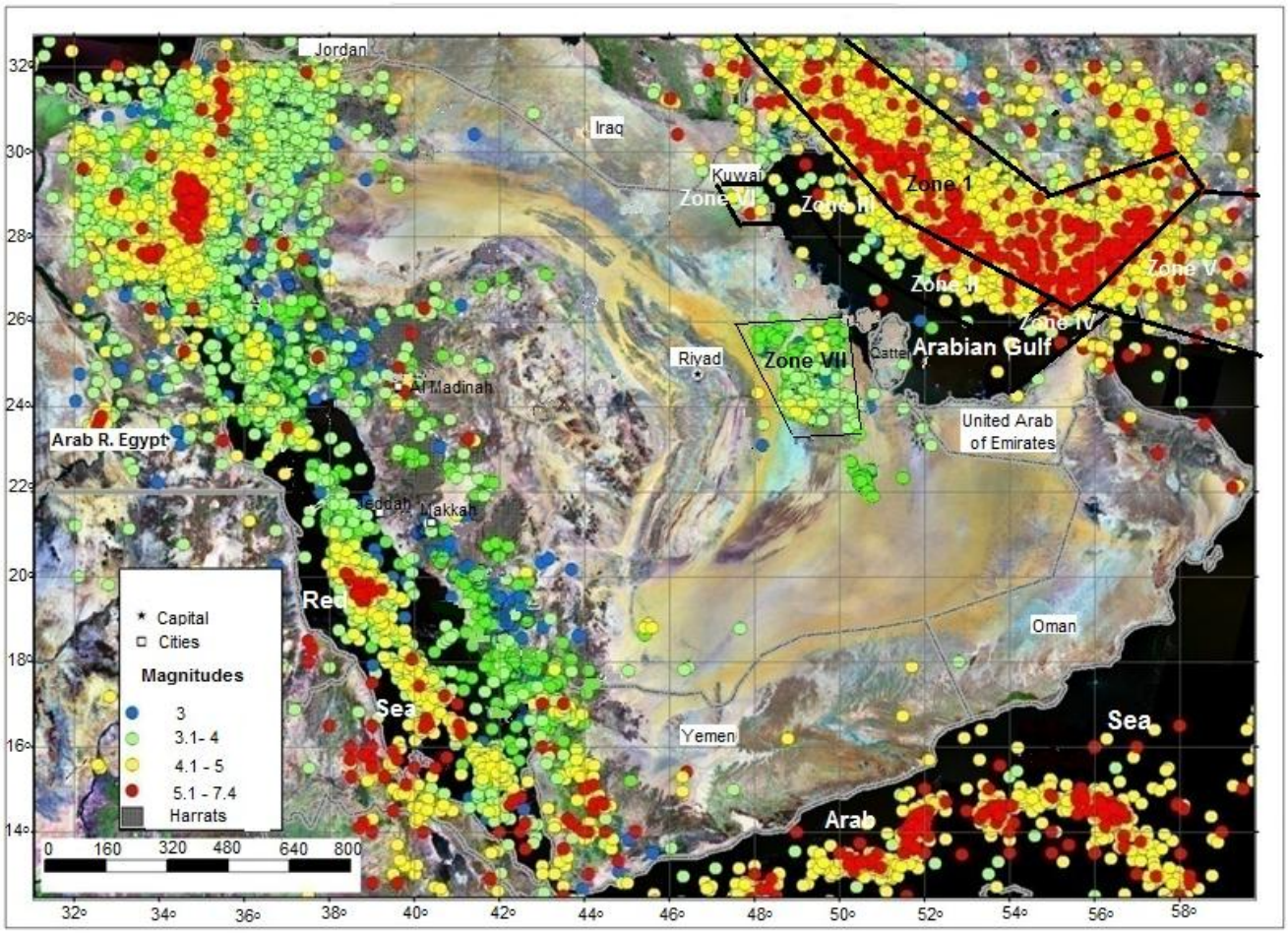

Figure 10: Seismic source zones affected the eastern province of Saudi Arabia.

A~4000 m thick Cambrian to Eocene sequence forms the so-called Competent Group. Apart from the initial Cambrian-Carboniferous clastic formations, the majority of this group until Upper Cretaceous consists of massive platform carbonate rocks (James and Wynd, 1965; Faure- Muret and Choubert, 1971; Szabo and

Kheradpir, 1978 and Sharland et al., 2001). The remainder of the stratigraphic sequence is represented by the Miocene to Recent clastic sediments of the Incompetent Group. These molasse-type sediments, derived from the uplift and erosion of the Zagros Mountains, show a typical coarsening-up evolution from marine-to-continental clastics to coarse proximal conglomerates at the top (James and Wynd, 1965; Edgell, 1996; Hessami et al., 2001).

The entire Zagros folded belt is the most active seismic area in this seismogenic source zone. The folded zone is characterized by both shallow and non-shallow earthquakes. The earthquakes locations in this folded belt define a zone of about 200 km wide that runs parallel to its central axis. Most of the earthquakes are crustal seismic events that occur in the portion of the Arabian plate. The continued convergence of the Afro-Arabian plate relative to the Iranian blocks is partially accommodated by folding of the Zagros sedimentary cover and by high angle reverse faulting of the underlying Precambrian Arabian basement. The present basement faulting beneath the Zagros fold belt as due to re-activation of pre-existing normal faults as reverse faults in the Arabian continental margin

Historical data indicates that an earthquake of magnitude 5.7 has occurred in March 21 1875. One 5.5 magnitude in Feb 4, 1934, and 3 magnitude 5.4 in 1925, 1939, and 1958 have occurred in this source zone. In 1972, a magnitude 6.1 has occurred which was followed by a magnitude 6 in 1976 in a span of 4 years. A survey of the range of magnitude in this zone is seen to be frequented many times

with magnitude 5 and above. These earthquakes could indeed cause a significant ground shaking in the eastern province of Saudi Arabia. The M_{max} expected of 7.4 for this zone is correlated well with the results of Berbrian and Yeats (1999), and Aldama-Bustos et al., (2009).

Zagros foredeep zone

Zagros fold-thrust belt can be divided into three tectonic zones from NE to the SW; Zagros fold-thrust belt, the Zagros Foredeep zone and Zagros Mesopotamian Foredeep zone (Falcon, 1974; Stőcklin 1984). The Zagros Foredeep Fault (Berberian, 1995), separates the present alluvial basin of the Zagros Belt from the simply Folded Belt. It partly controls the morphology of the Arabian Gulf and is marked by relatively long linear anticlines. Seismically, the Foredeep fault is active but less than Fold-thrust belt (Talebian and Jackson, 2004).

The foredeep in the Zagros system is localized in the coastal Plain and Arabian Gulf. The Coastal Plain is narrow feature that slopes gently to the south with an area of about 226.000 km^2; the Arabian Gulf is a shallow epicontinental sea with a tectonic origin (foreland depression) which covers the Arabian shelf platform with water depths less than 100 m. The evolution of the area can be subdivided into 3 main steps (Koop & Stoneley, 1982). The first step is characterized by a rifted continental shelf phase (Permian and Triassic) with thick marine deposition followed by thinning due to uplift and pre-Jurassic truncation associated to drift separation of the Arabian Plate. In the second step (Jurassic to Mid Cretaceous) thin sequences

typical of arid climates were deposited. In the early Cretaceous uplift is regionally replaced by subsidence, except the Arabian plate which remained elevated. In the Mid Cretaceous the first pre-tectonic effects are found and the Neotethys began to close. The third step concerns the collision and Zagros orogeny; at first a regional uplift is recognized in the whole area while in the Palaeocene-Eocene the subsidence starts and the first flysch sediment are deposited in an elongate foredeep with NW/SE direction.

Makran subduction zone

It is located in the north-eastern margin of the Arabian Plate where the Arabian Plate subducts beneath the Eurasian Plate (Farhoudi and Karig, 1977, Bayer et al., 2006 and Aldama-Bustos et al., 2009). The Makran accretionary wedge stretches from Iran to central Pakistan and off the south coast of this area (Schluter et al., 2002). It has been formed by the subduction of the oceanic portion of the Arabian Plate beneath Eurasia and is built up by sediments scraped off the Arabian Plate since early Tertiary (Berberian and King, 1981; Harms et al., 1984; Kopp et al., 2000). Subduction was probably initiated during Paleocene (Platt et al., 1988) and accretion started during Eocene times (Byrne et al., 1992). The modern Makran accretionary prism has developed since Late Miocene (Platt et al., 1985; Platt et al., 1988), and is still propagating seaward at a rate of ~10 mm yr-1 (White, 1982). Two features make this accretionary wedge unusual: (1) the sediment thickness on top of

the oceanic crust is extremely high (at least 6 km); and (2) the dip angle of subduction is extremely low (~5 degrees, Jacob and Quittmeyer, 1979; Byrne et al., 1992; Carbon, 1996).

The largest earthquake have been occurred in this zone was in 1945 with M_s of 8.0 (Quittmeyer and Jacob, 1979). The distribution of its aftershocks suggests that the length of the rupture zone between 100 and 200 km (Quitmeyer, 1979 and Byrne and Sykes, 1992).

Dibba Fault Line Zone (DFLZ)

The primary tectonic units in this source zone are the Dibba fault and the Hormuz salt basin south of the Arabian Gulf. This seismic source area is both historically and instrumentally active. Two earthquakes of magnitude 6.4 occurring in Jan 10, 1897 and the other in July 9, 1902 were located in the convergence zone. Likewise, two earthquakes of magnitude 6.2 have also occurred in March 21, 1977 and Apr 1, 1977 in almost the same location. It is noted that this seismogenic source zone seems to have frequent earthquakes of above magnitude 6 and many seismic events above magnitude 5. The maximum earthquake of this zone is 6.7. This is correlated well with Al-Amri, (2004) where he stated that M_{max} = 6.8 for this zone based on the statistical analysis of the historical and instrumental data.

Eastern Province (Al-Ghawar) Zone

The Ghawar structure consists of two subparallel, north-south trending structural crests, separated by a saddle. It is about 174 miles long and 12 miles wide. Major trend of this zone is almost north-northeast south- southwest (Al-Hariri and Abdullatif, 2001). To the north there is the N–S trending Kuwait Arch of basement horst (Carman, 1996). Al-Ghawar and Qatar arch area was experienced historically with earthquakes (Ambraseys et al., 1994). Recently some of seismic stations was deployed around the area and these stations have recorded number of earthquakes with magnitudes up to 5.0 (SGS, 2010) from Al-Ghawar area and its vicinity. Most of these seismic events are located south to southeast of the Al-Ghawar reservoir and the rest on the west of Qatar peninsula.

Al-Sayari and Zotle, 1978 recorded that the most prominent joint set strikes northwest, and another less prominent set strikes northeast. Saner et al., (2005) stated that, growth of the Al- Ghawar structure was active in the Pleistocene and probably even in the Quaternary. The average growth rate, indicated by tilting of the flanks, is 0.06^{o} per one million years. The origin of the recorded earthquakes in Ghawar area and its vicinity, to great extent, is the extraction of oil and/or recent tectonic activities of the area.

Southwestern Kuwait (Minagish-Umm Qudair) zone

The local seismicity of Kuwait reveals two main clusters of events. The first is around the Minagish-Umm Qudair oil fields in the south, and the second is around

the Raudhatain - Sabriya oil fields in the north (Bou-Rabee, 1994a, b; Bou-Rabee and Nur, 2002; Sadek, 2004; Al-Enezi et al., 2005). The spatial correlation of earthquakes and oil fields suggest that these seismic events have been induced by oil production (El-Enezi et al., 2008). The magnitude (ML) of these earthquakes ranges from 0.3 to 4.8 and occurred at depth ranging from 3.3 to 28 km. The maximum expected magnitude at southwestern Kuwait zone is 6.5 (El-Enezi et al., 2005).

III. 3 Ground motion attenuation characteristics

Estimation of Peak Ground Acceleration (PGA) or response spectral ordinates as a function of earthquake magnitude and distance, represent the key element for seismic hazard assessment and designing earthquake resistant structures. Ground-motion relations require a calibration for the region of interest because of commonly observed differences between diverse seismotectonic regimes, crustal structures, and site conditions. Available quantified strong motion information is completely absent in the eastern part of Saudi Arabia and for the eastern counters of Arabian Peninsula, engineers face, till the present time, a daunting problem in estimating ground motion levels for the future events in the area of interest. Therefore, most of the previous hazard studies in Saudi Arabia (e. g. Al-Haddad et al., 1994; Al-Amri et al., 2008), Kuwait (e.g. Sadek, 2004; El-Enezi et al., 2005), United Arab of Emirates (e.g. Abdalla and Al-Homoud, 2004) or for the Arabian Peninsula area (Peiris et al., 2006, and Pascucci et al., 2008) borrowed attenuation models from abroad to calculate the ground motions for their scenarios. The current paper is motivated by this need to

have a simple approach for understanding the ground motion attenuation for the eastern province of Saudi Arabia. Here, this difficulty is circumvented by adopting the seismological model for synthetic generation of peak ground acceleration (PGA) values following Boore's (1983) stochastic approach. The present study took into consideration the effect of probable variability in stress drop, radiation coefficient, cut-off frequency, and focal depth. Depending on large synthetic database, an attenuation relation for strong ground motion is obtained by a two way stratification approach (Joyner and Boore 1981; Deif et al., 2009).

III.3.1 Seismological model

Seismological models for eastern province, which lacks strong motion data, Boore (1983) are viable alternatives and are used worldwide for ground motion prediction (Atkinson and Boore 1995; Hwang and Huo 1997; Toro et al. 1997; Iyengar and Raghukanth 2004). The theory and application of such model have been discussed in detail by Boore (1983 and 2003). Fourier amplitude spectrum of ground acceleration at bedrock is expressed as:

$$A(f) = CS(f)D(f)P(f)$$

where S(f) is the source spectral function, D(f) is the path function characterizing the attenuation, P(f) is a filter to shape acceleration amplitudes beyond a high cut-off frequency fm to correspond the particular ground motion measure of interest, and **C**

is a scaling factor. In the present study, the single corner frequency model of Brune (1970) is used:

$$S(f) = (2\pi f)^2 M_0 / \left[1 + (f / f_c)^2\right]$$

where the corner frequency $\mathbf{f_c}$, the seismic moment $\mathbf{M_0}$, and the stress drop $\mathbf{\Delta\sigma}$ are related through:

$$f_c = 4.9 \times 10^6 V_s (\Delta\sigma / M_0)^{1/3}$$

where, the shear wave velocity **Vs** in the source region is a variable depends on the depth of the earthquake and the used crustal structure. The shear wave velocity values are taken from the velocity crustal structure for Arabian platform (Al-Amri el al., 2008). The diminution function D (f) (Boore 2003; Iyengar and Raghukanth, 2004) is defined as:

$$D(f) = G \exp\left[-\pi f R / V_s Q(f)\right]$$

where, **G** refers to the geometric attenuation and the other term to anelastic attenuation. In this equation, **Q** is the quality factor of the region. The high-cut filter in the seismological model is given by:

$$P(f, f_m) = \left[1 + (f / f_m)^8\right]^{-1/2}$$

where, $\mathbf{f_m}$ controls the high frequency fall of the spectrum. The scaling factor **C** is:

$$C = R_{\theta\varphi} K F / \left(4\pi\rho V_s^{\,3}\right)$$

where $\mathbf{R_{\theta\varphi}}$ is the radiation coefficient averaged over an appropriate range of azimuths and take-off angles, **K** is a factor for the partition onto two horizontal components, **F** is the free surface effect for the shear wave, **ρ** is the density at the source, and **Vs** is the shear wave velocity at the source. The three segments geometrical spreading operator of Atkinson and Boore (1995) is used in the current study. The geometrical attenuation term **G** for Aswan area is taken to be equal to R−1 for R<70 km and equal to R0.0 for distances from 70 to 130 km. Mokhtar et al., (2001) derived **Q** for the Arabian platform. The seismological model is implemented in the time domain by using the method of Boore (1983 and 2003). The simulation procedure essentially consists of three steps. First, a Gaussian stationary random process sample of strong ground motion duration (Boore and Atkinson 1987) is simulated.

$$T = 1/f_c + 0.05R$$

Second, the sample is windowed by multiplying it with the modulating function of Saragoni and Hart (1974) and is Fourier transformed into frequency domain. The Fourier amplitude spectrum is normalized by the square root of the mean square amplitude spectrum and multiplied by the target spectrum A(f) that was derived from the seismological model. Third, this is transformed back into the time domain to generate a sample of acceleration time history.

III.3.2 Ground motion attenuation

A considerable number of attenuation laws are used for predicting strong ground motion in terms of magnitude, distance, and local site geology. In some cases, other additional factors using a variety of models and data sets have been derived for different parts of the world (Joyner and Boore (1981); Ambraseys et al. (1996), and Ambraseys et al. (2005)).

The attenuation model is generally expressed as a mathematical function relating strong ground motion to parameters characterizing the earthquake source, propagation medium, and local site geology. The model should be simple as the available data and usually do not warrant excessive statistical analysis (Hasegawa et al. 1981). The proposed model of Joyner and Boore (1981) has been selected to be adopted in the present study. The basic form for the attenuation model can be expressed as:

$$\log(A) = \alpha + \beta M - \log R + bR + P\sigma \quad \text{.....(3.1)}$$

where **A** is the peak ground acceleration in gal (cm/s^2) and M its magnitude; **R** is the distance; and **α, β**, and **b** are the model parameters. **σ** is the standard deviation of log (A). The factor P is a dummy variable that represents the normal distribution: a value of P=0 implies mean (50-percentile) values of PGA, while the value of P=1 implies mean plus one standard deviation (84-percentile) values. The above equation is a linear function of magnitude and of distance dependent terms. The first term

represents the geometric losses, and it is constrained to spherical spreading from a point source while the second term accounts for anelastic losses (Ambraseys and Bommer 1991).

Joyner and Boore (1981) performed the regression analyses on the attenuation model in two stages; the first regression is on distance as:

$$\log(A) = \sum_{i=1}^{n} a_i E_i - \log R + br \qquad \ldots\ldots (3.2)$$

where

E_i = 1 for earthquake I and 0 otherwise

A is peak horizontal acceleration, **n** is the number of earthquakes in the data set, and **d** is the closest distance from the recording site to the surface projection of the fault rupture. Values of $\boldsymbol{\alpha_i}$ and **b** are determined by linear regression with average depth. Once the $\boldsymbol{\alpha_i}$ values are determined, they are used to find, by least squares, a first order polynomial representing the magnitude dependence. The second regression is then performed to determine the magnitude dependence:

$$a_i = \alpha + \beta M_i \ldots\ldots\ldots\ldots\ldots\ldots\ldots\ldots (3.3)$$

The employing of dummy variable E_i has the advantage that it decouples the determination of magnitude dependence from the determination of distance

dependence. To estimate σ_A, the standard error of a prediction equation, the following equation can be used;

$$\sigma_A = \left(\sigma_s{}^2 + \sigma_a{}^2\right)^{1/2} \quad \ldots\ldots\ldots\ldots\ldots\ldots \quad (3.4)$$

Where σ_s is the standard deviation for the residuals from the regression described by equation (3.2) and σ_a is the standard deviation of the residuals from the regression described by equation (3.3). This is based on two assumptions first, that the error in determining the attenuation curve in equation (3.1) is negligible compared to the residual of an individual data point relative to that curve and second, that all of the variability σ_a is due to the stochastic nature of the relationship between α_i and magnitude and none is due to measuring error in $\alpha_i M_i$ such as might be caused by inadequate sampling.

In the current research, the four model parameters, namely stress drop, focal depth, f_m, and the radiation coefficient are treated as random variables, were distributed uniformly around the mean value. The stress drop is taken to vary between 20 and 60 bars. The average focal depth in the affected zones (especially the nearest seismic zones of Zagros Foredeep, Zagros Mesopotamian Foredeep seismic source zones) has been estimated to be 25 km. while focal depth of the southwestern Kuwait seismic source ranges from 3.3 to 28 km. Accordingly, the focal depth is taken as a uniform random variable in the range of 3.0 –28 km. The cut-off frequency is taken in the interval 20–30 Hz. The range of the S-wave radiation

coefficient is taken as 0.48– 0.64 (Boore and Boatwright 1984). Here, it is noted that, Hwang and Huo (1997) and Iyengar and Raghukanth (2004) were also considered uncertainties in the model parameters for deriving the synthetic attenuation relationships for Central and Eastern United States and India Peninsula, respectively.

PGA values are simulated for moment magnitudes ranging from 3.5 to 7.5 in 0.5 magnitude unit increments (Fig. 11). The upper bound of magnitude is selected to be 7.5 representing the maximum magnitude that can be produced from Zagros seismogenic sources (Sadek, 2004). The distance is varied from 0 to 300 km (at 18 values of fault distances ranging from 1 to 300 km. as follows: 1, 2, 5, 10, 15, 20, 30, 40, 50, 60, 70, 80, 100, 120, 150, 200, 250 and 300 km.) representing the shortest distance between the projection of the rupture and the site of interest (Joyner and Boore 1981). The random vibration code written by Boore (1996) is used for generating the synthetic data. Regression by Joyner and Boore (1981) is carried out on the generated synthetic data to obtain the parameters of the attenuation equation for bed rock condition and the site effect at soft soil sites have to be estimated.

$$\mathbf{\log (A) = - 0.94 + 0.249\ M - \log r - 0.00233r + 0.19\ P}$$

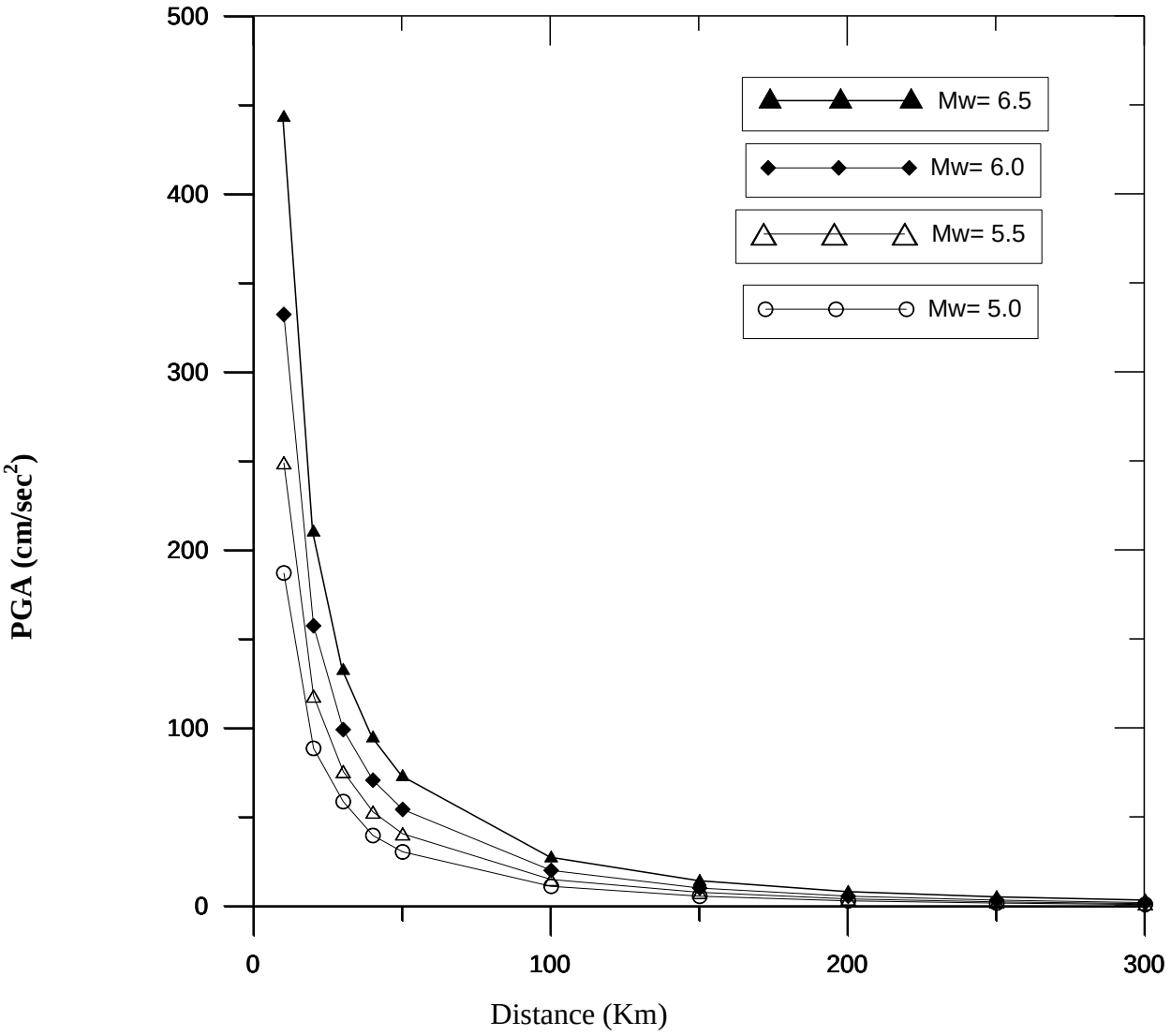

Figure 11: The estimated PGA through the eastern province of Saudi Arabia.

IV. SITE RESPONSE ASSESSMENT

IV. 1 SITE RESPONSE FUNDAMENTALS

Macroseismic observations, instrumental studies and theoretical or numerical investigations agree on the quasi-systematic occurrence of local effects in a small number of typical geological configurations. Their geometry and their mechanical parameters, such as S- and P-wave velocities, density, and material damping characterize these structures. It has been recognized that, earthquake damage is generally larger over soft sediments than on firm bedrock outcrops. This is particularly important, because most of the urban settlements have occurred along young, soft and surficial deposits. From the observations and investigations of the amplifications over soft sediments, the fundamentals of amplification on soft soils are established.

IV.1.1 Physical basis

The configuration of the underlying material also affects the amplitude of the seismic wave. When there are sharp changes in rock properties (impedance contrasts) below the earth's surface, several things happen. First, there is change (usually an increase) in amplitude as the upwardly propagating seismic wave traverses the change (usually a decrease) in impedance. A complication is that when a seismic wave traverses a sharp change in properties (boundary) some of its energy,

and therefore some amplitude, is lost in the form of reflections off that boundary and in the conversion to other wave types, such as from P- to S- waves. Second, resonance occurs as some of the seismic waves transmitted into the upper rock (or soil) layer themselves become trapped in this layer and begin to reverberate. This effect is a maximum when the reverberating waves are in phase with each other. Resonance is a frequency-dependent phenomenon. In the simplest case the maximum occurs for waves whose wavelength is four times the thickness of the layer in which the seismic waves are trapped. In other words, for shear waves the frequency which is amplified the most is that which is equal to $\beta/\mathbf{4h}$, where β the shear wave velocity of the layer and **h** is its thickness (Bard, 2007).

So the fundamental phenomenon responsible for the amplification of motion over soft sediments is the trapping of seismic waves due to the impedance contrast between sediments and the underlying bedrock. When the structure is horizontally layered (1-D structure), this trapping affects only body waves travelling up and down in the surface layers. When the surface sediments form a 2-D or 3-D structure, in other words when lateral heterogeneities such as thickness variations are present, this trapping also affects the surface waves, which develop on these heterogeneities and thus reverberate back and forth. The interference between these trapped waves leads to resonance patterns; the shape and the frequency of which are related with the geometrical and mechanical characteristics of the structure.

IV.1.2 Spectral characteristics

The resonance patterns show up as spectral peaks in the frequency domain. The frequencies of these peaks are related both to the thicknesses and velocities of the surface layers (Bard, 2007). For embanked 2-D or 3-D structures, they also depend on their width. For one layer structure, the peak frequency (fundamental frequency **Fo**) is given by:

$$\mathbf{F_o = \beta 1 / 4h}$$

where: β**1** is the horizontal shear wave velocity in the surface layer and **h** is its thickness. The amplitude of these peaks is related mainly to the impedance contrast between the surface layer and the underlying bedrock, to the material damping in the sediments, and to a somewhat lesser extent, to the characteristics of the incident wave field (types of waves, incident angle, near-field or far-field). In the case of 2-D or 3-D structures, the lateral geometry may also play an important role, especially in the case of small material damping. For the 1-D structure impinged by vertical plane S-wave, the amplification at the fundamental frequency **Fo** for the fundamental peak is given by:

$$\mathbf{Ao = 1 / ((1/C) + (0.5\ \pi\ \zeta 1))}$$

where: **C** is the impedance contrast = **(ρ2 β2/ ρ1β1)** and **ζ1** is the material damping in sediments.

IV.1.3 Time domain characteristics

In the time domain, these effects affect the peak amplitudes, the waveforms and motion duration, especially in the case of 2-D structures. It was thought that, peak ground accelerations (PGA) are not generally affected significantly by sediments, while peak ground velocities (PGV) are reaching higher values on soft soils. However, many investigations exhibited PGA values 4 times on soft sediments, such as the Mexico City records. On the other hand, it was also observed that, liquefied sandy deposits induce drastic reductions of peak accelerations.

There exist much fewer statistical analyses of strong motion duration and of its links with site conditions. All recent studies (Trifunac and Novikova, 1994; and Theodulidis et al., 1995) report a significant increase of duration on sediments, especially at long periods.

IV.1.4 Surface topographic effect

It has been often reported after destructive earthquakes that, buildings located at hill tops suffer much more intensive damage than those located at the base. There are also very strong instrumental evidences that surface topography considerably

affects the amplitude and frequency contents of ground motion (Géli et al. 1988; Faccioli, 1991 and Finn and Liam, 1991).

However, the number of instrumental studies about topographic effects is extremely low compared to studies dealing with soft soil amplification, so that it remains impossible to derive any statistics from the existing data. Basically these effects are related to three physical phenomena:

1- The sensitivity of the surface motions to the incidence angle, which is especially large for S-waves around the critical angle. The slope angle thus produces significant variations in the surface motion.

2- The focusing or defocusing of seismic waves reflected along the topographic surface (Bard, 2007). The wedge shape medium illustrates the effect (Fig. 12). If this wedge has an angle **2π/n** and is impinged by SH waves as depicted in figure 7, then one can easily compute the response by considering the multiple reflections within the wedge. The incoming waves will undergo **n-1** reflections and each single point within the wedge is reached by **n** waves. One may easily derive that, the motion amplitude at the vertex is equal to n times the incident one, since there is no phase lag between the incoming and reflected waves.

3- The diffraction of body and surface waves, which propagate down wards and outwards from the topographic features, lead to interference patterns between the direct and diffracted waves.

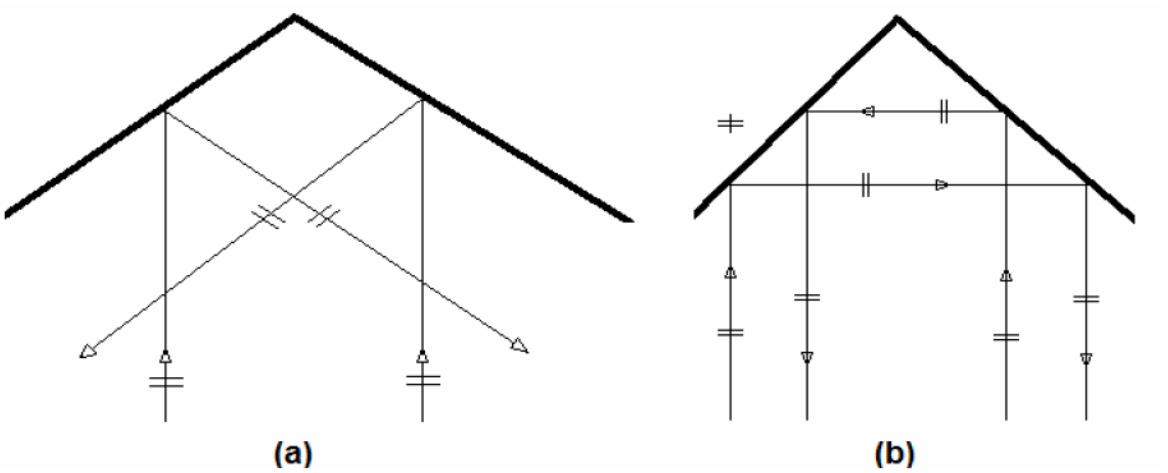

Figure 12: Response of a particular class of wedges to vertically incident SH waves. When the wedge angle is equal to $2\pi/n$, there exist n different waves passing through any point inside the wedge. All these waves interfere positively at wedge vertex, since there is no phase lag at this particular location, and the resulting amplitude of motion is n times larger than the incident wave (after Bard, 2007).

IV. 2 SITE RESPONSE ESTIMATION TECHNIQUES

There are several methods for site effect evaluation. These methods are classified according to various criteria into experimental, numerical and empirical approaches.

IV.2 .1 EXPERIMENTAL METHODS

They may be based on different kinds of data: macroseismic observations, microtremor measurements, weak seismicity surveys or strong motion accelerograms.

A- Macroseismic observations

It sometimes happens that, the site of interest has already undergone a destructive earthquake and that, detailed macroseismic observations are available. In that case, a detailed analysis of these data in the light of topographical and geometrical maps may lead to a qualitative appraisal of the most hazardous zones. Detailed macroseismic surveys immediately after destructive or well felt earthquakes are therefore of primary interest for microzonation purpose. Detailed questionnaires with an adequate format should therefore be carefully prepared. These macroseismic surveys have therefore to be complemented by the use of some empirical correlations between variations of intensity and variations of a few simple parameters, such as peak acceleration, peak velocity and duration.

B- Dynamic characteristics estimation using microtremor observations

Microtremors are ambient vibrations of ground excited by natural (oceanic and atmospheric) or artificial (humans) disturbances, such as wind, sea waves, traffic, industrial machinery, high waterfalls, lakes, heavy machinery, rapids of large river and railways (Field et al. 1990). Spectral feature of microtremors (background noise)

exhibit a gross correlation with the site geological conditions, for instance a short predominant period of microtremors (< 0.2 second) indicates a rather stiff rock, while a larger period indicates softer and thicker deposits. The noise sources are very different from one site to another (even a near-by one) especially in the short period range. There are also significant variations in the noise level during day and night times. A careful microtremor survey therefore requires precise measurements.

C- Spectral ratio (Nakamura's technique)

Nakamura, (1989) proposed the basis of qualitative arguments that, the H/V spectral ratio is a reliable estimation of the site response to S-wave, providing reliable estimates, not only of the resonance frequency, but also of the corresponding amplification. These ratios are much more stable than the noise spectra and that, on soft soil sites they exhibit a clear peak, which is well correlated with the fundamental resonance frequency.

D- Reference Site Techniques

The most common procedure for comparing records at nearby sites (where source and path effects are believed to be identical) through spectral ratios is the reference site technique or the traditional spectral ratio technique (TSRT). This technique is introduced first by Borcherdt (1970) and generalized by Andrews (1986). These spectral ratios constitute a reliable estimate of the site response, if the

reference site is free of any site effect. This means that, it should fulfill the two following conditions:

1- It should be located near enough to ensure that, differences between each site are only due to site conditions.

2- It should also be unaffected by any kind of site effect.

IV.2 .2 NUMERICAL METHODS

A- Numerical modeling of horizontal shear-waves in soil

The amplitude of earthquake ground motion can be increased or decreased by both the properties and configuration of the near surface material, through which seismic waves propagate. These properties, which affect the level of ground motion, are the impedance and absorption. As Aki and Richards (1980) pointed out, the impedance is the resistance to particle (rock or soil) motion. Particle velocity is inversely proportional to the square root of the impedance. As a seismic wave passes through a region of increasing impedance, the resistance to motion increases and, to preserve energy, the particle velocity and therefore the amplitude of the seismic wave decreases. Other factors aside, seismic waves of the same distance from an earthquake would be higher on low density and low velocity soil than on high density, high velocity rock. Mitigating the increase in amplitude is absorption, also

called damping or anelastic attenuation, which tends to be substantially greater on soft soils than on hard rocks.

When there are sharp changes in rock properties (impedance contrasts) below the earth's surface, several things happen. First, there is a change (usually an increase) in amplitude as the upwardly propagating seismic wave traverses the change (usually a decrease) in impedance. When a seismic wave traverses a sharp change in properties (boundary) some of its energy, and therefore some amplitude, is lost in the form of reflections off that boundary and in the conversion to other wave types, such as from P- to S- waves. Second, resonance occurs as some of the seismic waves transmitted into the upper rock (or soil) layer. They become trapped in this layer and begin to reverberate. This effect is a maximum when the reverberating waves are in phase with each other.

In this section we shall study the effect of the boundary between two half-spaces that are in contact along the plane Z = 0. If the half-spaces consist of a solid, a fluid or a vacuum, then there are five nontrivial cases: solid/solid, solid/fluid, solid/vacuum, fluid/fluid, and fluid/vacuum. One of the most important and commonly encountered problems in geotechnical earthquake engineering is the evaluation of ground response. Moreover, it is commonly known that during earthquakes the damage to structures is reasonably associated with the underlying subsoil conditions. So the dynamic properties of underlying soils are greatly reflected by the characteristics of earthquake ground motions at ground surface (i.e.,

ground response). It has also, been demonstrated that the geographic distribution of ground shaking-related damage and its intensity is strongly dependent on local lithological and physical properties (e.g., silt and clay content, void ratio) and conditions (depth-to-water table and basement) of the near surface sediments (Kanai, 1952; Ooba, 1957; Minakami and Sakuma, 1948; Chiaruttini and Siro, 1981; Mueller et al., 1982).

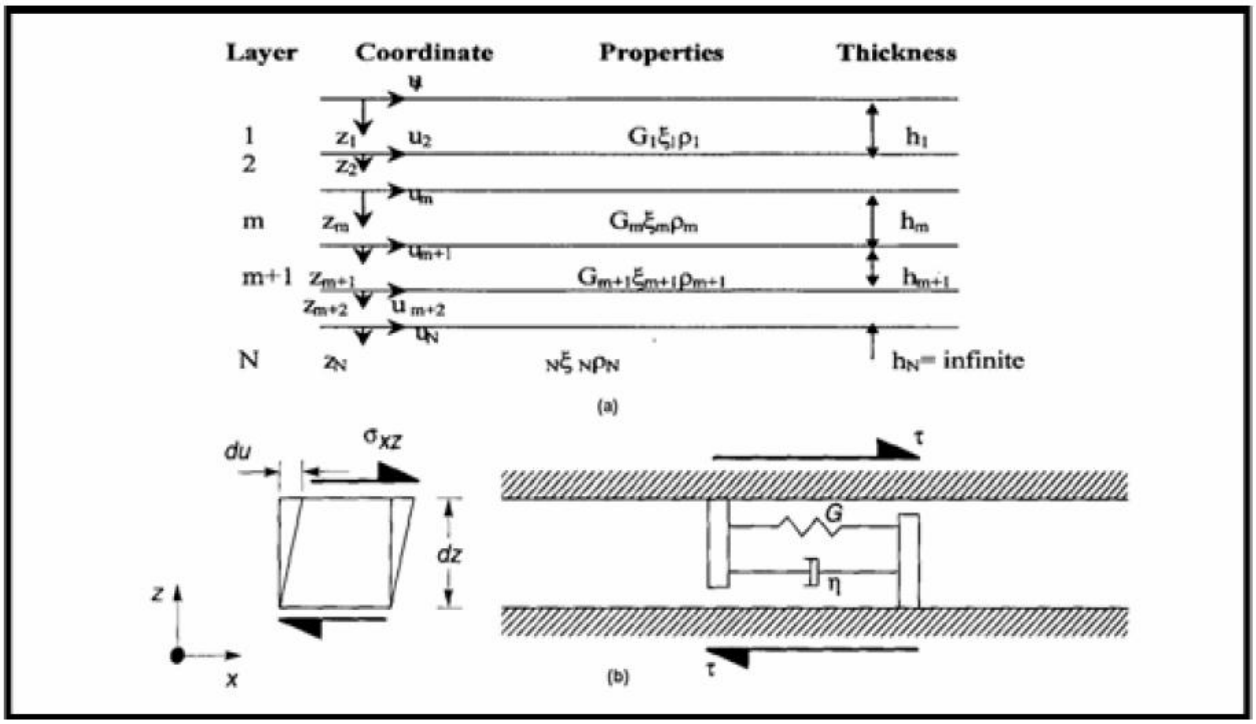

Figure (13): a-Nomenclature for layered soil deposits (1-D site response model) on elastic bedrock. b- Thin element of a Kelvin-Voigt solid subjected to horizontal shearing. Total resistance to shearing deformation is given by the sum of an elastic (spring) component and a viscous (dashpot) component (after Kramer, 1996).

where;

ξ ,ρ : damping coefficient and density respectively, h: layer thickness, G: shear modulus, u: displacement, z: layer depth, xz τ =σ : the shear stress, and η: the viscosity of the material.

This would cause upsurge of groundwater carrying sand, silt and clay in sedimentary areas of unconsolidated, pours, water-saturated and has a shallow water table (i.e., liquefaction). This is due to the fact, that the stress in such conditions reduces the shear resistance capacity of the soils. Consequently, understanding of the soil effect on seismic wave became an urgent need in order to map areas where amplification is likely and conveying this information to emergency mangers and community officials. Moreover, it can be used in land use planning, reducing business vulnerability, retrofitting building, producing guidelines for new constructions and assisting in infrastructure upgrade. Therefore, over the years, a great effort has been done in the level of theory (e.g., Ohsaki, 1981 and Kramer, 1996) and application (e.g., Faeh et al., 1990, 1993 and 1994; Zahradnik et al., 1991 & 1994, and Panza et al., 1996) in order to interpret the earthquake motion characteristics at a site. Both theory and application are often grouped according to the dimensionality of the problem they can address (Kramer, 1996).

After addressing the importance of ground response issue, an attempt to predict ground surface motions (taking into account the effect of local soils

conditions) using the one-dimensional ground response analysis approach (Fig. 13). This is relies on the theoretical model proposed by Kramer (1996). Next section describes the basics of the analysis used (i.e., 1-D ground response analysis approach) in this study and follows the general approach of Kramer (1996).

B. Geotechnical parameters-amplification relationship

The geotechnical data, such as the S-wave velocity or Standard Penetration Test value (NSPT), are sometimes available in addition to the simple information on surface geology. These parameters are used by several authors (Midorikawa, 1987; Joyner and Fumal, 1984; and Borcherdt et al., 1991) and they proposed relations between the average S-wave velocity of surficial deposits over a certain thickness and the relative amplification, as shown in Table (2). Applying these relations to the obtained shear wave velocities and the amplifications at the north western area of the Gulf of Suez, we found that, the obtained amplification values versus shear wave velocities obey Midorikawa relation (El-Shahat, 2003), as shown in Figure (14). The variation is due to the depth variation (the shear wave velocity with respect to the upper 30 meters in the used relation, but the calculated amplification with respect to the soil layer only about 5 meters).

Researchers	Equation
Midorikawa (1987)	$A = 68V_1^{-0.6}$ $(V_1 < 1100$ m/s.) $= 1.0$ $(V_1 > 1100$ m/s.)
Joyner and Fumal (1984)	$A = 23V_2^{-0.45}$
Brocherdt et al. (1991)	$AHSA = 700/V_1$ (for weak motion) $= 600/V_1$ (for strong motion)

Table 2: Shear wave velocity-amplification relationships.

Where;

A : relative amplification factors for peak ground velocity.

AHSA : average horizontal spectral amplification in period range of 0.4 to 2.0 sec.

V1 : average shear-wave velocity to a depth of 30 m. (in m/sec).

V2 : average shear-wave velocity to a depth of a one-quarter wavelength of a one second wave 30 m. (in m/sec).

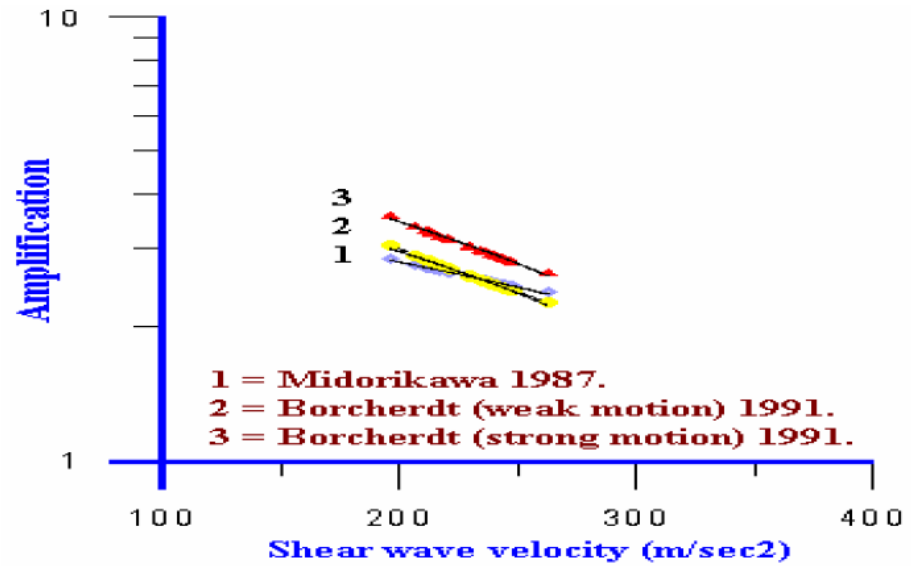

Figure 14: Amplification using shear wave velocities according to various authors (after El-Shahat, 2003).

IV.2 .3 EMPIRICAL METHODS

The effects of soft sediments on seismic response have been often observed. The very large number of observations has allowed researchers to develop empirical relations between surface geology and various measurements of earthquake motion. These relationships, derived from one particular set of data where both earthquake observations and information on surface geology are available, are then applied at other locations, where only the surface geology is known.

A- Geology-amplification relationship

The correlation between surface geology and relative amplification factors, according to various authors (Borcherdt and Gibbs 1976; Shima, 1978 and Midorikawa, 1987), is illustrated in Table (3).

B- Geology-intensity-increment relationship

Various empirical relationships between surface geology and seismic intensity increments have been proposed (Medvedev, 1962; Evernden and Thomson, 1985; Kagami et al, 1988; Astroza and Monage, 1991).

Table 3: Correlation between surface geology and relative amplification factor.

Geological Unit	Relative amplification factor
***Borchert and Gibbs (1976)**	
Bay mud	11.2
Alluvium	3.9
Santa Clara Formation	2.7
Great Valley sequence	2.3
Franciscan Formation	1.6
Granite	1.0
***Shima (1978)**	
Peat	1.6
Humus soil	1.4
Clay	1.3
Loam	1.0
Sand	0.9
***Midorikawa (1987)**	
Holocene	3.0
Pleistocene	2.1
Quaternary volcanic rocks	1.6
Miocene	1.5
Pre-Tertiary	1.0

Some of these relations have been obtained from sites where detailed intensity data were also available and it made it possible to develop empirical relationships between the average horizontal spectral amplification (AHSA) measured and the intensity increment are illustrated in Table (4).

IV.2. 4 Soil Structure Interaction Estimation

Ambient seismic noise measurements can be conducted inside any building for checking whether its frequencies of vibration fall into the range where soil amplification is expected. If this is the case, damage might increase in case of an earthquake due to an amplified structural response of the building. Two different techniques were used: the ratio between the horizontal and vertical components of

the spectra recorded at stations located inside the building and the ratio between the corresponding components of the spectra recorded simultaneously inside the building and at a reference station placed outside. The latter has the advantage of producing more stable results and deleting automatically the influence of the sedimentary cover, which might obscure some Eigen frequencies of vibration of the building.

Ambient seismic noise instead of earthquakes should be recorded inside the building using stations with 3D sensors (flat response in velocity between 1 and 40 Hz). Measurements should carry out at different floors in addition to the roof and the reference station outside the building simultaneously. There are different stations arrays can be used for measurements. The noise recording with a sampling rate of 100 Hz divided into 60-s windows. Ten or more windows tapered with a 5% cosine function were selected from the recordings at every site. The FFT is calculated for each component and spectra are first corrected for instrumental response and then smoothed using a Hanning window with constant relative bandwidth. Finally, the arithmetic mean of the results (H/V or RSM (Reference Site Measurements)) from the selected windows is computed. The natural period of the building is determined from the spectra of the two horizontal components and the effect of the soil structure interaction is determined from the H/V or RSM techniques.

Table 4. Correlation between surface geology and intensity increments (reproduced from TC4-ISSMGE, 1999).

Geological Unit	Intensity Increments
***Medvedev (1962)**	**(MSK scale)**
Granites	0
Limestone, Sandstone, Shales	0.2 ~ 1.3
Gypsum, Marl	0.6 ~ 1.4
Coarse-material ground	1.0 ~ 1.6
Sandy ground	1.2 ~ 1.8
Clayey ground	1.2 ~ 2.1
Fill	2.3 ~ 3.0
Moist ground	1.7 ~ 2.8
Moist fill and soil ground	3.3 ~ 3.9
***Evernden and Thomson (1985)**	**(MM scale)**
Granitic & Metamorphic rocks	0
Paleozoic rocks	0.4
Early Mesozoic rocks	0.8
Cretaceous to Eocene rocks	1.2
Undivided Tertiary rocks	1.3
Oligocene to middle Pliocene rocks	1.5
Pliocene-Pleistocene rocks	2.0
Tertiary volcanic rocks	0.3
Quaternary volcanic rocks	0.3
Alluvium (water table < 30 ft)	3.0
(100 ft < water table)	1.5
(others)	2.0
***Kagami et al. (1988)**	**(MM scale)**
Talus	0
Andesite	0
Gravel	0.2
River deposits	0.4
Volcanic ash	0.5
Sandy silt	0.7
Clayey silt	0.8
Silt	1.0
Peat	0.9
***Astroza and Monge (1991)**	**(MM scale)**
Granitic rock	0
Volcanic pumicite ashes	1.5 ~ 2.5
Gravel	0.5 ~ 1.0
Colluvium	1.0 ~ 2.0
Lacustrine deposits	2.5

V. SITE RESPONSE ESTIMATION IN AL_DAMMAM AND AL_KHOBAR CITIES

V.1 INTRODUCTION

The surface of the earth is always in motion even without earthquakes. These constant vibrations of the earth's surface are called microseisms or microtremors. The term "microtremor" is more commonly used in the field of earthquake engineering. Okada (2003) states that, amplitude of microtremors is, with some extreme exceptions, generally very small. Displacements are in the order of 10^{-4} to 10^{-2} mm; far below human sensing. Although, they are very weak, they represent a source of noise to the earthquake seismologists. If the amplifier gain is increased in order to record earthquake signals from a distant source, the amplitude of microtremors proportionally increases and the desired earthquake signal may be buried in the "noise" of microtremors. Elimination of this background noise is technically extremely difficult or impossible to achieve. Therefore the earthquake researchers call microtremors "seismic noise" or simply "noise".

It was not until the late nineteenth century, that seismologists could employ seismometers to observe the movement of the earth's surface. Since then, microtremors have been a focus of their strong interest, as is evident from large number of research papers published on the subject. Much of these publications concern the source of vibration and a variation in their character depending on time and location. It is well known that the microtremors are caused by daily human

activities such as movement of machinery in factories, motor cars and people walking; and natural phenomena such as flow of water in rivers, rain, wind, variation of atmospheric pressure, and ocean waves. Thus microtremors are not completely a natural phenomenon as human activities constitute some of their sources. However, at present microtremors are not regarded as nuisance "noise" but rather a useful "signal". In this sense, they are sometimes referred to as "uncontrolled signal".

Both human activity and natural phenomena (such as climate and oceanic conditions) vary with time as well, which sometime become very complex , irregular, and not repeatable. When microtremors are observed simultaneously at several spatially separated stations, it could be noted that these tremors are not completely random but some coherent waves are also contained in the records. In other words, microtremors are an assemblage of waves traveling in various directions. In fact, it is clearly demonstrated from the data of large-aperture seismic array that microtremors are an assemblage of body waves and surface waves. The microtremors originating from human activities are dominated by the components with periods shorter than one second or higher than 1Hz in frequency.

On the other hand, the microtremors due to natural phenomena such as climatic and oceanic condition have dominant periods greater than one second (frequency lower than 1 Hz), with associated amplitude and period variations corresponding to the natural phenomenon. The detailed analysis reveals that, microtremors variation depend upon location. The microtremor survey method has been devised to focus on

this variation. In this band, one can observe that the power spectra are affected by atmospheric pressure. However, the peak levels and their frequencies differ between the stations. A variation through time and the pattern is not consistent, as seen in the average of the day-time and night-time power spectra.

In 1960s, explanations about power spectra were presented in which the high power level of low frequency components (below 1.0 Hz) and the two characteristic spectral peaks have been attributed to oceanic activities, while the higher frequency components (above 1.0 Hz) were attributed to human activities and climatic conditions. It has been observed that the spectral characteristics show significant variation both locally and temporally. The microtremor survey method utilizes signals with periods shorter than several seconds, which always exists in seismic records, thereby demonstrating the ubiquitous applicability of this method.

Microtremor is a phenomenon which varies both spatially and temporally. As the microtremor survey method assumes both spatial and temporal microtremors, it is necessary to investigate this characteristic. The three-component microtremor records at different times show complex variations, but the degree of complexity does not vary during the recording period of three minutes. However, the amplitude envelope varies vastly between the microtremors recorded within one day or even as little as three hours apart.

Temporal variation of microtremors has a good inverse relationship with variation in atmospheric pressure: strength of microtremors increases with lower

atmospheric pressure with maxima soon after the trough. On the other hand, the strength decreases with the increasing of atmospheric pressure. Phenomena projecting a strong correlation between microtremors and atmospheric pressure and its lag by 3 to 15 hours present an interesting area for further research. As mentioned-above, the power spectra of higher-frequency microtremors are affected by human activities, where a range of frequencies between 4 Hz and 7 Hz clearly have diurnal variation. More precise observation may reveal that the power of microtremors diminishes relatively around lunchtime and also on public holidays.

V. 2 THE NAKAMURA TECHNIQUE

Nakamura, (1989) proposed the basis of qualitative arguments that, the H/V spectral ratio is a reliable estimation of the site response to S-wave, providing reliable estimates, not only of the resonance frequency, but also of the corresponding amplification. These ratios are much more stable than the noise spectra and that, on soft soil sites they exhibit a clear peak, which is well correlated with the fundamental resonance frequency. This alternative method gained much interest because of its low cost, rapid field operations and simple analytical procedure. Figure (15) shows a simple model proposed by Nakamura, which is based on the assumption that:

(1) Microtremors are composed mainly of Rayleigh waves, propagating in soft surface layers overlying a half-space;

(2) The vertical motions are not affected by the soft soils;

(3) The microtremors are originated by local surface sources (traffic and industrial noise) without any contribution from deep sources;

(4) Amplification of the vertical component is exclusively associated with the depth of surface (Rayleigh) wave's motion.

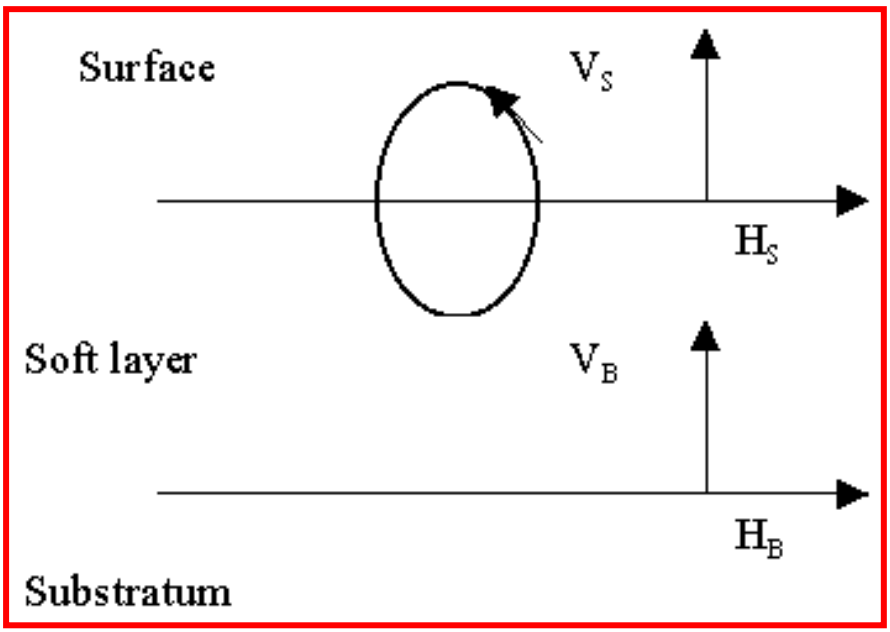

Figure 15: Simple model of Nakamura method (Nakamura, 1989).

According to Nakamura, the transfer function (i.e., the site response function) for Rayleigh waves compensated for the source spectrum is:

$$S_M = \frac{Zs}{Zb}$$

Where Zs= Hs/Vs and Zb=Hb/Vb. Under the prescribed assumptions, the vertical component is not amplified by the surface layer, i.e.,

$$\frac{Vs}{Vb} \sim 1$$

thus

$$S_M = \frac{Hs}{Vs}$$

i.e. the vertical component of microtremors on the surface retain the characteristics of horizontal component for the hard rock.

For each site the microtremor record is corrected for the base-line effect using the running average technique. This is done by sliding an average window of a given length over the data series. For each window position, the baseline is calculated as the average value in the data window. Various numbers of windows with 40 seconds (8000 samples) duration were selected among the quietest part of the signal. This time window is proven to be sufficiently long to provide stable results. The time series was tapered with a cosine taper and an amplitude spectrum is computed for each component. The FFT spectra were smoothed with a triangular moving Hanning window. In a final step, the geometrical mean is computed to merge the two horizontal components in one outcome H component.

V.2.1 EQUIPEMENTS AND DATA ACQUISITION

V.2.1.1 EQUIPEMENTS

V.2.1.1.1 Taurus data Logger

Due to the Al-Dammam and Al-Khobar cites are crowded all time, the Taurus Portable Seismograph which is a compact, self-contained digitizer and data logger that combines exceptional performance with versatility and low power consumption (Fig. 16) has been used. The Taurus can be used either as a stand-alone time-series data logger or as a component in a data acquisition network. Taurus incorporates a three-channel 24-bit Digitizer, GPS receiver and system clock, removable data storage, and remote communication options. Taurus is configurable locally using the color display screen and integrated browser or remotely using web browser over a TCP/IP connection. This instrument is equipped with three 24-bit data channels. Time-series data are stored in Steim (1) format which can be extracted to MiniSEED, Seisan, or ASCII format, and streamed in Nanometrics NP format.

As a portable unit, Taurus can be deployed to record continuous data for extended periods of time. For example, when recording 3 channels at 100sps, up to 600 days of data can be recorded using a 40GB 1.8” hard disk drive. A Compact-Flash card may also be used as an alternative to a hard drive, for example to use at more extreme temperatures or altitudes, or to realize optimal power consumption. Media are removable for easy data retrieval from the field. The extensive storage

combined with low power consumption make the Taurus ideal for long term unattended data acquisition.

Figure 16: Taurus data logger (seismograph) for the microtremors.

V.2.1.1.2 Trillium Compact

Standing at just 128 mm (5.04”) tall with a diameter of only 90 mm (3.54”), Trillium Compact combines the superior performance of a broadband seismometer with the installation convenience of a rugged geophone (Fig. 17). The instrument incorporates a symmetric triaxial force feedback sensor with a response flat to velocity from 120 seconds to 100 Hz. Scientists no longer need to compromise on performance in applications demanding small, highly portable seismometers. Data

output can be remotely switched between XYZ and UVW, allowing calibration of the elements independently of the electronics. UVW may be continuously recorded, if desired. The transfer function is approximately flat from 120s to 100 Hz, as shown in figure (18). Typical Trillium self-noise is plotted in figure (19). Curves indicating Peterson's new high- and low-noise models are included for references.

Figure 17: The Trillium compact 120s seismometer (Nanometrics Inc.).

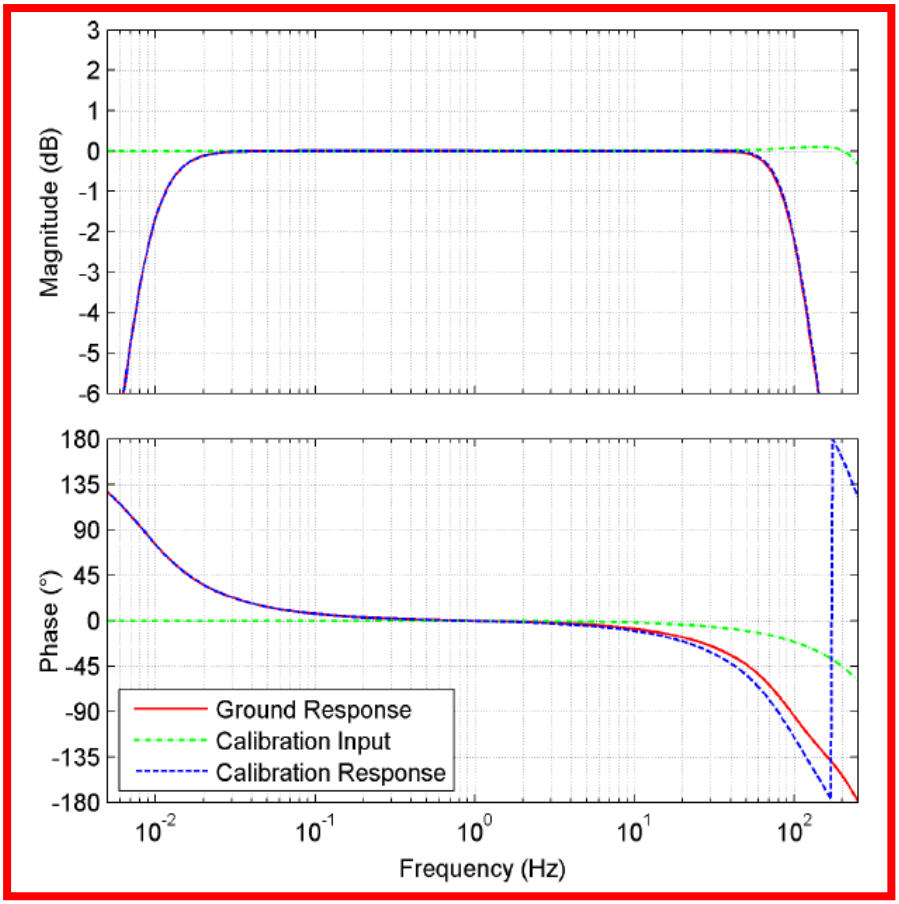

Figure 18: Trillium Compact 120s Nominal frequency response.

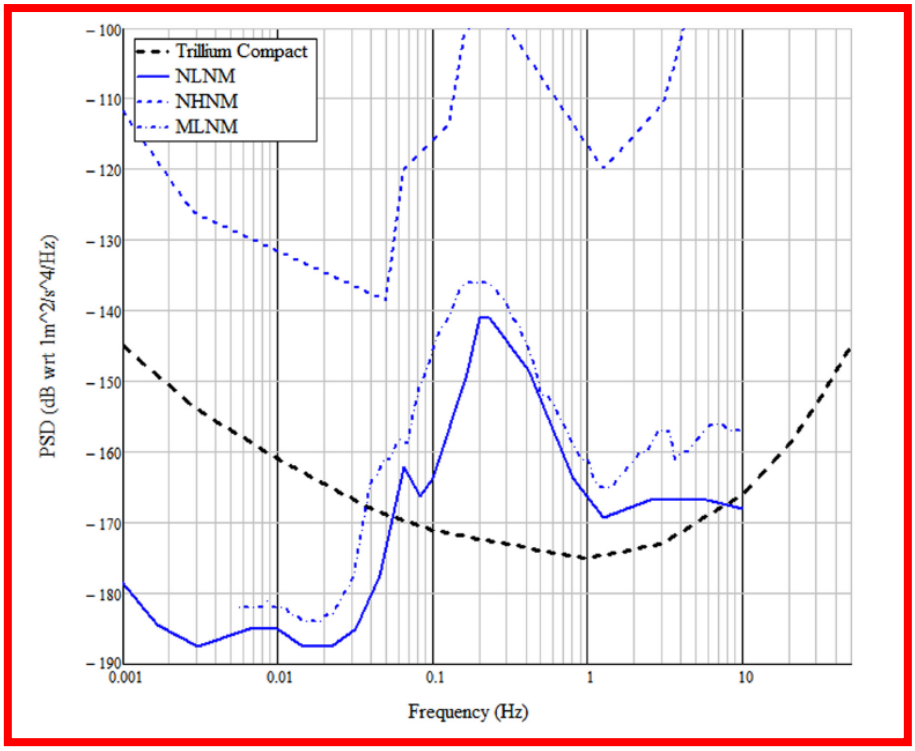

Figure 19: The Trillium Compact 120s seismometer self noise.

V.2.1.2 Microtremor measurements

Al-Dammam and Al-Khobar Cities have been bisected in a grid of 500m x 500m, each comprising a discrete measurement site. Microtremor measurements were acquired through the period from February 2010 – June 2011. Figures (20 and 21) illustrates the locations of 112 observation points in Al-Khobar city while, Figures 22 and 23 present 113 of measuring sites of in Al-Dammam city. At each site, the microtremors were recorded continuously for, almost, one hour. The Microtremors have been recorded at the measuring sites with the following precautions according to Nakamura (1996); Mucciarelli et al., (1998); Mucciarelli (1998); Bard and SESAME-Team (2005):

1- Measurements were carried out using 1-second (or higher) triaxial velocimeter, for analysis at periods longer than 1 second carried out measurements.

2- Avoided long external wiring, for reducing any mechanical and electronic interference.

3- Avoided measurements in windy or rainy days, which can cause large and unstable distortions at low frequencies.

4- Avoided recordings close to roads with heavy vehicles, which cause strong and rather long transients.

It is highly recommended that the above mentioned precautions in addition to the following guidelines (Tables 5& 6) should be read carefully before and during the field acquisition.

Digital records were obtained in the range of 0.2 – 25 Hz band-pass filter with a sampling rate of 100 samples per second. Tables 7 and 8 present the time of measurements at various sites in Al-Khobar and Al-dammam cities respectively. The length of recording for each measurement is an important parameter where, too short a period will result in unreliable average spectral ratios. The sensors used were calibrated before recording and installed in good coupling with soil. Furthermore, it was isolated thermally against temperature changes using thick foam box and covered to reduce the interference of wind. Then, these sensors were oriented horizontally (north-south and east-west) and vertically leveled.

Type of parameter	Main recommendations	
Recording duration	Minimum expected f_0 [Hz]	Recommended minimum recording duration [min]
	0.2	30'
	0.5	20'
	1	10'
	2	5'
	5	3'
	10	2'
Measurement spacing	→ Microzonation: start with a large spacing (for example a 500 m grid) and, in case of lateral variation of the results, densify the grid point spacing, down to 250 m, for example. → Single site response: never use a single measurement point to derive an f_0 value, make at least three measurement points.	
Recording parameters	→ level the sensor as recommended by the manufacturer. → fix the gain level at the maximum possible without signal saturation.	
In situ soil-sensor coupling	→ set the sensor down directly on the ground, whenever possible. → avoid setting the sensor on "soft grounds" (mud, ploughed soil, tall grass, etc.), or soil saturated after rain.	
Artificial soil-sensor coupling	→ avoid plates from "soft" materials such as foam rubber, cardboard, etc. → on steep slopes that do not allow correct sensor levelling, install the sensor in a sand pile or in a container filled with sand. → on snow or ice, install a metallic or wooden plate or a container filled with sand to avoid sensor tilting due to local melting.	
Nearby structures	→ Avoid recording near structures such as buildings, trees, etc. in case of wind blowing (faster than approx. 5 m/s). It may strongly influence H/V results by introducing some low frequencies in the curves → Avoid measuring above underground structures such as car parks, pipes, sewer lids, etc.	
Weather conditions	→ Wind: Protect the sensor from the wind (faster than approx. 5 m/s). This only helps if there are no nearby structures. → Rain: avoid measurements under heavy rain. Slight rain has no noticeable influence. → Temperature: check sensor and recorder manufacturer's instructions. → Meteorological perturbations: indicate on the field sheet whether the measurements are performed during a low-pressure meteorological event.	
Disturbances	→ Monochromatic sources: avoid measurements near construction machines, industrial machines, pumps, generators, etc. → Transients: In case of transients (steps, cars,...), increase the recording duration to allow for enough windows for the analysis, after transient removal.	

Table 5: Guidelines for Microtremor measurements.

Table 6: Sheet of Microtremor Field Measurements.

DATE: **10/2/1011**						PLACE: **Al-Dammam City**, **Al-Hamrah District (Cornish Street)**	
Operator: **Meteb Al-Malki**						GPS type and No.	
Latitude: **26° 28.168'**						Longitude: **50° 5.784'**	Altitude: **22 m**
Station type: **Broad-Band**						Sensor type: **Trillium Compact**	
Station No.: **2208**						Sensor Serial No.: **000190**	Disk No.: **SanDisk**
File Name:						Point No.: **1**	
Gain:						Sample Freq.: **100 SPS** Hz	Rec. Duration: **35** Minutes
Weather Conditions						Wind ☐ **None** ☐ weak ☐ medium ☐ strong Rain ☐ **None** ☐ weak ☐ medium ☐ strong Temperature (approx.): **25° C** Remarks……	
Ground Type						☐ earth {☐ hard} ☐ gravel ☐ **sand** ☐ rock ☐ grass = {☐ short} {☐ soft} {☐ tall} ☐ asphalt ☐ cement ☐ concrete ☐ paved ☐ other	
						☐ **dry soil** ☐ wet soil remarks …….	
Artificial Ground-Sensor Coupling ☐ **No** ☐ yes, type …….. ……							
Building Density ☐ none ☐ **scattered** ☐ dense ☐ other, type							
Transients	None	few	moderate	Many	Very dense	Distance	Monochromatic Noise sources (factories, works, pumps, rivers,…) ☐ **No** ☐ yes, type ……
Cars				√			Nearby Structures (trees, buildings, bridges, underground structures) (description, height, distance) **Nothing**
Trucks		√					
Pedestrians	√						
other							
Observations							

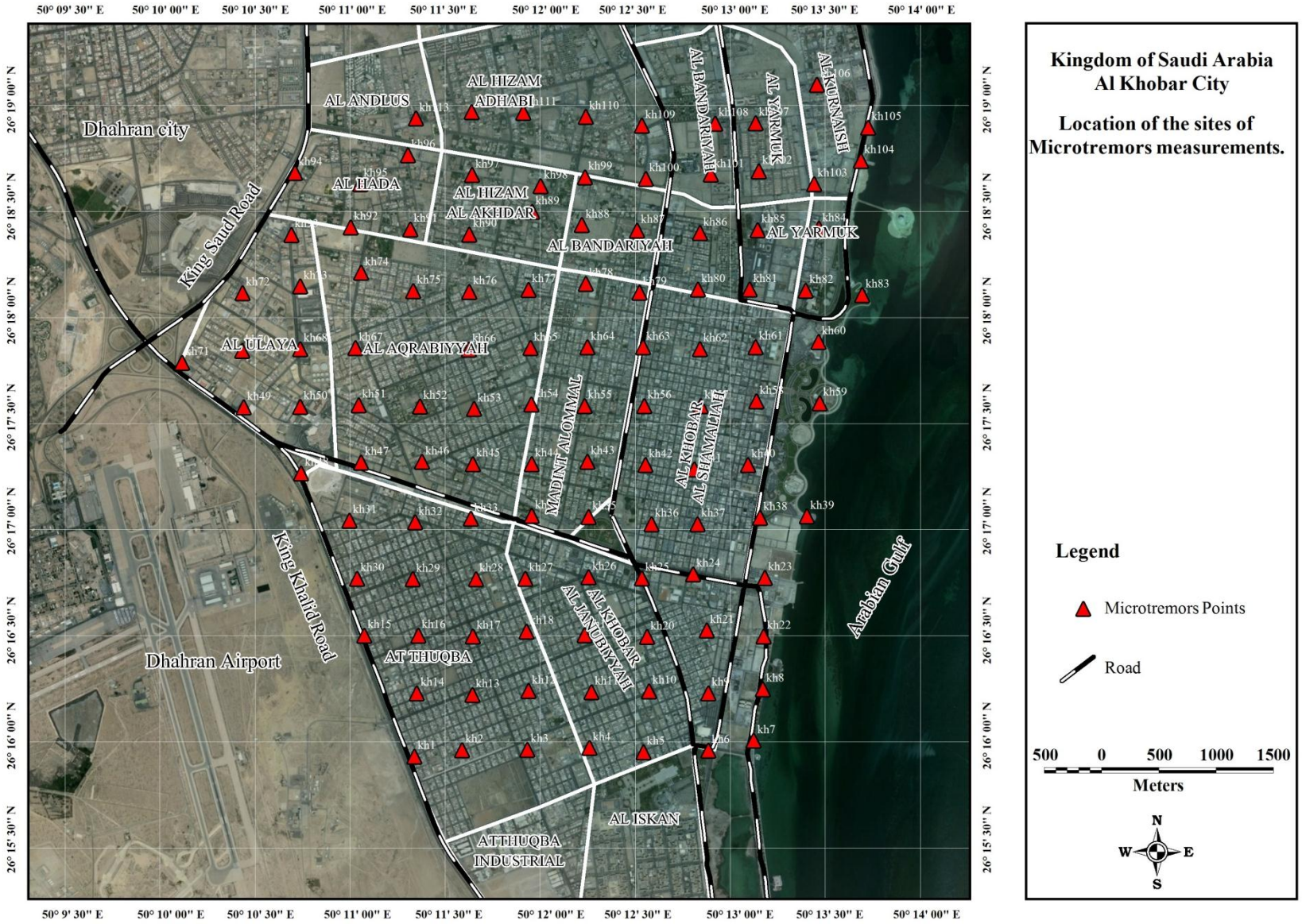

Figure 20: Location of the microtremor measurements in Al-Khobar City.

Table 7: Parameters of microtremor measurements sites at Al-Khobar City.

Site Code	Latitude	Longitude	Date	Start Time	End time	Duration	Sampling Frequency
Kh01	26° 15.936`	50° 11.337`	11/4/2011	10:23:00	10:53:33	30	100
Kh02	26° 15.966`	50° 11.588`	11/4/2011	11:32:00	12:02:00	30	100
Kh03	26° 15.969`	50° 11.931`	11/4/2011	13:33:00	14:03:00	30	100
Kh04	26° 15.977`	50° 12.258`	12/4/2011	06:44:00	07:14:00	30	100
Kh05	26° 15.957`	50° 12.543`	12/4/2011	08:28:00	08:58:00	30	100
Kh06	26° 15.964`	50° 12.883`	12/4/2011	09:45:00	10:15:00	30	100
Kh07	26° 16.011`	50° 13.123`	12/4/2011	11:31:00	12:01:00	30	100
Kh08	26° 16.254`	50° 13.171`	14/4/2011	07:10:00	07:41:00	30	100
Kh09	26° 16.235`	50° 12.884`	14/4/2011	08:22:00	08:52:00	30	100
Kh10	26° 16.244`	50° 12.572`	14/4/2011	10:10:00	10:40:00	30	100
Kh11	26° 16.240`	50° 12.268`	14/4/2011	11:50:00	12:20:00	30	100
Kh12	26° 16.245`	50° 11.937`	15/4/2011	11:03:00	11:24:00	20	100
Kh13	26° 16.227`	50° 11.643`	15/4/2011	13:08:00	13:29:00	20	100
Kh14	26° 16.235`	50° 11.351`	15/4/2011	14:34:00	14:55:00	20	100
Kh15	26° 16.507`	50° 11.073`	15/4/2011	15:52:00	16:13:00	20	100
Kh16	26° 16.506`	50° 11.358`	16/4/2011	06:48:00	07:09:00	20	100
Kh17	26° 16.503`	50° 11.646`	16/4/2011	07:39:00	08:00:00	20	100
Kh18	26° 16.526`	50° 11.927`	16/4/2011	09:16:00	09:37:00	20	100
Kh19	26° 16.509`	50° 12.232`	16/4/2011	10:05:00	10:26:00	20	100
Kh20	26° 16.500`	50° 12.561`	16/4/2011	10:56:00	11:17:00	20	100
Kh21	26° 16.530`	50° 12.875`	16/4/2011	12:32:00	12:53:00	20	100
Kh22	26° 16.503`	50° 13.175`	16/4/2011	13:25:00	13:55:00	30	100
Kh23	26° 16.779`	50° 13.181`	16/4/2011	14:20:00	14:51:00	30	100
Kh24	26° 16.795`	50° 12.804`	16/4/2011	16:33:00	16:59:00	25	100
Kh25	26° 16.776`	50° 12.535`	17/4/2011	07:15:00	07:36:00	20	100
Kh26	26° 16.781`	50° 12.255`	17/4/2011	08:16:00	08:37:00	20	100
Kh27	26° 16.775`	50° 11.922`	17/4/2011	09:12:00	09:33:00	13	100
Kh28	26° 16.773`	50° 11.662`	17/4/2011	10:20:00	10:51:00	30	100
Kh29	26° 16.772`	50° 11.329`	17/4/2011	12:00:00	12:31:00	30	100
Kh30	26° 16.775`	50° 11.036`	17/4/2011	13:00:00	13:31:00	30	100
Kh31	26° 17.049`	50° 10.996`	17/4/2011	13:50:00	14:21:00	30	100
Kh32	26° 17.040`	50° 11.342`	17/4/2011	14:40:00	15:01:00	20	100
Kh33	26° 17.057`	50° 11.634`	17/4/2011	15:48:00	16:09:00	20	100
Kh34	26° 17.070`	50° 11.954`	17/4/2011	07:46:00	08:07:00	20	100
Kh35	26° 17.065`	50° 12.255`	18/4/2011	16:10:00	16:41:00	30	100
Kh36	26° 17.031`	50° 12.584`	18/4/2011	17:25:00	17:46:00	20	100
Kh37	26° 17.031`	50° 12.828`	18/4/2011	18:05:00	18:26:00	20	100
Kh38	26° 17.061`	50° 13.156`	18/4/2011	19:27:00	19:48:00	20	100
Kh39	26° 17.068`	50° 13.402`	18/4/2011	20:20:00	20:41:00	20	100
Kh40	26° 17.311`	50° 13.093	19/4/2011	07:44:00	08:05:00	20	100
Kh41	26° 17.290`	50° 12.810`	19/4/2011	16:25:00	16:46:00	20	100
Kh42	26° 17.311`	50° 12.554`	19/4/2011	17:55:00	18:16:00	20	100
Kh43	26° 17.326`	50° 12.247`	19/4/2011	18:49:00	19:10:00	20	100
Kh44	26° 17.314`	50° 11.954`	19/4/2011	19:38:00	19:59:00	20	100
Kh45	26° 17.314`	50° 11.644`	19/4/2011	20:22:00	20:43:00	20	100
Kh46	26° 17.325`	50° 11.378`	19/4/2011	21:14:00	21:45:00	30	100
Kh47	26° 17.322`	50° 11.058`	20/4/2011	16:00:00	16:21:00	20	100
Kh48	26° 17.271`	50° 10.742`	20/4/2011	17:08:00	17:29:00	20	100
Kh49	26° 17.582`	50° 10.440`	20/4/2011	18:07:00	18:28:00	20	100
Kh50	26° 17.584`	50° 10.736`	20/4/2011	18:50:00	19:11:00	20	100
Kh51	26° 17.592`	50° 11.045`	20/4/2011	20:21:00	20:52:00	30	100
Kh52	26° 17.587`	50° 11.366`	20/4/2011	21:22:00	21:53:00	30	100
Kh53	26° 17.574`	50° 11.651`	20/4/2011	22:20:00	22:51:00	30	100
Kh54	26° 17.595`	50° 11.952`	30/4/2011	18:26:00	18:57:00	30	100
Kh55	26° 17.588`	50° 12.232`	30/4/2011	19:49:00	20:19:00	30	100
Kh56	26° 17.589`	50° 12.547`	30/4/2011	20:48:00	21:09:00	20	100
Kh57	26° 17.589`	50° 12.845`	30/4/2011	21:33:00	21:54:00	20	100
Kh58	26° 17.610`	50° 13.137`	30/4/2011	22:15:00	22:36:00	20	100
Kh59	26° 17.601`	50° 13.469`	30/4/2011	23:17:00	23:48:00	30	100
Kh60	26° 17.890`	50° 13.464`	01/5/2011	15:38:00	15:59:00	20	100
Kh61	26°17.866`	50°13.133`	01/5/2011	17:21:00	17:42:00	20	100

Kh62	26°17.857`	50°12.839`	01/5/2011	19:14:00	19:39:00	25	100
Kh63	26°17.865`	50°12.540`	01/5/2011	21:16:00	21:37:00	20	100
Kh64	26°17.865`	50°12.248`	01/5/2011	22:15:00	22:46:00	30	100
Kh65	26°17.861`	50°11.948`	01/5/2011	23:10:00	23:31:00	20	100
Kh66	26°17.854`	50°11.624`	02/5/2011	16:38:00	17:09:00	30	100
Kh67	26°17.861`	50°11.027`	02/5/2011	17:49:00	18:10:00	20	100
Kh68	26°17.857`	50°10.737`	02/5/2011	19:06:00	19:45:00	20	100
Kh69	26°17.856`	50°10.737`	02/5/2011	20:50:00	21:11:00	20	100
Kh70	26°17.849`	50°10.432`	02/5/2011	21:40:00	22:10:00	30	100
Kh71	26°17.792`	50°10.115`	02/5/2011	22:38:00	22:59:00	20	100
Kh72	26°18.121`	50°10.433	03/5/2011	16:22:00	16:43:00	20	100
Kh73	26°18.152`	50°10.736`	03/5/2011	17:22:00	17:43:00	20	100
Kh74	26°18.216`	50°11.058`	03/5/2011	18:16:00	18:47:00	30	100
Kh75	26°18.130`	50°11.332`	03/5/2011	19:12:00	19:33:00	20	100
Kh76	26°18.127`	50°11.627 `	03/5/2011	20:23:00	20:44:00	20	100
Kh77	26°18.136`	50°11.938`	03/5/2011	21:59:00	22:20:00	20	100
Kh78	26°18.164`	50°12.239`	03/5/2011	22:46:00	23:17:00	30	100
Kh79	26°18.123`	50°12.521`	03/5/2011	22:48:00	00:09:00	20	100
Kh80	26°18.137`	50°12.829`	04/5/2011	00:45:00	01:06:00	20	100
Kh81	26°18.137`	50°13.102`	04/5/2011	16:07:00	16:28:00	20	100
Kh82	26°18.132`	50°13.397`	04/5/2011	17:22:00	17:43:00	20	100
Kh83	26°18.111`	50°13.693`	04/5/2011	18:32:00	18:53:00	20	100
Kh84	26°18.424`	50°13.466`	04/5/2011	20:02:00	20:23:00	20	100
Kh85	26°18.417`	50°13.144`	04/5/2011	22:28:00	22:49:00	20	100
Kh86	26°18.403`	50°12.840`	05/5/2011	17:13:00	17:34:00	20	100
Kh87	26°18.416`	50°12.510`	05/5/2011	18:15:00	18:36:00	20	100
Kh88	26°18.441`	50°12.219`	05/5/2011	19:06:00	19:27:00	20	100
Kh89	26°18.503`	50°11.957`	05/5/2011	19:54:00	20:25:00	30	100
Kh90	26°18.397`	50°11.627`	05/5/2011	21:12:00	21:33:00	20	100
Kh91	26°18.421`	50°11.316`	06/5/2011	18:10:00	18:31:00	20	100
Kh92	26°18.431`	50°11.003`	06/5/2011	19:01:00	19:22:00	20	100
Kh93	26°18.395`	50°10.690`	06/5/2011	19:49:00	20:10:00	20	100
Kh94	26°18.687`	50°10.710`	06/5/2011	20:40:00	21:01:00	20	100
Kh95	26°18.635`	50°11.053`	06/5/2011	21:21:00	21:42:00	20	100
Kh96	26°18.771`	50°11.303`	07/5/2011	15:40:00	16:11:00	30	100
Kh97	26°18.677`	50°11.640`	07/5/2011	17:06:00	17:27:00	20	100
Kh98	26°18.625`	50°12.001`	07/5/2011	18:01:00	18:22:00	20	100
Kh99	26°18.666`	50°12.235`	08/5/2011	21:24:00	21:45:00	20	100
Kh100	26°18.659`	50°12.556`	08/5/2011	16:28:00	16:49:00	20	100
Kh101	26°18.679`	50°12.896`	08/5/2011	17:56:00	18:17:00	20	100
Kh102	26°18.695`	50°13.150`	08/5/2011	18:51:00	19:12:00	20	100
h103	26° 18.634`	50°13.440`	09/5/2011	20:50:00	21:11:00	30	100
Kh104	26° 18.744`	50°13.687`	11/5/2011	21:40:00	22:10:00	30	100
Kh105	26° 18.900`	50°13.724`	11/5/2011	22:38:00	22:59:00	20	100
Kh106	26° 19.103`	50°13.455`	12/5/2011	16:22:00	16:43:00	20	100
Kh107	26° 18.921`	50°13.133`	12/5/2011	17:22:00	17:43:00	20	100
Kh108	26° 18.920`	50°12.920`	12/5/2011	18:16:00	18:47:00	20	100
Kh109	26° 18.909`	50°12.535`	12/5/2011	19:12:00	19:33:00	20	100
Kh110	26° 18.951`	50°12.240`	12/5/2011	20:23:00	20:44:00	20	100
Kh111	26° 18.970`	50°11.910`	13/5/2011	21:59:00	22:20:00	20	100
Kh112	26° 18.974`	50°11.638`	13/5/2011	22:46:00	23:17:00	20	100
Kh113	26° 18.943`	50°11.346``	13/5/2011	22:48:00	00:09:00	20	100

Figure 21: Microtremors field measurements in Al-Khobar City.

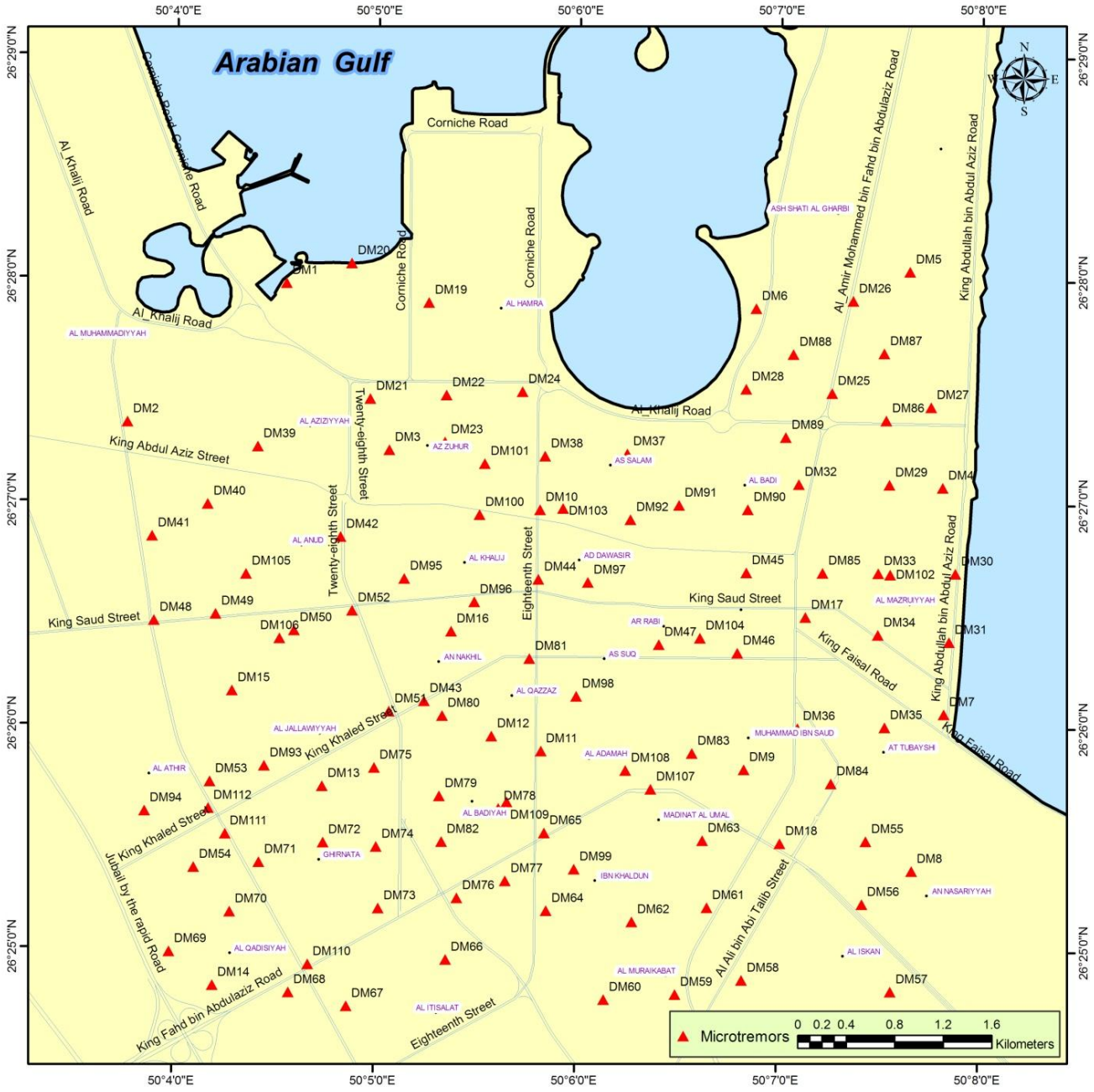

Figure 22: Location of the Microtremors measurements in Al-Dammam City.

Table 8: Parameters of microtremor measurements in Al- Dammam City.

Site	Lat.	Long.	Date	S.T.	E.T.	D. Min)	Sensor	S. Freq.	G.T.
DM1	26.4663	50.0758	10/2/2011	07:50	08:20	30	T.C.	100	asphalt
DM2	26.4559	50.0627	10/2/2011	13:30	13:55	25	T.C.	100	sand
DM3	26.4539	50.0844	10/2/2011	15:00	15:20	20	T.C.	100	gravel
DM4	26.4513	50.1302	11/2/2011	06:30	07:05	35	T.C.	100	sand
DM5	26.4674	50.1274	11/2/2011	08:16	08:46	30	T.C.	100	asphalt
DM6	26.4646	50.1147	11/2/2011	09:43	10:09	26	T.C.	100	asphalt
DM7	26.4344	50.1304	11/2/2011	11:09	11:35	26	T.C.	100	paved
DM8	26.4227	50.1278	11/2/2011	12:21	12:53	32	T.C.	100	asphalt
DM9	26.4302	50.1139	11/2/2011	13:30	13:50	20	T.C.	100	cement
DM10	26.4495	50.0969	12/2/2011	10:05	10:48	43	T.C.	100	asphalt
DM11	26.4315	50.0971	12/2/2011	12:31	12:51	20	T.C.	100	cement
DM12	26.4326	50.093	13/2/2011	06:33	07:08	35	T.C.	100	asphalt
DM13	26.4288	50.079	13/2/2011	08:30	09:00	30	T.C.	100	asphalt
DM14	26.4139	50.07	13/2/2011	10:00	10:25	25	T.C.	100	asphalt
DM15	26.4359	50.0715	13/2/2011	11:20	11:54	34	T.C.	100	asphalt
DM16	26.4404	50.0896	13/2/2011	12:35	13:00	25	T.C.	100	asphalt
DM17	26.4416	50.1189	13/2/2011	14:00	14:30	30	T.C.	100	asphalt
DM18	26.4247	50.1169	14/2/2011	09:00	09:31	31	T.C.	100	cement
DM19	26.4649	50.0876	8/4/2011	05:40	06:10	30	T.C.	100	asphalt
DM20	26.4678	50.0812	8/4/2011	07:11	07:41	30	T.C.	100	asphalt
DM21	26.4577	50.0828	8/4/2011	13:10	13:40	30	T.C.	100	sand
DM22	26.458	50.0891	8/4/2011	14:04	14:35	31	T.C.	100	sand
DM23	26.4545	50.089	8/4/2011	14:58	15:28	30	T.C.	100	sand
DM24	26.4583	50.0954	8/4/2011	17:25	17:52	27	T.C.	100	sand
DM25	26.4583	50.121	9/4/2011	04:27	04:47	20	T.C.	100	asphalt
DM26	26.4652	50.1227	9/4/2011	05:33	05:53	20	T.C.	100	sand
DM27	26.4573	50.1292	9/4/2011	06:15	06:35	20	T.C.	100	asphalt
DM28	26.4586	50.1139	9/4/2011	07:00	07:27	27	T.C.	100	asphalt
DM29	26.4515	50.1258	9/4/2011	08:03	08:23	20	T.C.	100	asphalt
DM30	26.4449	50.1313	9/4/2011	08:50	09:12	22	T.C.	100	asphalt

DM31	26.4398	50.1308	9/4/2011	09:35	09:55	20	T.C.	100	cement
DM32	26.4515	50.1183	9/4/2011	12:00	12:20	20	T.C.	100	asphalt
DM33	26.4449	50.1249	9/4/2011	14:12	14:35	23	T.C.	100	asphalt
DM34	26.4403	50.1249	9/4/2011	15:00	15:20	20	T.C.	100	asphalt
DM35	26.4334	50.1255	9/4/2011	16:00	16:20	20	T.C.	100	paved
DM36	26.4333	50.1183	9/4/2011	16:50	17:10	20	T.C.	100	asphalt
DM37	26.4537	50.1041	10/4/2011	05:20	05:40	20	T.C.	100	asphalt
DM38	26.4535	50.0973	10/4/2011	06:08	06:28	20	T.C.	100	asphalt
DM39	26.4541	50.0735	10/4/2011	07:00	07:20	20	T.C.	100	asphalt
DM40	26.4498	50.0694	10/4/2011	09:00	09:20	20	T.C.	100	concrete
DM41	26.4474	50.0648	10/4/2011	10:10	10:30	20	T.C.	100	asphalt
DM42	26.4474	50.0804	10/4/2011	12:00	12:20	20	T.C.	100	asphalt
DM43	26.4352	50.0874	10/4/2011	13:00	13:22	22	T.C.	100	asphalt
DM44	26.4443	50.0968	10/4/2011	16:03	16:23	20	T.C.	100	sand
DM45	26.4449	50.114	11/4/2011	05:50	06:20	30	T.C.	100	asphalt
DM46	26.4389	50.1133	11/4/2011	06:48	07:18	30	T.C.	100	asphalt
DM47	26.4395	50.1068	11/4/2011	07:55	08:25	30	T.C.	100	asphalt
DM48	26.4411	50.065	11/4/2011	14:26	14:48	22	T.C.	100	asphalt
DM49	26.4416	50.0701	11/4/2011	15:21	15:46	25	T.C.	100	sand
DM50	26.4404	50.0766	11/4/2011	16:15	16:35	20	T.C.	100	asphalt
DM51	26.4344	50.0845	12/4/2011	05:57	06:22	25	T.C.	100	asphalt
DM52	26.4419	50.0814	12/4/2011	06:45	07:09	24	T.C.	100	asphalt
DM53	26.4291	50.0697	12/4/2011	09:07	09:37	30	T.C.	100	asphalt
DM54	26.4227	50.0684	12/4/2011	14:52	15:02	10	T.C.	100	asphalt
DM55	26.4249	50.124	11/5/2011	16:54	17:14	20	T.C.	100	asphalt
DM56	26.4202	50.1237	11/5/2011	17:33	17:58	25	T.C.	100	asphalt
DM57	26.4137	50.1261	11/5/2011	18:15	18:38	23	T.C.	100	sand
DM58	26.4145	50.1138	11/5/2011	19:44	20:04	20	T.C.	100	asphalt
DM59	26.4134	50.1083	12/5/2011	02:19	02:39	20	T.C.	100	asphalt
DM60	26.413	50.1024	12/5/2011	03:05	03:30	25	T.C.	100	asphalt
DM61	26.4199	50.1109	12/5/2011	03:57	04:22	25	T.C.	100	asphalt
DM62	26.4188	50.1047	12/5/2011	04:43	05:08	25	T.C.	100	asphalt
DM63	26.4249	50.1105	21/5/2011	15:50	16:10	20	T.C.	100	asphalt

DM64	26.4196	50.0976	3/6/2011	16:26	16.47	21	T.C.	100	Sand
DM65	26.4254	50.0974	3/6/2011	17:10	17.30	20	T.C.	100	Sand
DM66	26.4159	50.0893	3/6/2011	17:50	18:10	20	T.C.	100	cement
DM67	26.4114	50.0811	3/6/2011	18:25	18:45	20	T.C.	100	Cement
DM68	26.4134	50.0763	3/6/2011	19:00	19:20	20	T.C.	100	Asphalt
DM69	26.4164	50.0664	3/6/2011	19:40	20:00	20	T.C.	100	asphalt
DM70	26.4194	50.0714	3/6/2011	20:22	20:42	20	T.C.	100	asphalt
DM71	26.4231	50.0738	4/6/2011	6:15	06:35	20	T.C.	100	asphalt
DM72	26.4246	50.0791	4/6/2011	6:51	07:11	20	T.C.	100	asphalt
DM73	26.4197	50.0837	4/6/2011	15:30	15:50	20	T.C.	100	asphalt
DM74	26.4243	50.0835	4/6/2011	16:12	16:32	20	T.C.	100	sand
DM75	26.4302	50.0833	4/6/2011	17:04	17:24	20	T.C.	100	asphalt
DM76	26.4205	50.0902	4/6/2011	17:48	18:08	20	T.C.	100	sand
DM77	26.4218	50.0942	4/6/2011	18:30	18:50	20	T.C.	100	cement
DM78	26.4272	50.0936	4/6/2011	19:11	19:31	20	T.C.	100	asphalt
DM79	26.4281	50.0887	4/6/2011	19:50	20:10	20	T.C.	100	asphalt
DM80	26.4341	50.0889	4/6/2011	20:25	20:45	20	T.C.	100	asphalt
DM81	26.4384	50.0961	4/6/2011	21:06	21:26	20	T.C.	100	asphalt
DM82	26.4247	50.0889	5/6/2011	13:54	14:15	21	T.C.	100	asphalt
DM83	26.4341	50.1096	5/6/2011	14:37	15:00	23	T.C.	100	sand
DM84	26.4292	50.1211	5/6/2011	15:20	15:42	22	T.C.	100	Sand
DM85	26.4449	50.1203	5/6/2011	16:06	16:26	20	T.C.	100	asphalt
DM86	26.4563	50.1255	5/6/2011	16:55	17:15	20	T.C.	100	asphalt
DM87	26.4613	50.1253	5/6/2011	17:38	17:58	20	T.C.	100	asphalt
DM88	26.4612	50.1178	5/6/2011	18:20	18:40	20	T.C.	100	asphalt
DM89	26.455	50.1172	5/6/2011	19:02	19:22	20	T.C.	100	asphalt
DM90	26.4496	50.1141	5/6/2011	19:52	20:12	20	T.C.	100	sand
DM91	26.4499	50.1084	6/6/2011	13:10	13:35	25	T.C.	100	asphalt
DM92	26.4488	50.1044	6/6/2011	13:55	14:15	20	T.C.	100	asphalt
DM93	26.4303	50.0742	6/6/2011	16:20	16:44	24	T.C.	100	asphalt
DM94	26.4269	50.0643	6/6/2011	17:10	17:40	20	T.C.	100	asphalt
DM95	26.4443	50.0857	6/6/2011	18:15	18:35	20	T.C.	100	sand
DM96	26.4426	50.0915	6/6/2011	18:56	19:16	20	T.C.	100	asphalt

DM97	26.4441	50.1009	7/6/2011	04:00	04:20	20	T.C.	100	asphalt
DM98	26.4356	50.1	7/6/2011	04:51	05:11	20	T.C.	100	asphalt
DM99	26.4227	50.0999	7/6/2011	05:45	06:05	20	T.C.	100	asphalt
DM100	26.4491	50.0919	7/6/2011	15:10	15:30	20	T.C.	100	sand
DM101	26.4529	50.0923	7/6/2011	16:00	16:20	20	T.C.	100	sand
DM102	26.4448	50.1259	8/6/2011	14:00	14:05	5	T.C.	100	asphalt
DM103	26.4496	50.0988	8/6/2011	14:45	14:50	5	T.C.	100	asphalt
DM104	26.44	50.1102	8/6/2011	15:30	15:35	5	T.C.	100	concrete
DM105	26.4446	50.0726	8/6/2011	17:08	17:13	5	T.C.	100	concrete
DM106	26.4398	50.0754	8/6/2011	17:35	17:40	5	T.C.	100	concrete
DM107	26.4287	50.1062	9/6/2011	14:42	14:48	6	T.C.	100	concrete
DM108	26.4301	50.1041	9/6/2011	15:05	15:10	5	T.C.	100	asphalt
DM109	26.4277	50.0943	9/6/2011	15:35	15:40	5	T.C.	100	asphalt
DM110	26.4155	50.0779	9/6/2011	15:55	16:00	5	T.C.	100	concrete
DM111	26.4252	50.071	9/6/2011	16:30	16:46	16	T.C.	100	cement
DM112	26.4271	50.0696	9/6/2011	17:00	17:15	15	T.C.	100	asphalt

Figure 23: Microtremors field measurements in Al-Dammam City.

V. 3 BOREHOLE GEOTECHNICAL DATA

Shear wave velocity is a critical factor to identify stiffness of the sediment in determining the amplitude of ground motion (Joyner and Fumal, 1985; Boore et al., 1993 and Anderson et al., 1996) and might be a useful parameter to characterize local geologic conditions quantitatively for calculating site response (Park and Elrick, 1998). As an alternative, the relations between shear wave velocity and several other physical properties (i.e. Standard Penetration Test) can be identified; this can be mapped more readily on a regional scale (Fumal, 1978). These correlations can be applied to areal distribution, physical properties and thickness of the geologic units to estimate and map shear wave velocity potential that is useful for seismic zonation studies.

The method used here identifies soil profiles in site characterization and merges in-situ measurements of dynamic properties with geologic information according to design code of IBC 2006. Twenty-nine boreholes have been drilled through Al-Khobar city (Fig. 24) and Tables (9 and 10) present the parameters from these boreholes. Thirteen geotechnical boreholes have been conducted through Al-Dammam City (Fig. 25) and tables (11 and 12) present the parameters from these boreholes. The maximum penetrated depth of these logs is about 30 m. The SPT was performed at 1.5 m interval in every borehole (ASTM D1586-84), and their respective blow counts were recorded. Measurements of the ambient noise have been carried out very close to or directly at the boreholes sites, where detailed

information about the subsurface structure, namely the thickness of the sediments, is available.

Finally, the borehole information were combined with the observed site response functions to develop a 1-D model for the subsurface and to calculate the S-wave velocity values for the soils that characterize the investigated region.

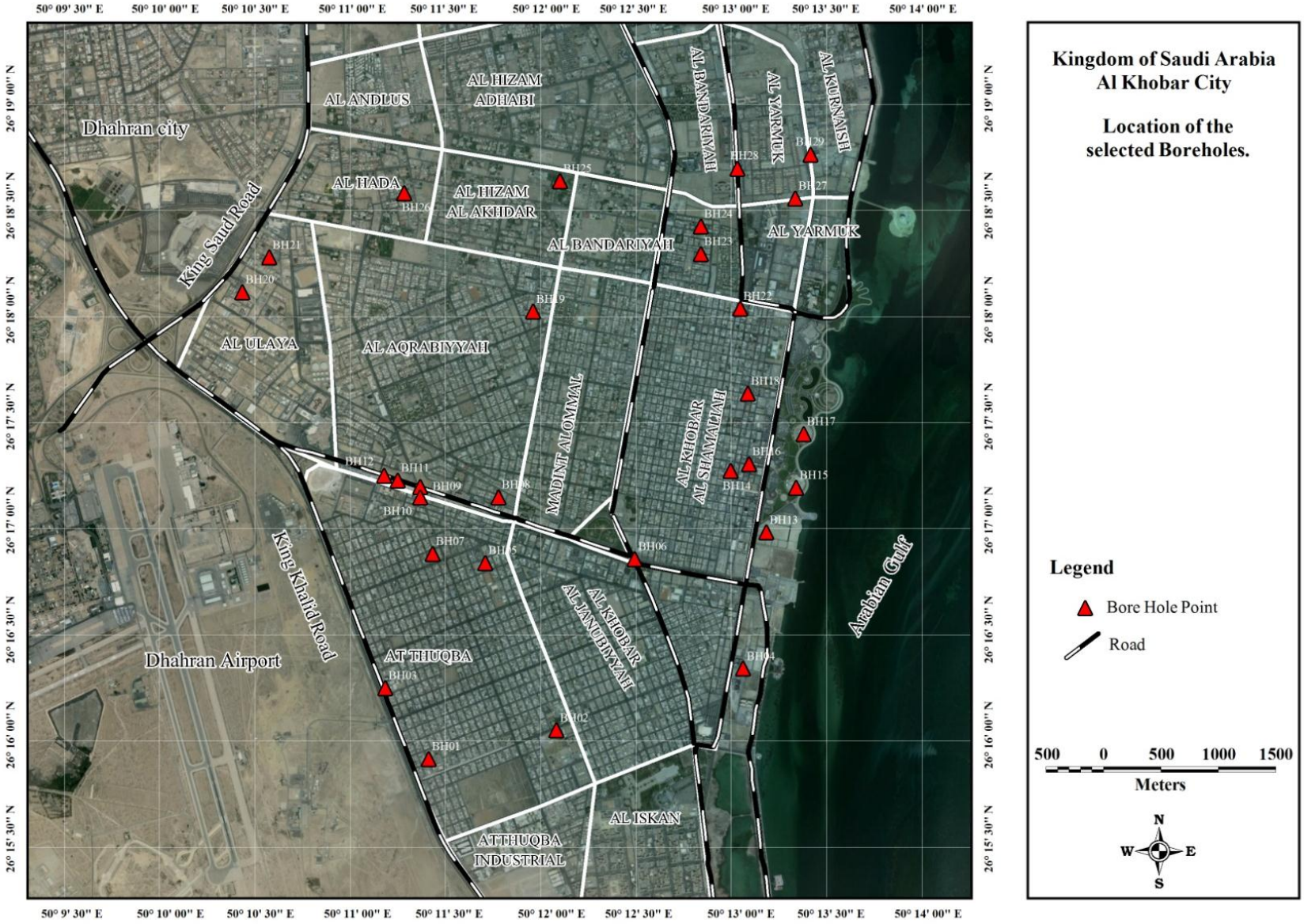

Figure 24: Location of Boreholes in Al-Khobar City.

Table 9: Parameters of the drilled boreholes in Al-Khober City.

Borehole	Name	Latitude	Longitude	depth*(m)*	W. L.*(m)*
BH01	Al-Mamoon Primary School	26° 15.921`	50° 11.411`	10.00	3.70
BH02	Jabber Bin Hayan School	26° 16.056`	50° 12.082`	10.00	No G.T
BH03	Al Tabri School	26° 16.255`	50° 11.184`	10.00	No G.T
BH04	Al Fahad Tower Bulding	26° 16.347`	50° 13.062`	20.00	02.40
BH05	Abdurrahman Bin Al Qasim School	26° 16.844`	50° 11.709`	10.00	07.00
BH06	King Abdullah /King Abdulaziz Interchange	26° 16.863`	50° 12.493`	20.00	03.65
BH07	King Abdullah /King Abdulaziz Interchange	26° 16.888`	50° 11.432`	20.00	03.70
BH08	Al Zajil for Realestate Investment Est.	26° 17.154`	50° 11.778`	09.00	No G.T
BH09	King Abdullah /Makkah Interchange	26° 17.202`	50° 11.367`	10.00	02.00
BH10	King Abdullah /Makkah Interchange	26° 17.154`	50° 11.367`	10.50	02.10
BH11	Water Front Project , Sport Hall	26° 17.234`	50° 11.249`	25.50	08.60
BH12	King Abdullah /Makkah Intersection	26° 17.255`	50° 11.177`	25.50	08.58
BH13	King Abdullah /Makkah Intersection	26° 16.989`	50° 13.183`	24.50	02.00
BH14	Al Oula Tower , Phase –B	26° 17.279`	50° 12.995`	15.27	00.48
BH15	Dar Ghassan Consultants	26° 17.199`	50° 13.340`	100.0	No G.T
BH16	Tamimi Safeway	26° 17.311`	50° 13.093`	21.00	00.30
BH17	Al Oula Tower , Phase –A	26 °17.452`	50° 13.379`	40.00	02.10
BH18	Al-Mana Tower (Hospital)	26° 17.643`	50° 13.087`	25.00	01.63
BH19	Jasim Al Gawahmed Engineering Office	26° 18.029`	50° 11.959`	07.50	04.80
BH20	Accuracy & Innovation Est	26° 18.121`	50° 10.433`	10.10	No G.T
BH21	Abdurrahman Al Dable Est	26° 18.284`	50° 10.575`	08.27	No G.T
BH22	Abdurrahman Al Siekh	26° 18.043`	50° 13.047`	30.50	01.85
BH23	Bulding Eyes General Cont. Est	26° 18.300`	50° 12.840`	08.45	01.70
BH24	Al-Nahdi Realestate Group	26° 18.430`	50° 12.839`	15.00	02.70
BH25	Abdullah A.M.Al-Khodari & Sons Co.	26° 18.644`	50° 12.100`	08.00	No G.T
BH26	Girls School	26° 18.587`	50° 11.282`	08.00	No G.T
BH27	Anmatt Al Amar Construction Co.Ltd	26° 18.562`	50° 13.334`	12.29	01.85
BH28	Mosa & Sultan Sons of AbdulAziz Al-Mosa	26° 18.702`	50° 13.031`	20.00	00.50
BH29	Al Sharq Architects & Design	26° 18.768`	50° 13.416	20.00	03.20

Where; G.W.L: the Ground Water Level (m)*;* SAFCO: Soil & Foundation Company

Table 10 : Geotechnical parameters for borehole No.29 in Al-Khobar City.

BH No	Depth		H	SPT
29	0		0.5	
	0.5	Brown, medium dense, poorly graded fine to medium	0.5	
	1	sillceous carbonate SAND with silt & seashells.	0.5	17
	1.5		0.5	
	2	Ditto,	0.5	27
	2.5		0.5	
	3	Ditto, gray	0.5	17
	3.5		0.5	
	4	Ditto, loose	0.5	10
	4.5		0.5	
	5	Ditto, light gray, medium dense	0.5	11
	5.5		0.5	
	6	Ditto,	0.5	13
	6.5		0.5	
	7		0.5	
	7.5	Light gray, medium dense poorly graded, fine	0.5	16
	8	to medium SAND with seashells	0.5	
	8.5		0.5	
	9	Ditto,	0.5	20
	9.5		0.5	
	10		0.5	
	10.5	Light gray, medium dense cermented silty	0.5	40
	11	SAND (gravel sizes)	0.5	
	11.5		0.5	
	12	Ditto, medium dense	0.5	15

	12.5	Light gray, medium dense, cemented silty Sand	0.5	
	13		0.5	
	13.5	Gray, medium dense, fine to medium silty SAND	0.5	20
	14		0.5	
	14.5		0.5	
	15	Ditto,	0.5	15
	15.5		0.5	
	16		0.5	
	16.5	Ditto,	0.5	18
	17		0.5	
	17.5		0.5	
	18	Brownish gray, dense, silty clayey SAND with	0.5	40
	18.5	cementation	0.5	
	19		0.5	
	19.5	Ditto, very dense	0.5	
	20	.	0.5	53

Figure (25): Location of boreholes in Dammam city.

DB1	Al Zahour school	26.4539	50.0913	6.45	3.50
DB2	Al Maarif Primary School	26.4162	50.0944	10	9.00
DB3	Yazeed Al-Shibani Primary School	26.4288	50.0880	10	
DB4	Girls School	26.4496	50.0988	10	1.10
DB5	School	26.4342	50.0971	10	3.30
DB6	38 Primary School girls.	26.4446	50.0726	8.5	1.20
DB7	Girls School	26.4448	50.1259	10	1.20
DB8	General Girls Education Management	26.4495	50.0969	10.5	4.50
DB9	Girls School	26.4309	50.0742	8	1.10
DB10	Zaid Bin Al Khattab Medium School	26.4104	50.0785	10	7.00
DB11	Intersection	26.4411	50.0650	25	0.60
DB12	Intersection	26.4251	50.1146	35	2.70
DB13	Civil Defense.	26.4301	50.1041	12	2.60

Where; G.W.L: the Ground Water Level (m), SAFCO: Soil & Foundation Company

Table 11: Parameters of the collected bore-hole data through Al-Dammam City.

Table 12 : Geotechnical parameters for borehole No.11 in Al-Dammam City.

Depth(m)	SPT	N60	(N1)60	Description	H
0.15				Backfill, consist of gravels, sand and silt.	0.85
1	7	5	10	light brown to gray, very loose to loose silty sand	1
2	5	4	7	light brown to gray, very loose to loose silty sand	1
3	6	5	8	light brown to gray, very loose to loose silty sand	1
4	7	5	10	light brown to gray, very loose to loose silty sand	1

5	11	8	15	light gray, medium dense silty sand and shells.	1
6	35	26	49	light brown, dense sand with silt and shells	1.5
7.5	38	29	53	light brown, dense sand with silt and shells	1.5
9	R			off white, hard elastic silt with sand (marl)	3
10.5	R			off white, hard elastic silt with sand (marl)	
12	R			brown, hard fat clay with sand	4.5
13.5	R			brown, hard fat clay with sand	
15	R			brown, hard fat clay with sand	
16.5	R			dark grey, hard sandy elastic silt.	
18	R			dark grey, hard sandy elastic silt.	
19.5	R			dark grey, hard sandy elastic silt.	
21	R			dark grey, hard sandy elastic silt.	
22.5	R			dark grey, hard sandy elastic silt.	
24	R			dark grey, hard sandy elastic silt.	
25				**end of boring**	

VI. DATA PROCESSING AND RESULTS

VI. 1 MICROTREMOR MEASUREMENTS

The collected data have been processed through **Geopsy_software** developed within the framework of the great European project SESAME. At each site, the field measurements sheet proposed by SESAME project (SESAME Guidelines, 2004) was filled in terms of time, date, operator name, coordinates, etc. All the necessary and

recommended information about the recorded signals were applied according to these guidelines.

VI. 1 .1 Criteria for Reliability of results

The SESAME project recommended several criteria for reliability of results as follows;

$$F_0 > 10/I_w$$

According to this condition, at the frequency of interest, there is at least 10 significant cycles in each window. Although not mandatory, but if the data allows, it is always fruitful to check whether a more stringent condition ($f_0 > 20 / I_w$) can be fulfilled, which allows at least ten significant cycles for frequencies half the peak frequency , and thus enhances reliability of the whole peak

$$N_c (f_0) > 200$$

According to this condition, a large number of windows are needed. The total number of significant cycles: $n_c = I_w.f_0$ is larger than 200 (which means, for instance, for a peak of 1 Hz, there are at least 20 windows of 10 seconds each; or, for a peak of 0.5 Hz, 10 windows of 40 seconds each). In case no window selection is considered all transients are taken into account.

$$\sigma A (f) < 2 \quad \text{for} \quad 0.5f0 < f < 2f_0 \quad \text{if} \quad f_0 > 0.5 \text{ Hz}$$

$$\text{or } \sigma A(f) < 3 \quad \text{for} \quad 0.5f_0 < f < 2f_0 \quad \text{if} \quad f_0 < 0.5 \text{ Hz}$$

This condition takes into account an acceptably low level of scattering between all windows.

VI. 1. 2 Criteria for clear H/V Peak

According to the SESAME Guidelines, at least five of the following criteria must be achieved for the clarity of H/V peaks.

$$\exists\, \boldsymbol{f}^{-} \quad \in \left[\frac{\boldsymbol{f}_0}{\boldsymbol{4}}, \boldsymbol{f}_0\right] | \boldsymbol{A}_{H/V}\ \left(\boldsymbol{f}^{-}\right) < A_0/\boldsymbol{2}$$

one frequency f^-, should be lying between $f_0/4$ and f_0, such as A_0 / AH/V (f^-) > 2

$$\exists\, \boldsymbol{f}^{+} \quad \in \left[\boldsymbol{f}_0, \boldsymbol{4f}_0\right] | \boldsymbol{A}_{H/V}\ \left(\boldsymbol{f}^{+}\right) < A_0/\boldsymbol{2}$$

Another frequency f^+, should be lying between f_0 and $4f_0$, such as $A_0/A_{H/V}$ (f^+) > 2

$$\mathbf{A_0 > 2}$$

$$f_{peak}\left[A_{H/V}(f) \pm \sigma_A(f)\right] = f_0 \pm 5\%$$

The peak should appears at the same frequency (within a percentage ± 5 %) on the H/V curves corresponding to mean + and – one standard deviation.

$$\sigma f < \varepsilon(f_0)$$

σ f should be lower than a frequency dependent threshold ε (f_0) , as in Table 13

$$\sigma A\ (f_0) < \theta(f_0)$$

$\sigma_A(f_0)$ should be lower than a frequency dependent threshold θ (f_0), as in Table 13

Table 13: Threshold values for σ_f and σ_A (f_0)

Frequency range (Hz)	**< 0.2**	**0.2 – 0.5**	**0.5 – 1.0**	**1.0- 2.0**	**> 2.0**
$\varepsilon(f_0)$ (Hz)	0.25 f_0	0.20 f_0	0.15 f_0	0.10 f_0	0.05 f_0
θ (f_0) for σ_A (f_0)	3.0	2.5	2.0	1.78	1.58
Log θ (f_0) for $\sigma_{logH/V}(f_0)$	0.48	0.40	0.30	0.25	0.20

Where;

I_w = window length

n_w = number of windows selected for the average H/V curve

n_c = $I_w.n_w.f_0$ is the number of significant cycles

f = current frequency

f_{sensor} = sensor cut-off frequency

f_0 = H/V peak frequency

σ_f = standard deviation of H/V peak frequency ($f_0 \pm \sigma_f$)

$\varepsilon (f_0)$ = threshold value for the stability condition $\sigma_f < \varepsilon (f_0)$

A_0 = H/V peak amplitude at frequency f_0

$A_{H/V} (f)$ = H/V curve amplitude at frequency f

f^- = frequency between $f_0/4$ and f_0 for which $A_{H/V}(f^-) < A_0/2$

f^+ = frequency between f_0 and $4f_0$ for which $A_{H/V}(f^+) < A_0/2$

σ_A (f) = "standard deviation" of $A_{H/V}$ (f) , σ_A (f) is the factor by which the mean $A_{H/V}$ (f) curve should be multiplied or devided

$\sigma_{logH/V}$ (f) = standard deviation of the log $A_{H/V}$ (f) curve, $\sigma_{logH/V}$ (f) is an absolute value which should be added to or subtracted from the mean log $A_{H/V}$(f) curve

θ (f_0) = threshold value for the stability condition σ_A (f) < $\theta(f_0)$

$V_{s,av}$ = average S-wave velocity of the total deposits

$V_{s,\ surf}$ = S-wave velocity of the surface layer

H = depth to bedrock

H_{min} = lower-bound estimate of h

VI. 1. 3 Microtremors Mesurements

At each site, the microtremors data file was divided into several time windows of 30 -50 sec for spectral calculations (Fig. 26). This time window is proven to be sufficiently long to provide stable results. The selected time windows were Fourier transformed using cosine tapering before transformation. The spectra were then smoothed with a Konno & Ohmachi algorithm (Konno and Ohmachi, 1998). After data smoothing the spectra of EW and NS channels at a site were

divided by the spectra of the vertical channel (Nakamura estimate) in order to obtain spectral ratios. The geometrical average of the two component ratios is the site amplification function. However, in most cases, due to the influence of sources like dense population, high traffic and industries activities the resonance frequency cannot be directly identified from microtremors spectra (Duval et al., 2004).

Figure (27) presents an average horizontal-to- vertical spectral ratio for point No. 72 (in Al-Khobar City). As shown, the dominant peak is near 3.9 Hz, while the observed amplification factor is about 3.6. The solid line represents the average value.

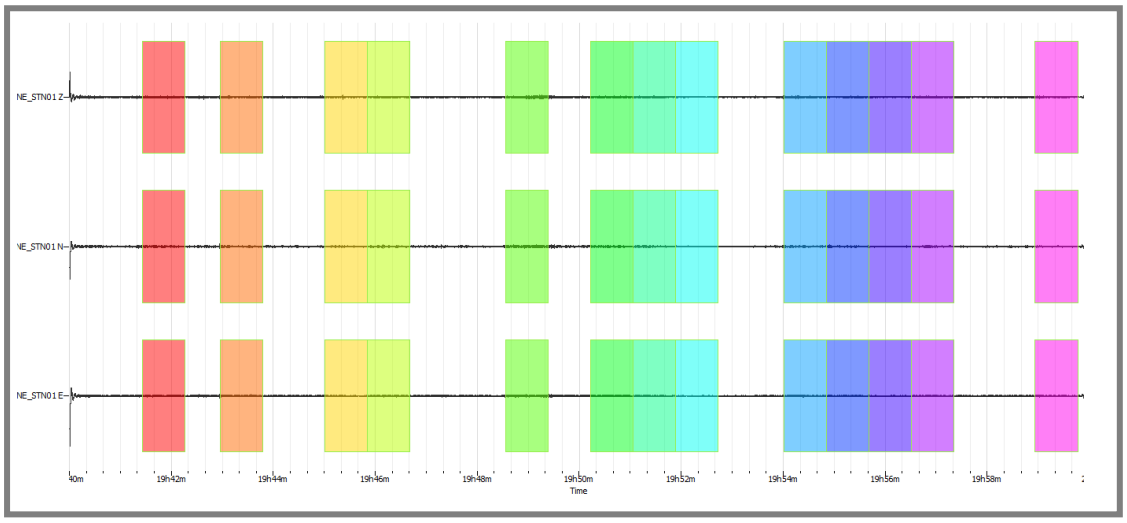

Figure 26: Colored- window noise for point No. 72 in Al-Khobar City.

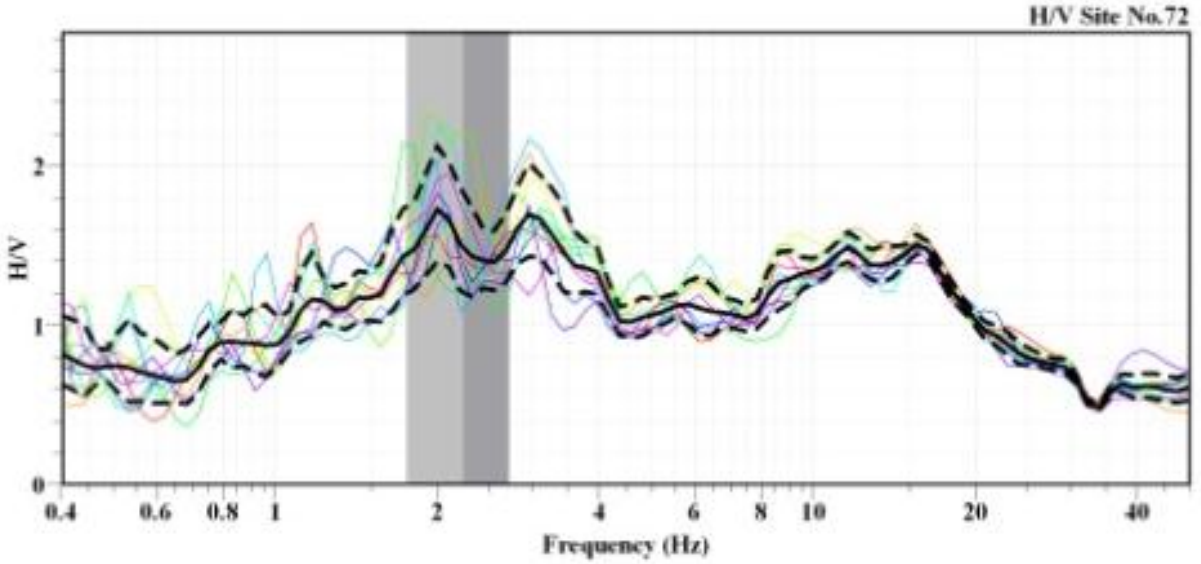

Figure 27: HVSR for the point No. 72 in Al-Khobar City.

VI. 1. 3 .1 Criteria for H/V industrial origin Peaks

It often occurs in urban environments where H/V curves exhibit local narrow peaks – or troughs. In most cases, such peaks or troughs are related to some kind of machinery (turbine, generators, etc…), are recognized by the following general characteristics:

- They may exist over a significant area, may be up to a distance of several kilometers from their source in the same localities.
- As the source is more or less "permanent" (at least within working hours), the original (non-smoothed) Fourier spectra should exhibit sharp narrow peaks at the same frequency for all the three components, as seen in Figure (28).

- Reprocessing with less and less smoothing: in the case of industrial origin, the H/V peak should become sharper and sharper, which is not the case for a site effect peak linked to soil characteristics.
- If other measurements have been performed in the same area, determine whether a peak exists at the same frequencies with comparable sharpness (the amplitude of the associated peak, even for fixed smoothing parameters, may vary significantly from site to site, being transformed sometimes into a trough).
- Another very effective check is to apply the random decrement technique (Dunand et al., 2002) to the ambient vibration recordings in order to derive the "impulse response" around the frequency of interest: if the corresponding damping (z) is very low (below 1%), an anthropogenic origin may be assumed almost certainly, and the frequency should not be considered for the interpretation purposes (Fig. 29).

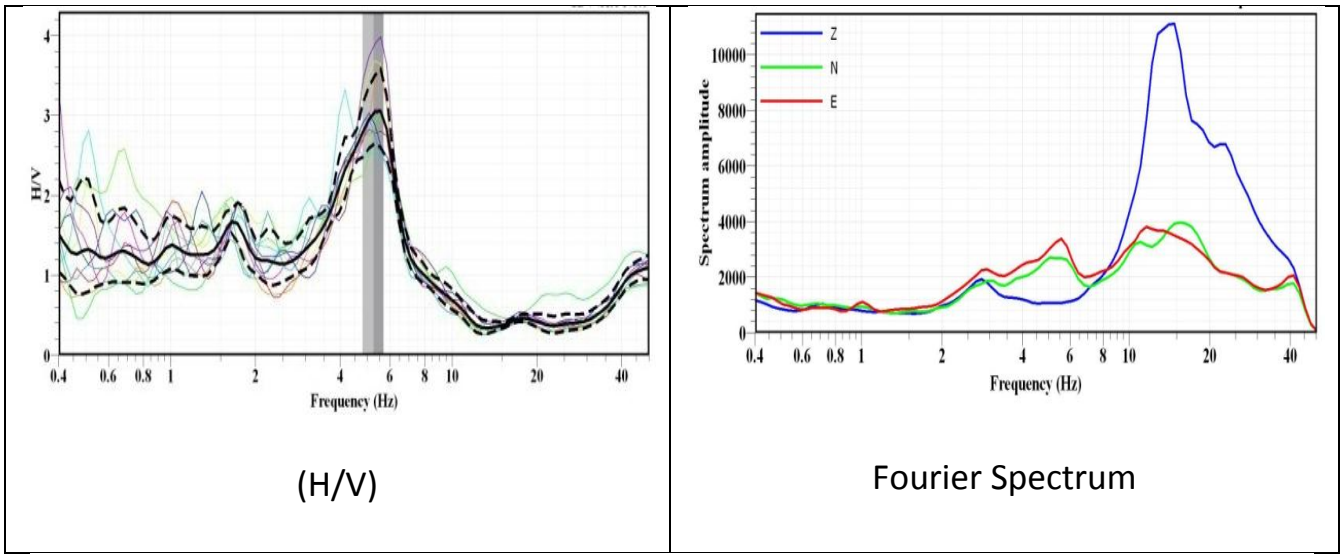

Figure 28: Detection of industrial origin peaks.

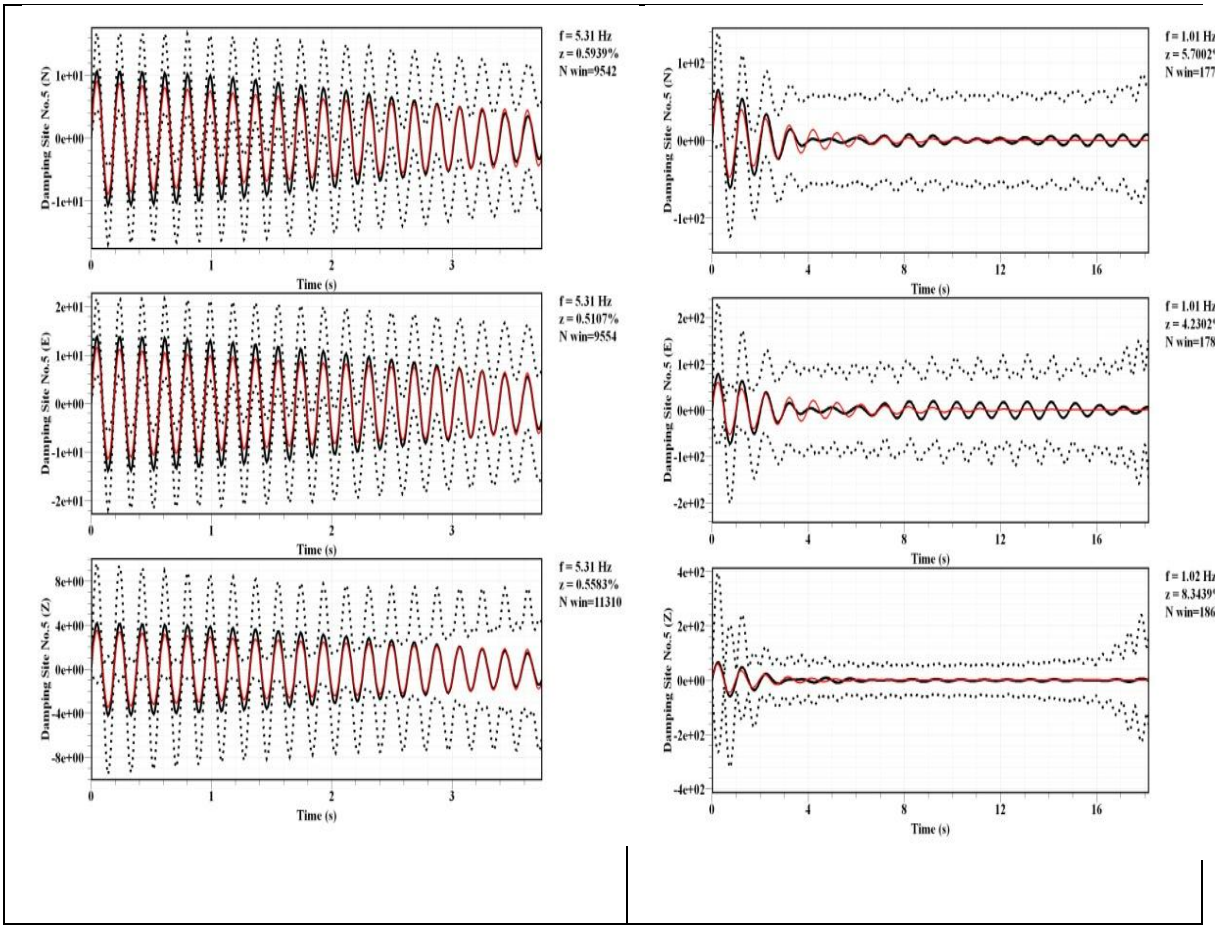

Figure 29: peaks for industrial and natural origin with damping test.

Fundamental frequencies and the corresponding amplifications from all measurement sites across Al-Khobar City are summarized in Table 14 and Figures 30 and 31 while Figure 32, represents the predominant periods through the city. The site response functions of the soil sites exhibit peaks at dominant frequencies between 0.3 to 7.8 Hz. The lower resonance frequencies (range from 0.3 to 3.9 Hz) are attained at sites in the northern part. On the other hand the higher resonance frequencies (range from 5.2- 7.8 Hz) are attained at sites in the southern part. As a

consequence, intermediate values of frequencies (3.9 – 5.2 Hz) are distributed in the central part of the city.

The map of maximum amplification (Fig. 32) reflects a variation in the impedance values between the bedrock and the overlying sediments. The highest amplifications (greater than 4) are attained at the northern areas with relatively thick sediments, while the lower amplification (range from 1-2.5) prevailed in the central areas of shallow bedrock. But the intermediate values of amplification (2.5 - 4) are encountered through the central part of the area. Accordingly, Al-Khobar City is divided into three zones, each characterized by a fundamental resonance frequency of the soil column as follows:

Zone 1: Characterized by a resonance frequency between 0.33 and 1.03 Hz.

Zone2: Characterized by a resonance frequency between 1.03 and 1.23 Hz.

Zone 3: Characterized by a resonance frequency between 1.23 and 1.73 Hz.

While these parameters (Table 15, Figs. 33, 34 and 35) has been noticed that parameters for site effects are remarkably robust in Al-Dammam City. Comparison of the two neighboring points reveals that differences in the location of the fundamental frequencies and amplification levels are small and the general shapes of two horizontal components are similar. These findings significantly increase the reliability of the obtained information and emphasize the importance of a densely laid observation points in microzoning studies. Accordingly, the study area is

divided into four zones, each characterized by a fundamental resonance frequency of the soil column as follows:

Zone 1: Characterized by a resonance frequency between 0.3 and 3.9 Hz.

Zone2: Characterized by a resonance frequency between 3.9 and 5.2 Hz.

Zone 3: Characterized by a resonance frequency between 5.2 and 6.5 Hz.

Zone 4: Characterized by a resonance frequency between 6.5 and 7.8 Hz.

Table 14: Results of Microtremor Measurements in Al-Khobar City.

Site Code	No. of samples	No. of windows (nw)	Window length (lw)	No. of cycles (nc)	H/V Peak amplitude (A0)	Standard Deviation σA(f)	Fundamental Frequency (F0)	Standard Deviation (σf)	Remarks
KH01	180000	10	30	8778	2.02	1.08	29.26	2.52	Industrial
	180000	10	30	369	1.53	0.37	1.23	0.08	Natural
KH02	180000	10	40	11828	1.87	1.08	29.57	1.33	Industrial
	180000	10	40	528	1.36	0.5	1.32	0.09	Natural
KH03	180000	10	40	6700	2.13	1.05	16.75	1.14	Industrial
	180000	10	40	620	1.31	0.33	1.55	0.07	Natural
KH04	180000	--	--	--	--	--	---	--	No Industrial
	180000	12	50	852	2.52	1.15	1.42	0.23	Natural
KH05	180000	10	30	1593	3.09	1.13	5.31	0.32	Industrial
	180000	10	30	498	1.64	0.21	1.66	0.08	Natural
KH06	180000	11	50	5500	3.64	1.06	10	0.43	Industrial
	180000	11	50	550	1.3	1.16	1	0.06	Natural
KH07	180000	10	50	3070	3.75	1.08	6.14	0.3	Industrial
	180000	10	50	505	1.2	1.19	1.01	0.07	Natural
KH08	180000	10	50	3740	3.13	1.1	7.48	0.29	Industrial
	180000	10	50	500	1.2	1.3	1	0.08	Natural
KH09	180000	10	50	2915	2.84	1.11	5.83	0.48	Industrial
	180000	10	50	435	1.5	1.14	0.87	0.09	Natural
KH10	180000	12	25	9675	4.23	1.14	32.25	1.04	Industrial
	180000	12	25	594	1.19	0.27	1.98	0.07	Natural
KH11	180000	10	25	3507.5	4.33	1.28	14.03	0.72	Industrial
	180000	10	25	432.5	1.11	1.35	1.73	0.09	Natural

KH12	120000	10	40	6200	1.55	1.03	15.5	0.79	Industrial
	120000	10	40	628	0.93	0.19	1.57	0.04	Natural
KH13	120000	10	30	9678	3.09	1.07	32.26	1.07	Industrial
	120000	10	30	465	0.88	0.18	1.55	0.11	Natural
KH14	120000	10	40	14932	2.87	1.1	37.33	2.66	Industrial
	120000	10	40	760	0.77	0.17	1.9	0.06	Natural
KH15	120000	11	40	14907.2	2.55	1.07	33.88	1.9	Industrial
	120000	11	40	545.6	0.84	0.1	1.24	0.51	Natural
KH16	120000	10	40	14924	3.4	1.14	37.31	1.46	Industrial
	120000	10	40	648	0.71	1.17	1.62	0.08	Natural
KH17	--	--	--	--	--	--	--	--	No Industrial
	120000	10	20	230	1.09	1.35	1.15	0.24	Natural
KH18	120000	10	40	7356	2.87	1.1	18.39	0.46	Industrial
	120000	10	40	480	2.05	1.5	1.2	0.04	Natural
KH19	120000	12	30	4377.6	3.08	1.07	12.16	1.36	Industrial
	120000	12	30	604.8	1.25	0.36	1.68	0.08	Natural
KH20	120000	10	25	1087.5	1.75	1.18	4.35	0.63	Industrial
	120000	10	25	177.5	1.81	1.45	0.71	0.11	Natural
KH21	120000	10	30	1443	3.19	1.07	4.81	0.45	Industrial
	120000	10	30	291	1.2	1.17	0.97	0.07	Natural
KH22	120000	10	40	2228	3.81	1.08	5.57	0.54	Industrial
	180000	10	40	380	1.2	1.19	0.95	0.1	Natural
KH23	180000	10	40	2220	2.96	1.1	5.55	0.4	Industrial
	180000	10	40	348	1.08	1.18	0.87	0.07	Natural
KH24	150000	10	30	1593	1.72	1.18	5.31	0.53	Industrial
	150000	10	30	273	1.34	1.28	0.91	0.07	Natural
KH25	120000	10	40	2988	1.35	1.1	7.47	0.79	Industrial
	120000	10	40	304	1.35	1.14	0.76	0.09	Natural
KH26	120000	10	30	4656	3.40	1.07	15.52	0.83	Industrial
	120000	10	30	480	1.14	0.43	1.60	0.08	Natural
KH27	089583	10	30	6072	4.44	1.07	20.24	0.34	Industrial
	089583	11	25	440	1.01	0.24	1.60	0.09	Natural
KH28	180000	15	30	11884.5	1.43	0.37	26.41	2.72	Industrial
	180000	15	30	684	1.01	0.31	1.52	0.09	Natural
KH29	180000	10	30	14232	1.69	0.40	47.44	2.53	No Industrial
	180000	10	30	477	0.89	0.14	1.59	0.08	Natural
KH30	--	--	--	--	--	--	--	--	No Industrial
	180000	10	50	585	0.94	1.4	1.17	0.18	Natural
KH31	--	--	--	--	--	--	--	--	No Industrial
	180000	10	50	480	1.26	1.23	0.96	0.19	Natural
KH32	--	--	--	--	--	--	--	--	No Industrial
	120000	10	50	480	0.92	1.23	0.96	0.15	Natural
KH33	120000	10	40	12084	1.84	1.1	30.21	2.13	Industrial
	120000	10	40	404	1.05	1.21	1.01	0.06	Natural

KH34	120000	10	30	6246	3.39	1.07	20.82	0.74	Industrial
	120000	10	30	273	1.7	1.54	0.91	0.08	Natural
KH35	180000	10	40	7176	3.85	1.09	17.94	0.41	Industrial
	180000	10	40	320	0.95	1.24	0.8	0.1	Natural
KH36	120000	10	30	1758	2.05	1.1	5.86	1.02	Industrial
	120000	10	30	273	1.3	1.37	0.91	0.08	Natural
KH37	120000	10	18	473.4	3.31	1.22	2.63	0.14	Industrial
	120000	10	18	160.2	2.14	1.82	0.89	0.07	Natural
KH38	120000	13	50	2977	4.29	1.12	4.58	0.6	Industrial
	120000	13	50	591.5	1.21	1.26	0.91	0.04	Natural
KH39	120000	10	50	322.5	4.31	1.07	6.45	0.2	Industrial
	120000	10	50	785	1.18	1.22	1.57	0.09	Natural
KH40	--	--	--	--	--	--	--	--	No Industrial
	120000	10	25	75	1.63	0.86	0.30	0.03	Natural
KH41	120000	10	40	1748	2.82	1.15	4.37	0.55	No Industrial
	120000	18	50	198	2.96	1.76	0.22	0.02	Natural
KH42	120000	10	40	8656	4.17	0.64	21.64	6.91	Industrial
	120000	10	40	108	1.06	0.69	0.27	0.03	Natural
KH43	120000	10	50	1980	3.95	1.11	3.96	0.4	Industrial
	120000	12	50	192	3.54	1.29	0.32	0.05	Natural
KH44	120000	10	50	12650	2.97	1.09	25.3	0.60	Industrial
	120000	10	50	505	1.25	1.26	1.01	0.06	Natural
KH45	120000	13	50	18973.5	2.16	1.08	29.19	0.75	Industrial
KH46	180000	10	50	23790	11.6	1.11	47.58	1.98	Industrial
	180000	10	50	525	2.97	1.55	1.05	0.10	Natural
KH47	--	--	--	--	--	--	--	--	No Industrial
	120000	10	50	490	1.46	1.16	0.98	0.17	Natural
KH48	--	--	--	--	--	--	--	--	Industrial
	120000	10	50	200	4.76	1.30	0.40	0.05	Natural
KH49	120000	10	50	2405	2.27	1.1	4.81	0.34	Industrial
	120000	10	50	500	2.02	1.21	1.00	0.05	Natural
KH50	--	--	--	--	--	--	--	--	No Industrial
	180000	10	50	790	3.24	1.19	1.58	0.25	Natural
KH51	180000	10	50	19975	3.07	1.04	39.95	0.96	Industrial
	180000	10	50	500	2.11	1.15	1	0.05	Natural
KH52	180000	10	50	500	1.49	1.21	1	0.14	Natural
KH53	180000	13	50	8060	3.59	1.05	12.4	0.51	Industrial
	180000	13	50	650	1.53	1.2	1	0.07	Natural
KH54									
	180000	10	50	505	0.8	1.21	1.01	0.23	Natural
KH55	180000	11	30	6854.1	4.02	1.11	20.77	1.2	Natural
	180000	10	30	489	1.08	1.35	1.63	0.09	Industrial
KH56	120000	10	30	1515	2.98	1.09	5.05	0.46	Natural
	120000	10	30	303	1.00	1.16	1.01	0.09	Industrial

KH57	120000	10	25	1090	2.11	1.24	4.36	0.84	Industrial
	120000	10	25	240	1.00	1.23	0.96	0.06	Natural
KH58	120000	10	40	1436	3.8	1.11	3.59	0.24	Industrial
	120000	10	40	332	1.05	1.23	0.83	0.1	Natural
KH59	180000	10	50	1885	4.00	1.10	3.77	0.17	Industrial
	180000	10	50	425	0.92	1.19	0.85	0.07	Natural
KH60	120000	10	40	1372	3.98	1.11	3.43	0.30	Industrial
	120000	10	40	400	1.42	1.21	1.00	0.07	Natural
KH61	120000	10	25	3550	2.06	1.11	13.4	0.5	Industrial
	120000	10	25	252.5	1.42	1.32	1.01	0.05	Natural
KH62	150000	10	40	1660	2.66	1.13	4.15	0.61	Industrial
	150000	10	40	248	0.98	1.5	0.62	0.09	Natural
KH63	120000	10	40	2988	2.84	1.07	7.47	0.63	Industrial
	120000	10	40	400	1.00	1.23	1	0.05	Natural
KH64	180000	10	50	8145	3.51	1.06	16.29	1.12	Industrial
	180000	10	50	500	0.86	1.13	1	0.05	Natural
KH65	120000	10	40	6860	3.82	1.05	17.15	0.32	Industrial
	120000	10	40	400	1.03	1.21	1.00	0.07	Natural
KH66	180000	10	50	6690	1.95	1.05	13.38	0.78	Industrial
	180000	10	50	910	0.88	1.28	1.82	0.09	Natural
KH67	180000	10	25	11382.5	2.71	1.20	45.53	1.93	Industrial
	120000	10	25	227.5	0.88	1.33	0.91	0.05	Natural
KH68	120000	10	50	17755	1.73	1.1	35.51	1.18	Industrial
	120000	10	50	955	1.26	1.21	1.91	0.07	Natural
KH69	--	--	--	--	--	--	--	--	No Industrial
	120000	10	50	1005	2.05	1.17	2.01	0.32	Natural
KH70	180000	10	50	12800	2.58	1.12	25.6	3.82	Industrial
	180000	10	50	530	1.17	1.13	1.06	0.08	Natural
KH71	120000	10	50	2290	1.57	1.12	4.58	0.06	Industrial
	120000	10	50	505	1.32	1.16	1.01	0.06	Natural
KH72	--	--	--	--	--	--	--	--	No Industrial
	120000	10	50	1000	1.72	1.23	2	0.48	Natural
KH73	--	--	--	--	--	--	--	--	No Industrial
	120000	10	50	1455	1.87	1.13	2.91	0.28	Natural
KH74	180000	10	50	20550	1.36	1.16	41.1	1.27	Industrial
	180000	10	50	710	1.17	1.18	1.42	0.07	Natural
KH75	120000	10	50	22890	1.57	1.08	45.78	0.92	Industrial
	120000	10	50	820	0.97	1.12	1.64	0.07	Natural
	120000	10	50	855	0.85	1.14	1.71	0.09	Natural
KH91	120000	10	50	13250	1.78	1.07	26.5	1.34	Industrial
	120000	10	50	825	1.1	1.2	1.65	0.06	Natural
KH92	120000	10	50	21600	1.37	1.06	43.2	2.25	Industrial
	120000	10	50	580	0.91	1.17	1.16	0.09	Natural
KH93	120000	10	50	16130	1.94	1.05	32.26	0.74	Industrial

	120000	10	50	610	1.53	1.21	1.22	0.05	Natural
KH94	120000	10	50	19585	1.67	1.04	39.17	0.96	Industrial
	120000	10	50	860	1.06	1.2	1.72	0.09	Natural
KH95	120000	10	50	14620	1.43	1.03	29.24	4.49	Industrial
	120000	10	50	505	1.11	1.11	1.01	0.09	Natural
KH96	180000	10	50	21625	2.23	1.06	43.25	2.13	Industrial
	180000	10	50	505	1.21	1.19	1.01	0.05	Natural
KH97	120000	10	50	8140	2.37	1.04	16.28	1.54	Industrial
	120000	10	50	405	1.08	1.23	0.81	0.09	Natural
KH98	120000	10	50	8555	4.55	1.06	17.11	0.36	Industrial
	120000	10	50	400	0.87	1.21	0.8	0.07	Natural
KH99	120000	10	20	2984	3.78	1.27	14.92	0.92	Industrial
	120000	10	20	180	1.28	1.44	0.9	0.1	Natural
KH100	120000	10	50	4650	2.46	1.09	9.30	0.61	Industrial
	120000	15	50	195	1.73	1.11	0.26	0.05	Natural
KH101	120000	10	50	2290	2.65	1.09	4.58	0.09	Industrial
	120000	19	50	370.5	1.20	0.68	0.39	0.04	Natural
KH102	120000	10	30	2460	2.28	1.05	8.20	0.31	Industrial
	120000	16	30	115.2	2.03	2.68	0.24	0.02	Natural
KH103	--	--	--	--	--	--	--	--	No Industrial
	180000	14	50	154	1.96	2.10	0.22	0.02	Natural
KH104	180000	10	30	1026	3.48	1.19	3.42	0.31	Industrial
	180000	10	30	69	2.01	2.08	0.23	0.02	Natural
KH105	120000	10	50	1375	3.68	1.12	2.75	0.43	Industrial
	120000	13	50	279.5	1.06	0.48	0.43	0.06	Natural
KH106	--	--	--	--	--	--	--	--	No Industrial
	120000	11	50	275	1.51	0.41	0.50	0.04	Natural
KH107	--	--	--	--	--	--	--	--	No Industrial
	120000	10	40	144	2.53	1.59	0.36	0.07	Natural
KH108	--	--	--	--	--	--	--	--	No Industrial
	120000	16	50	264	2.35	1.33	0.33	0.07	Natural
KH109	120000	10	40	4656	2.97	1.05	11.64	0.71	Industrial
	120000	10	40	172	2.46	1.35	0.43	0.04	Natural
KH110	120000	10	15	1659	1.86	1.14	11.06	0.54	Industrial
	120000	10	15	148.5	1.13	1.69	0.99	0.08	Natural
KH111	120000	10	50	7330	4.91	1.06	14.66	0.26	Industrial
	120000	10	50	835	0.85	0.21	1.67	0.05	Natural
KH112	120000	10	40	18308	4.02	1.12	45.77	3.76	Industrial
	120000	10	40	292	1.26	1.28	0.98	0.07	Natural
KH113	120000	10	50	5510	3.68	1.05	11.02	0.25	Industrial
	120000	10	50	505	1.49	1.22	1.01	0.03	Natural

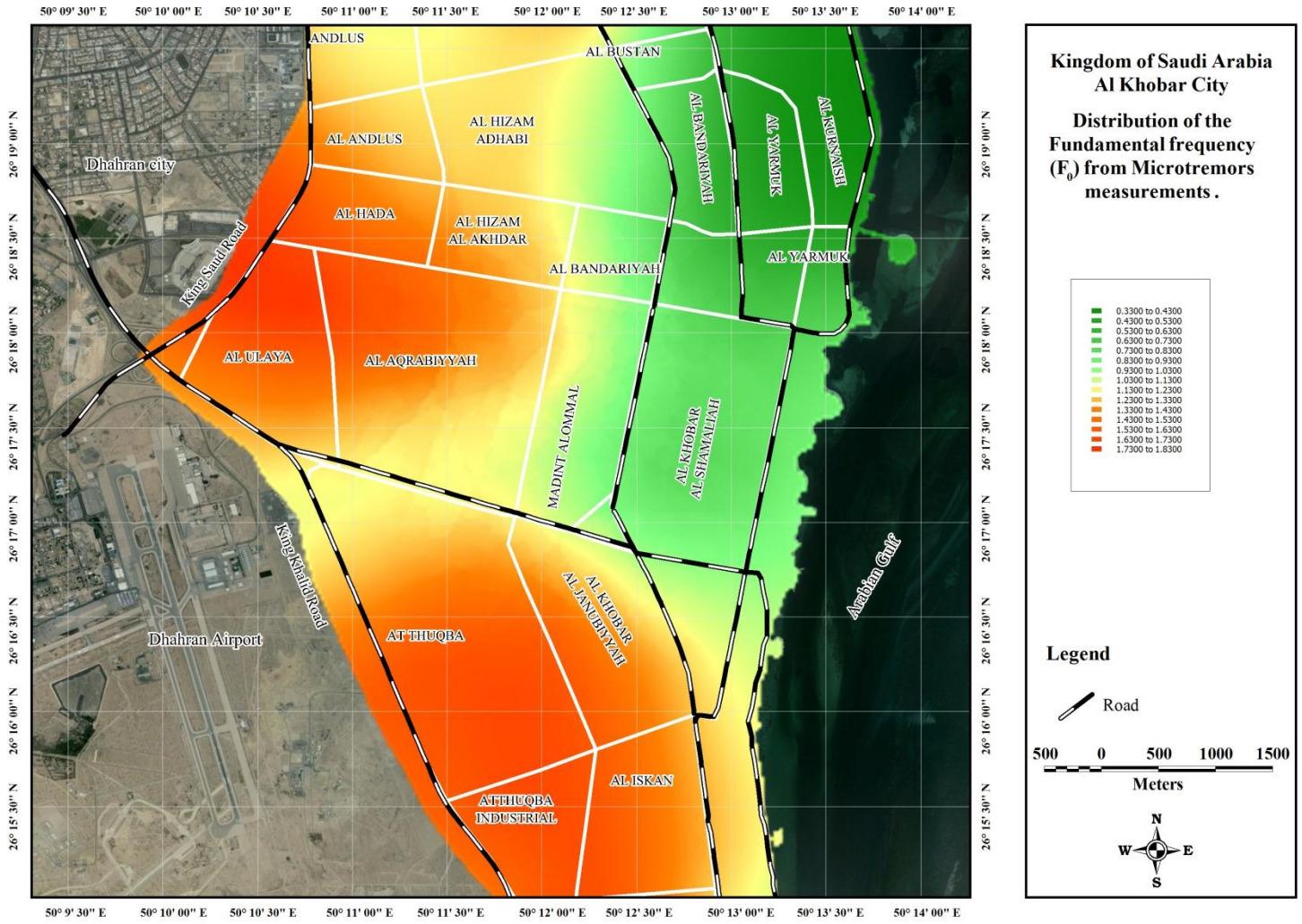

Figure 30: Distribution of the fundamental frequencies (F_0) through Al-Khobar City.

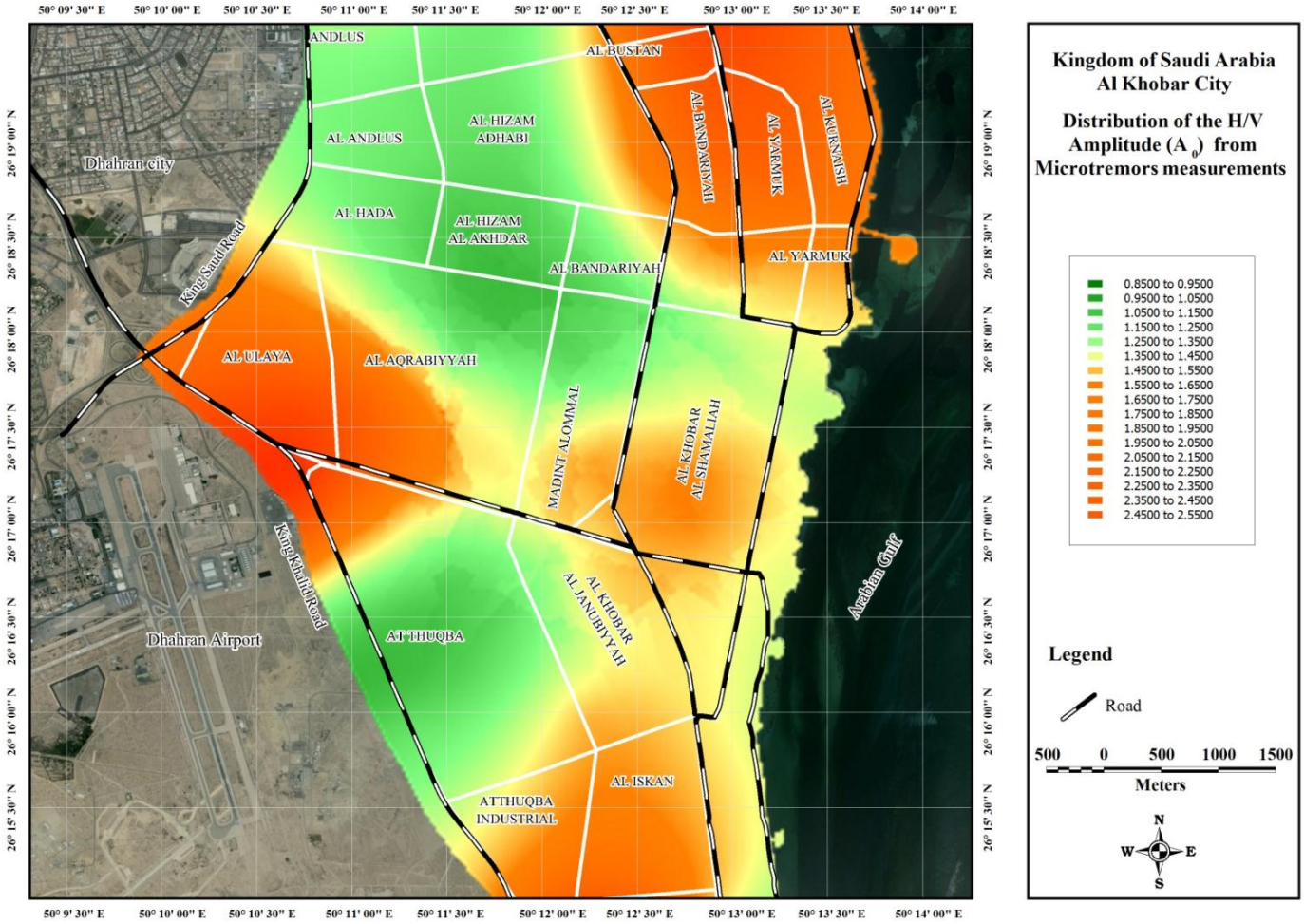

Figure 31: Distribution of H/V Amplitude (A_0) through Al-Khobar City.

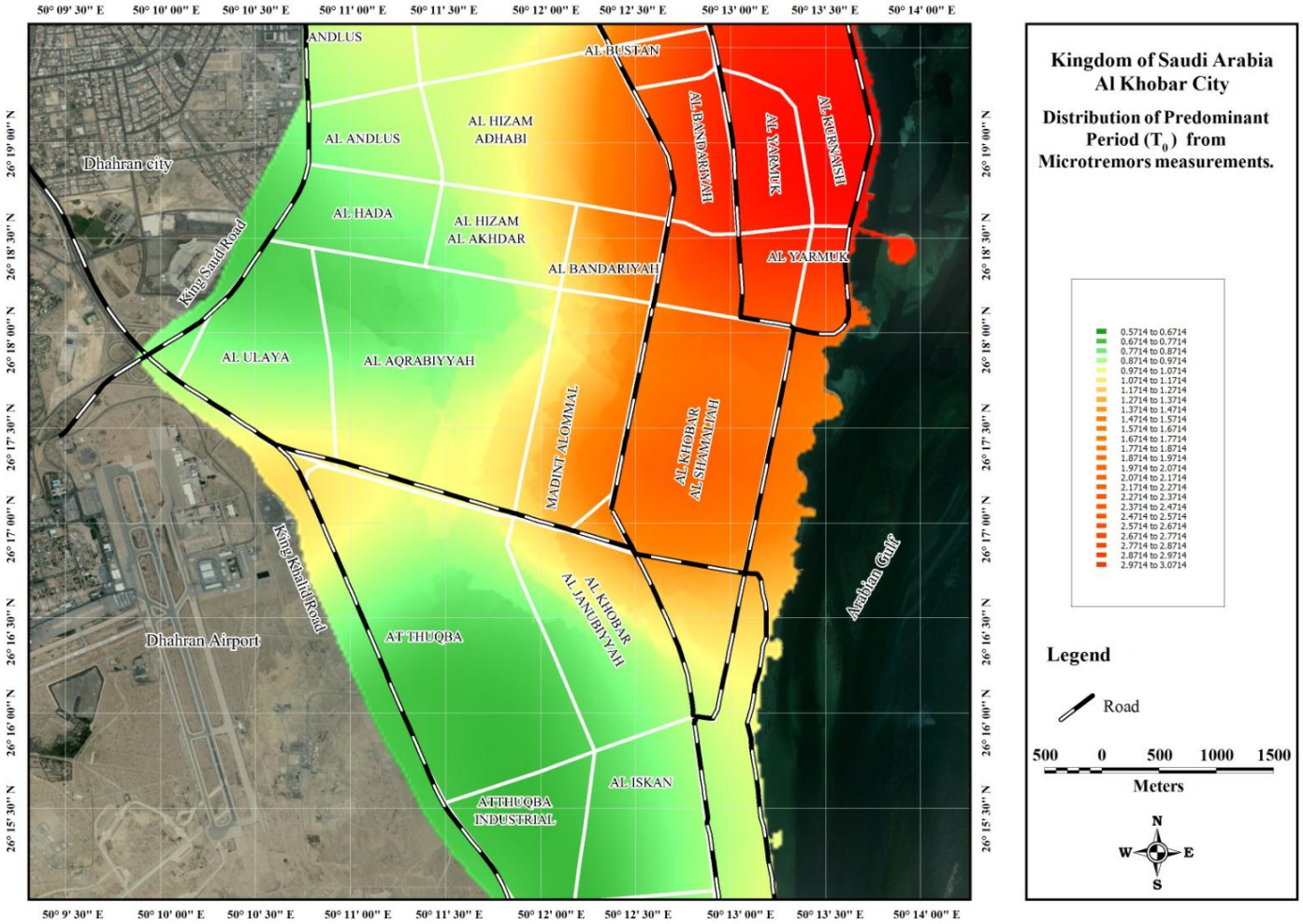

Figure 32: Distribution of the fundamental period (T_0) through Al-Khobar City.

Table 15: Results of Microtremor Measurements through Al-Dammam City.

Site Code	No. of samples	No. of windows (n_w)	Window length (I_w)	No. of cycles (n_c)	H/V Peak amplitude (A_0)	Standard Deviation $\sigma_A(f)$	Fundamental Frequency (F_0)	Standard Deviation (σ_f)	Remarks
DM1	177184	25	50	375	3.3	1.8	0.3	0.02	Natural
DM2	150000	16	50	2480	2.21	1.18	3.1	0.53	Natural
DM3	120000	12	50	3492	2.53	1.1	5.82	0.35	Natural
DM4	210000	10	50	1535	1.92	1.15	3.07	0.59	Natural
DM5	180000	11	50	2002	2.17	1.1	3.64	0.88	Natural
DM6	156000	19	50	4332	2.7	1.17	4.56	0.43	Natural
DM7	156000	14	50	4200	2.4	1.16	6	0.46	Natural
DM8	191613	12	50	13260	2.3	1.13	22.1	1.48	Industrial
	191613	12	50	618	1.48	1.35	1.03	0.07	Natural
DM9	150000	16	50	2480	2.22	1.19	3.10	0.53	Natural
DM10	258000	43	50	16770	2.66	1.12	7.8	0.35	Natural
DM11	120000	10	15	567	1.95	1.48	3.78	0.49	Natural
DM12	210000	18	50	15381	2.3	1.1	17.09	0.89	Industrial
	210000	18	50	3600	1.77	1.13	4	0.58	Natural
DM13	180000	15	50	2850	2.44	1.14	3.8	0.30	Natural
DM14	150000	12	45	2457	3.15	1.13	4.55	0.52	Natural
DM15	203212	10	35	1890	2.99	1.25	5.4	0.94	Natural
DM16	150000	18	50	3600	2.53	1.16	4	0.71	Natural
DM17	180000	12	50	3168	3.39	1.14	5.28	0.25	Natural
DM18	180000	10	50	670	1.79	1.19	1.34	0.17	Natural
DM19	180000	10	30	84	5.9	1.36	0.28	0.04	Natural
DM20	180000	10	35	105	2.0	1.7	0.3	0.06	Natural
DM21	180000	16	50	3984	3.67	1.1	4.98	0.42	Natural
DM22	186000	10	40	120	2.3	1.5	0.3	0.03	Natural
DM23	180000	10	50	135	1.8	1.4	0.27	0.02	Natural
DM24	162000	10	40	120	3.9	2.3	0.3	0.03	Natural
DM25	120000	10	25	1250	3.29	1.18	5.0	0.69	Natural
DM26	120000	10	50	2535	3.14	1.12	5.07	0.51	Natural
DM27	120000	13	50	1931	2.43	1.12	2.97	0.37	Natural
DM28	162000	10	50	2470	3.64	1.1	4.94	0.39	Natural
DM29	120000	10	50	1315	2.45	1.17	2.63	0.37	Natural
DM30	132000	10	45	126	5.5	1.5	0.28	0.03	Natural
DM31	120000	10	45	3492	3.1	1.25	7.76	0.73	Natural
DM32	120000	10	50	3305	3.32	1.2	6.61	0.63	Natural
DM33	138000	14	50	3626	2.79	1.15	5.18	0.31	Natural
DM34	120000	10	25	1430	2.86	1.16	5.72	0.51	Natural
DM35	120000	10	40	2060	1.9	1.1	5.15	0.82	Natural
DM36	120000	12	50	9168	2.21	1.08	15.28	0.98	Industrial
	120000	12	50	1020	1.25	1.13	1.7	0.087	Natural

DM37	120000	10	35	1337	1.07	1.09	3.82	0.09	Natural
DM38	120000	10	50	1315	2.55	1.17	2.63	0.61	Natural
DM39	120000	10	45	1373	2.61	1.27	3.05	0.34	Natural
DM40	120000	10	50	1710	2.76	1.09	3.42	0.19	Natural
DM41	126000	14	50	2401	2.29	1.2	3.43	0.43	Natural
DM42	132000	10	35	1225	1.68	1.13	3.5	0.14	Natural
DM43	120000	15	50	2633	1.71	1.17	3.51	0.28	Natural
DM44	174840	20	50	5030	2.63	1.09	5.03	0.43	Natural
DM45	180000	16	50	2232	2.15	1.1	2.79	0.24	Natural
DM46	180000	10	50	2000	1.46	1.11	4	0.1	Natural
DM47	180000	10	50	1960	1.56	1.13	3.92	0.09	Natural
DM48	150000	15	50	2528	2.85	1.12	3.37	0.28	Natural
DM49	126124	10	50	1950	2.69	1.11	3.9	0.51	Natural
DM50	150000	15	50	2978	2.8	1.16	3.97	0.35	Natural
DM51	144000	15	50	2783	2.42	1.17	3.71	0.42	Natural
DM52	138000	10	50	2155	2.45	1.18	4.31	0.39	Natural
DM53	117655	10	40	1780	2.92	1.08	4.45	0.55	Natural
DM54	120000	10	50	500	1.29	1.2	1	0.11	Natural
DM55	150000	10	50	825	3.05	1.2	1.65	0.038	Natural
DM56	138000	10	40	620	1.25	1.4	1.55	0.096	Natural
DM57	120000	10	50	165	4.2	1.2	0.33	0.05	Natural
DM58	150000	10	50	800	1.33	1.15	1.6	0.03	Natural
DM59	120000	10	50	3850	4.19	1.11	7.7	0.55	Natural
DM60	150000	10	50	2570	2.94	1.15	5.14	0.55	Natural
DM61	150000	13	50	3471	2.54	1.14	5.34	0.47	Natural
DM62	150000	14	50	3990	3.18	1.14	5.7	0.14	Natural
DM63	120000	10	35	1782	1.39	1.14	5.09	0.1	Natural
DM64	126000	20	50	5260	2.36	1.09	5.26	0.76	Natural
DM65	120000	19	50	4950	0.92	1.08	5.21	0.13	Natural
DM66	120000	10	30	1200	1.5	1.32	4	0.1	Natural
DM67	120000	10	50	2930	2.88	1.07	5.86	1.17	Natural
DM68	119130	16	50	4000	1.9	1.1	5	0.87	Natural
DM69	120000	15	50	2828	3.66	1.1	3.77	0.17	Natural
DM70	120000	13	50	2555	3.6	1.12	3.9	0.23	Natural
DM71	120000	10	50	2260	2.99	1.13	4.52	0.72	Natural
DM72	120000	13	50	3328	2.46	1.13	5.12	0.49	Natural
DM73	120000	14	50	3794	2.14	1.11	5.42	0.61	Natural
DM74	120000	14	50	3325	1.45	1.09	4.75	0.83	Natural
DM75	119305	18	50	4437	2.29	1.11	4.93	0.54	Natural
DM76	120000	15	50	3675	1.22	1.13	4.9	0.12	Natural
DM77	120000	16	50	3728	2.4	1.12	4.66	0.75	Natural
DM78	117957	13	50	3465	2.42	1.1	5.33	0.33	Natural
DM79	120000	11	35	1964	2.1	1.19	5.1	0.68	Natural
DM80	120000	13	50	2529	2.12	1.11	3.89	0.27	Natural

DM81	120000	10	45	1665	2	1.13	3.7	0.51	Natural
DM82	132000	15	50	3795	2.32	1.11	5.06	0.16	Natural
DM83	138000	10	45	1395	1.77	1.16	3.1	0.37	Natural
DM84	132000	10	50	140	3.76	1.58	0.28	0.03	Natural
DM85	120000	10	30	1515	2.52	1.15	5.05	0.89	Natural
DM86	120000	10	50	1330	3.15	1.22	2.66	0.34	Natural
DM87	120000	10	50	1580	3.33	1.18	3.16	0.5	Natural
DM88	120000	14	50	3150	3.23	1.09	4.50	0.53	Natural
DM89	120000	13	50	3341	3.56	1.1	5.14	0.49	Natural
DM90	120000	14	50	2954	3.89	1.09	4.22	0.61	Natural
DM91	150000	10	25	1448	2.22	1.17	5.79	0.66	Natural
DM92	120000	10	50	6340	2.08	1.07	12.68	1.1	Industrial
	120000	10	50	2000	1.4	1.13	4	0.1	Natural
DM93	144000	10	50	1860	3.08	1.09	3.72	0.22	Natural
DM94	180000	10	50	1910	1.63	1.16	3.82	0.54	Natural
DM95	117105	12	50	2220	1.52	1.11	3.7	0.49	Natural
DM96	115629	10	35	1341	2.8	1.15	3.83	0.24	Natural
DM97	115535	10	40	1496	1.89	1.14	3.74	0.35	Natural
DM98	120000	11	35	1448	2.27	1.19	3.76	0.25	Natural
DM99	120000	10	50	6635	2.3	1.06	13.27	0.27	Industrial
	120000	10	50	2815	1.52	1.13	5.63	0.12	Natural
DM100	120000	16	50	3040	1.81	1.12	3.8	0.44	Natural
DM101	116668	13	50	4219	2.85	1.07	6.49	0.68	Natural
DM102	30000	10	20	1158	3.03	1.4	5.79	0.72	Natural
DM103	30000	10	15	2762	1.9	1.07	18.41	1.14	Industrial
	30000	10	15	483	1.33	1.2	3.22	0.08	Natural
DM104	30000	11	15	774	1.96	1.29	4.69	0.79	Natural
DM105	26759	10	15	533	2.85	1.19	3.55	0.45	Natural
DM106	26475	10	15	552	2.72	1.17	3.68	0.43	Natural
DM107	36000	10	20	400	1.4	1.14	2	0.27	Natural
DM108	30000	10	15	804	1.98	1.3	5.36	0.58	Natural
DM109	30000	11	10	513	1.77	1.29	4.66	0.73	Natural
DM110	30000	10	10	306	1.79	1.42	3.06	0.58	Natural
DM111	96000	10	50	2035	2.7	1.11	4.07	0.5	Natural
DM112	90000	10	50	2010	2.34	1.15	4.02	0.49	Natural

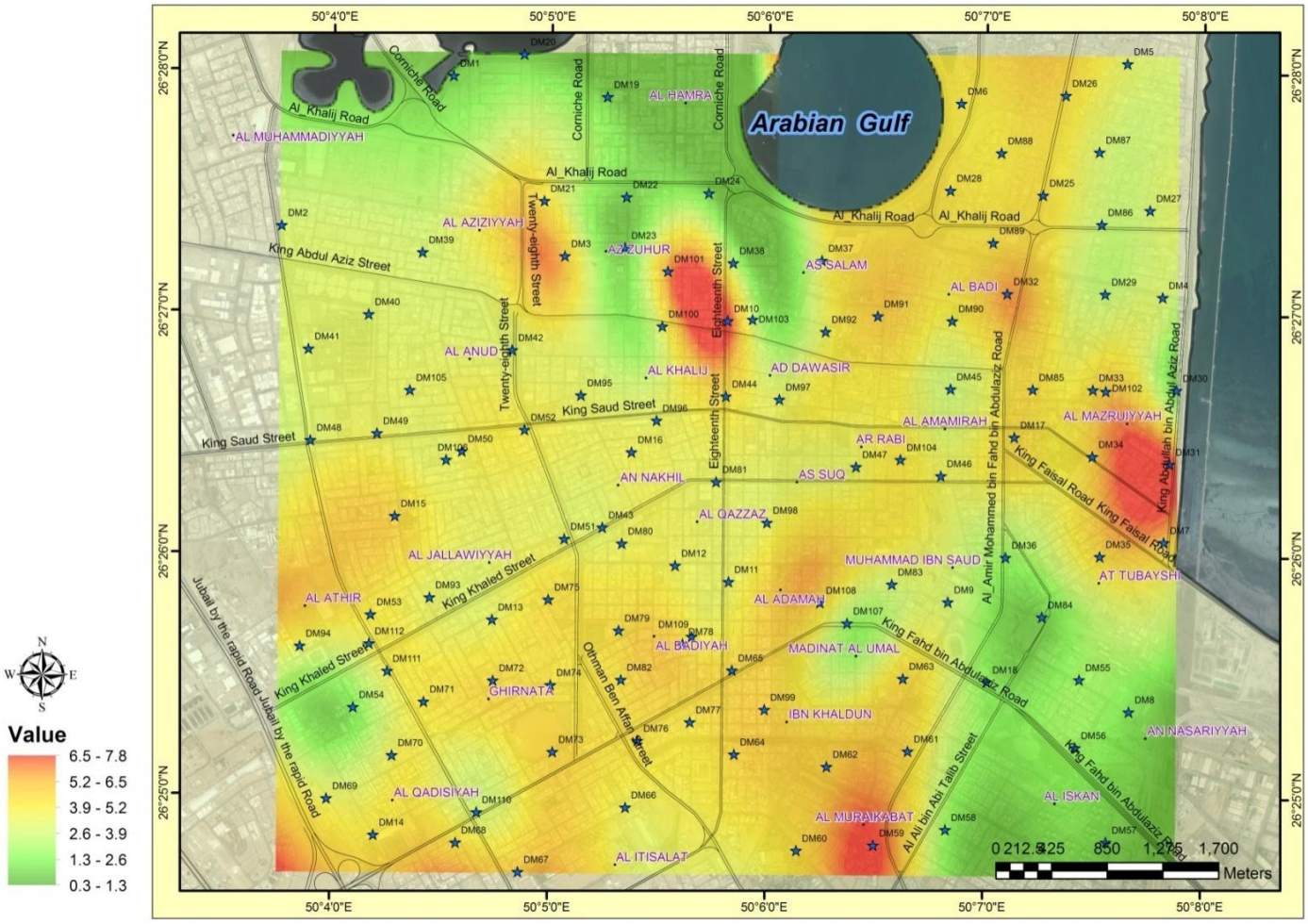

Figure 33: Distribution of fundamental resonance frequency (F_0) in Al-Dammam City.

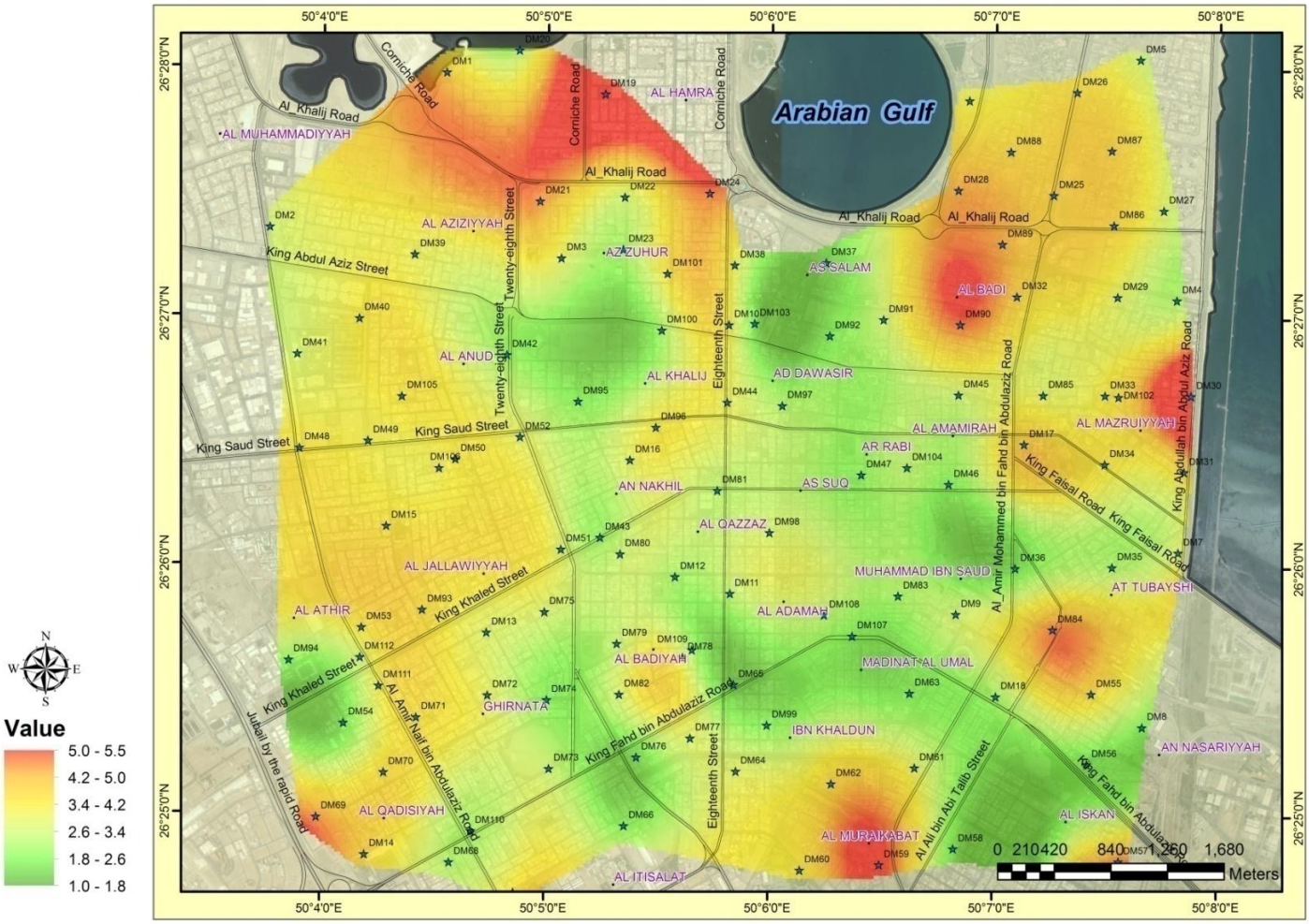

Figure 34: Distribution of H/V Amplitude (A_0) through Al-Dammam City.

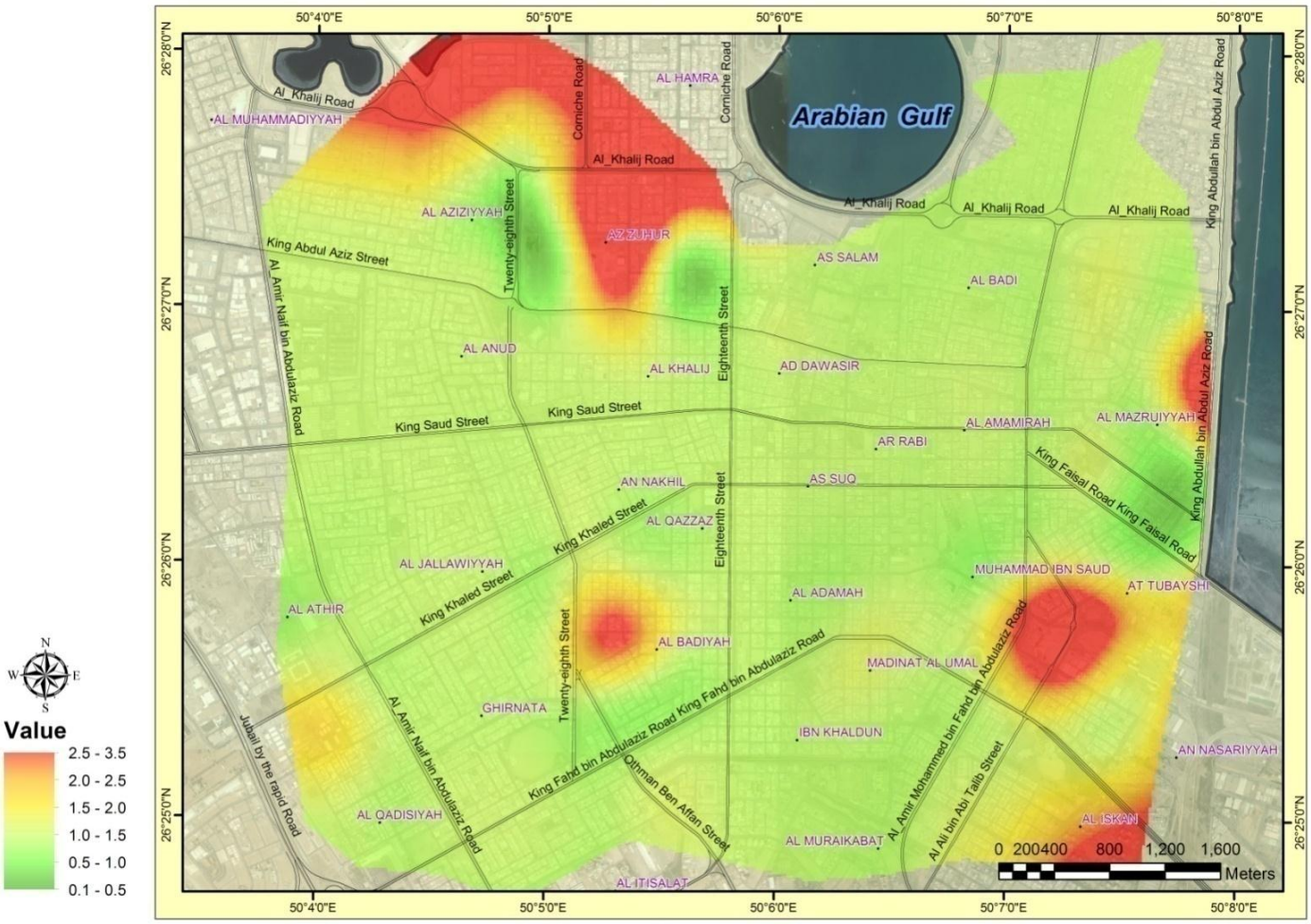

Figure 35: Distribution of Predominant Period (T_0) through Al-Dammam City.

VI. 2 BOREHOLES GEOTECHNICAL DATA

Recent seismic code provisions have adapted site classification using average shear wave velocity and standard penetration results in the upper 30 m of a site as the sole parameter for site classification (Borcherdt, 1994; Borcherdt and Glassmoyer, 1994; Dobry et al., 2000). The site conditions specified by IBC 2006 (Table 16) are identical to the provisions of IBC 2003, and practically distinguish soil profiles in the five main categories. Each category is assigned factors appropriate for the site conditions. The average shear wave velocity and correlated index measurements of the average standard penetration resistance to 30 m [(V_s (30) and N (30)] have been calculated in accordance with the following equations, and then used to develop categories for local site conditions.

$$V_s(30) = \frac{\sum_{i=1}^{n} di}{\sum_{i=1}^{n} \frac{di}{v_{si}}}$$

$$N(30) = \frac{\sum_{i=1}^{n} di}{\sum_{i=1}^{n} \frac{di}{N_i}}$$

Where V_{si} is the shear wave velocity (m/s), N_i is the standard Penetration resistance (ASTM D 158-84) not exceeding 100 blows/0.3 m as directly measured

in the field without corrections and d_i is the thickness of any layer between 0 and 30 m.

Thirteen of geotechnical boreholes have been conducted in Al-Dammam City and twenty-nine in Al-Khobar City, including the values of standard penetration resistance for different depths (Table 17). Following this, the standard penetration tests have been corrected and compensate field testing procedure (Skempton, 1986) according to the following Eq.;

$$N_{60} = 1.6 E_m C_b C_r N$$

where;

N_{60} = standard penetration test N value corrected for field testing procedures

E_m = hammer efficiency (for U.S. equipment, E_m is 0.6 for a safety hammer and 0.45 for a doughnut hammer)

C_b = borehole diameter correction (C_b = 1.0 for boreholes of 65-115-mm diameter, 1.05 for 150-mm diameter, and 1.15 for 200- mm diameter hole).

C_r = rod length correction (C_r = 0.75 for up to 4 m of drill rods, 0.85 for 4 to 6

m of drill rods, 0.95 for 6 to 10 m of drill rods, 1.0 for drill rods in excess of 10 m)

N = measured standard penetration test N-value.

After this procedure, the shear wave velocity has been calculated using the extrapolation method entitled "extrapolation assuming constant velocity "as proposed by Boore (2004b) for boreholes of less than 30 m depth. Accordingly, the values of shear wave velocities ranges from 200 – 500 m/s (Table 18).

Table 16: IBC 2006 site class definitions using the average shear wave velocity and the average standard resistance up to 30 m (ICC 2006).

Site class	Soil profile name	Average properties in top 30m	
		S-wave V_s (m/s)	SPT N (blows/0.3 m)
A	Hard rock	$V_s > 1500$	N/A
B	Rock	$760 < V_s \leq 1500$	N/A
C	Very dense soil and soft rock	$360 < V_s \leq 760$	N > 50
D	Stiff soil profile	$180 < V_s \leq 360$	$15 < N \leq 50$
E	Soft soil profile	$V_s < 180$	

After the estimation of shear wave velocities, the fundamental frequency values (F_0) can be identified at each borehole site. Using the following equation;

$$F_0 = \beta 1/4h$$

Where,

β_1 = the shear wave velocity in the surficial layer

h = the thickness of the surficial layer

Accordingly, resonance frequencies from boreholes are presented in Table 17 and Figure 36. On the basis of these frequencies, Al-Khobar City can be divided into three zones as follows:

Zone 1: has resonance frequency between 0.27 and 1.07 Hz.

Zone2: has resonance frequency between 1.07 and 1.23 Hz.

Zone 3: has resonance frequency between 1.23 and 1.95 Hz.

The spectral amplitudes (A_0) are then calculated using the equation of Brochert et al. (1991) as follows;

$$AHSA = 700/V_1$$

Where,

AHSA = average horizontal spectral amplification

V_1 = average shear wave velocities up to a depth of 30 m (m/sec.)

Accordingly, the estimated values of amplification factor (A_0) are presented in Table 17 and Figure (37), while Figure (38) illustrates the predominant periods in Al-Khobar City. Based on the values of resonance frequencies from boreholes (Table 18 and Fig. 39), Al-Dammam City can be divided into four zones as follows:

Zone 1: Characterized by a resonance frequency between 2.9 and 3.9 Hz.

Zone2: Characterized by a resonance frequency between 4.0 and 5.1 Hz.

Zone 3: Characterized by a resonance frequency between 5.2 and 6.3 Hz.

Zone 4: Characterized by a resonance frequency between 6.3 and 7.0 Hz.

The estimated values of amplification factor in Al-Dammam City (A_0) are presented in Table 19 and Figure 40, while the predominant periods are presented in Figure 41.

VI.3 THE SOIL CLASSIFICATION (V_{S30}) MAPS

The vertically averaged shear wave velocity to 30 m (V_{s30}), computed by dividing 30m by the traveltime from the surgace to 30m, has become a widely used parameter for classifying sites to predict their potential to amplify seismic shaking (Boore, 2004b) and is now adopted in recent building codes (Doherty et al, 2000, BSSC, 2001) and loss estimation. The classification of soil – profile types based on V_{s30}included in the NEHRP building code is also a part of the International Building Code adopted in 2001 (IBC, 2002) (Table 16).

The griding algorithm was selected so as to preserve original data and produce minimum artifacts, if any, in accordance with the extensive treatment presented by Reuter et al. (2007) on various methods to interpolate missing data in the Shuttle Radar Topography Mission (SRTM) spatial datasets.

Accordingly, the calculated values of shear-wave velocities ranges from 106 - 577 m/sec in Al-Khobar City and matched well with C, D and E classes (Fig. 42). This suggests that, the southern districts of Al-Khobar City have good bedrock rather than the eastern and coastal districts. While, average V_{s30} ranges from 200-500 m/sec in Al-Dammam City which fall in C and D classes (Fig. 43) according to the IBC. Accordingly, the southern districts of Al-Dammam City have good foundation layer rather than the eastern and coastal districts.

Table 17: Results of the Microtremors at drilled boreholes in Al-Khobar City.

Site Code	No. of samples	No. of windows (n_w)	Window length (I_w)	No. of cycles (n_c)	H/V Peak amplitude (A_0)	Standard Deviation $\sigma_A(f)$	Fundamental Frequency (F_0)	Standard Deviation (σ_f)	Remarks
BH03	30000	11	15		1.56	1.11	24.01	2.90	Industrial
	30000	11	15		0.84	1.14	1.81	0.09	Natural
BH04	30000	10	15		2.50	1.26	12.60	0.69	Industrial
	30000	10	15		1.25	1.24	1.04	0.06	Natural
BH05	30000	10	09		3.48	1.14	35.40	1.42	Industrial
	60000	10	09		0.86	1.47	1.19	0.08	Natural
BH06	60000	11	30		2.60	1.20	8.44	0.64	Industrial
	30000	11	30		1.44	1.52	2.00	0.06	Natural
BH 07	30000	10	15		--	--	--	--	No Industrial
	60000	10	15		1.23	1.21	1.00	0.22	Natural
BH08	60000	13	15		2.25	1.25	9.06	1.30	Industrial
	60000	13	15		1.68	1.60	01.17	0.10	Natural
BH09	60000	12	30		3.45	1.14	7.10	0.484	Industrial
	60000	12	30		1.11	1.36	1.71	0.05	Natural
BH10	60000	12	30		1.73	1.08	21.15	0.77	Industrial
	60000	12	30		1.23	1.15	1.20	0.07	Natural
BH11	60000	10	15		1.69	1.17	47.76	4.45	Industrial
	60000	10	15		1.28	1.82	0.91	0.10	Natural
BH 12	60000	12	25		2.20	1.05	42.64	1.33	Industrial
	60000	12	25		0.96	1.31	0.96	0.08	Natural
BH13	60000	11	25		1.87	1.21	39.11	2.81	Industrial
	60000	11	25		1.40	1.15	01.01	0.07	Natural
BH14	60000	12	20		6.49	1.11	37.83	1.25	Industrial
	30000	12	20		1.84	1.21	00.98	0.06	Natural
BH15	30000	10	15		4.17	1.63	6.12	0.74	Industrial
	60000	10	15		1.20	1.24	1.73	0.08	Natural
BH16	60000	10	30		1.69	1.14	1.57	0.10	Natural
		16	30		1.18	1.40	1.67	0.08	Natural

BH18	20000	11	50	--	--	--	--	No Industrial
	120000	11	50	3.80	1.09	3.93	0.39	Natural
BH19	60000	11	30	4.07	1.16	4.38	0.20	Industrial
	60000	11	30	1.33	1.17	1.57	0.08	Natural
BH20	60000	10	30	--	--	--	--	Industrial
	60000	10	30	2.89	1.17	3.57	0.60	Natural
BH21	60000	11	20	3.14	1.06	25.20	0.55	Industrial
	60000	11	20	1.68	1.18	2.00	0.45	Natural
BH22	120000	15	50	--	--	--	--	No Industrial
	120000	15	50	1.68	1.18	2.00	0.45	Natural
BH23	60000	10	30	1.91	1.03	5.25	0.49	Industrial
	60000	10	30	1.72	1.36	2.98	0.08	Natural
BH24	60000	12	40	4.25	1.21	5.05	0.07	Industrial
	60000	12	40	1.86	1.17	2.00	0.06	Natural
BH25	60000	12	20	--	--	--	--	Industrial
	60000	12	20	2.45	1.27	3.15	0.62	Natural
BH26	60000	16	30	--	--	--	--	Industrial
	60000	16	30	2.40	1.09	3.29	0.35	Natural
BH27	60000	12	30	2.48	1.07	17.15	0.52	Industrial
	60000	12	30	0.97	1.26	1.60	0.06	Natural
BH28	60000	12	30	2.80	1.11	22.66	0.29	Industrial
	60000	12	30	1.04	1.26	0.96	0.09	Natural
BH30	30000	11	30	--	--	--	--	Industrial
	30000	11	30		1.21	3.61	0.38	Natural
BH31	79630	12	20	3.37	--	--	--	No Industrial
	79630	12	20	--	1.20	3.58	0.29	Natural
BH32	60000	12	15	2.35	--	--	--	No Industrial
	60000	12	15	2.91	1.19	2.91	0.49	Natural

Table 18 : Results of the conducted geotechnical boreholes in Al-Khobar city.

No. Borehole	Name	V_{av}	V_{30}	T_0 (s)	F_0 (Hz)	A_0	NEHRP-class
BH01	Al-Mamoon Primary School	136	236	0.76	1.32	1.40	D
BH02	Jabber Bin Hayan School	300	366	0.65	1.53	1.61	C
BH03	Al Tabri School	160	171	0.8	1.25	1.20	E
BH04	Al Fahad Tower Building	88	153	1.05	0.95	1.27	E
BH05	Abdurrahman Bin Al Qasim School	222	229	0.73	1.4	1.04	D
BH06	King Abdullah /King Abdulaziz Interchange	125	236	1.17	0.9	1.28	D
BH07	King Abdullah /King Abdulaziz Interchange	250	277	0.81	1.3	0.94	D
BH08	Al Zajil for Realestate Investment Est.	308	345	1.02	0.97	1.31	D
BH09	King Abdullah /Makkah Interchange	500	577	1.01	0.98	1.97	C
BH10	King Abdullah /Makkah Interchange	375	405	1.03	0.96	1.66	C
BH11	Water Front Project , Sport Hall	375	379	1.01	0.98	1.87	C
BH12	King Abdullah /Makkah Intersection	303	326	1.01	0.98	1.72	D
BH13	King Abdullah /Makkah Intersection	161	150	1.06	0.96	1.18	E
BH14	Al Oula Tower , Phase –B	108	152	3.37	0.35	2.00	E
BH15	Dar Ghassan Consultants	118	121	1.22	1.2	1.22	E
BH16	Tamimi Safeway	82	136	3.2	0.34	1.62	E
BH17	Al Oula Tower , Phase –A	95	154	1.25	1.01	1.08	E

BH18	Al-Mana Tower (Hospital)	66	106	1.23	0.82	1.08	E
BH19	Jasim Al Gawahmed Engineering Office	242	303	0.69	1.49	1.06	D
BH20	Accuracy & Innovation Est	327	492	0.52	1.95	1.68	C
BH21	Abdurrahman Al Dable Est	214	268	0.61	1.73	1.58	D
BH22	Abdurrahman Al Siekh	87	122	2.4	0.53	1.40	E
BH23	Building Eyes General Cont. Est	66	140	2.85	0.51	1.63	E
BH24	Al-Nahdi Realestate Group	104	167	3.8	0.27	1.89	E
BH25	Abdullah A.M.Al-Khodari & Sons Co.	241	268	1.17	0.86	1.02	D
BH26	Girls School	204	236	0.82	1.29	1.13	D
BH27	Anmatt Al Amar Construction Co.Ltd	120	129	3.61	0.3	1.59	E
BH28	Mosa & Sultan Sons of AbdulAziz Al-Mosa	94	116	3.28	0.32	1.69	E
BH29	Al Sharq Architects & Design	96	142	3.73	0.29	1.92	E

Where; V_{av}: Shear wave velocity / T_0: Natural period/ F_0: Fundamental Frequency/ A_0: Relative Amplification

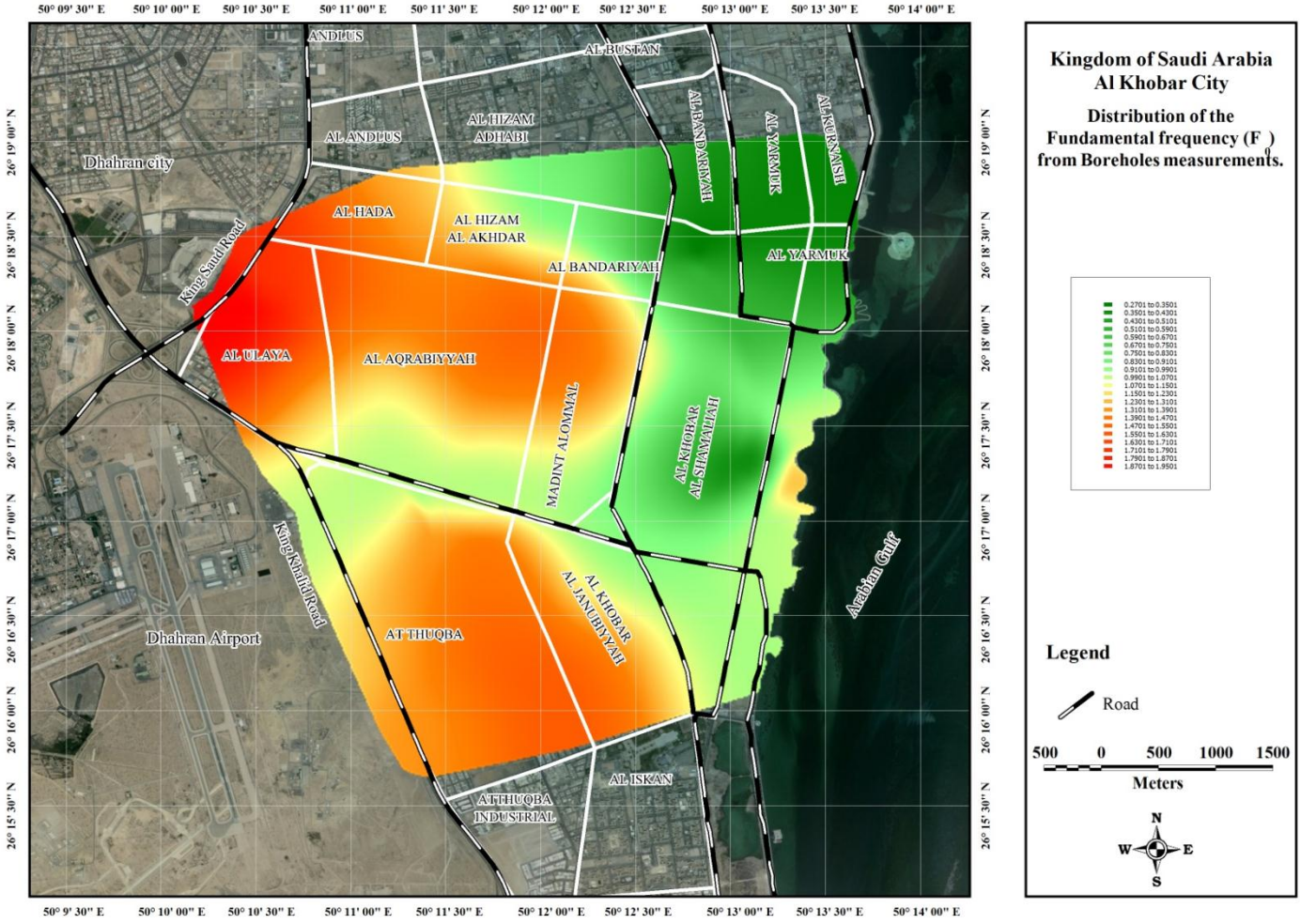

Figure 36: Distribution of the fundamental frequencies (F_0) from boreholes in Al-Khobar City.

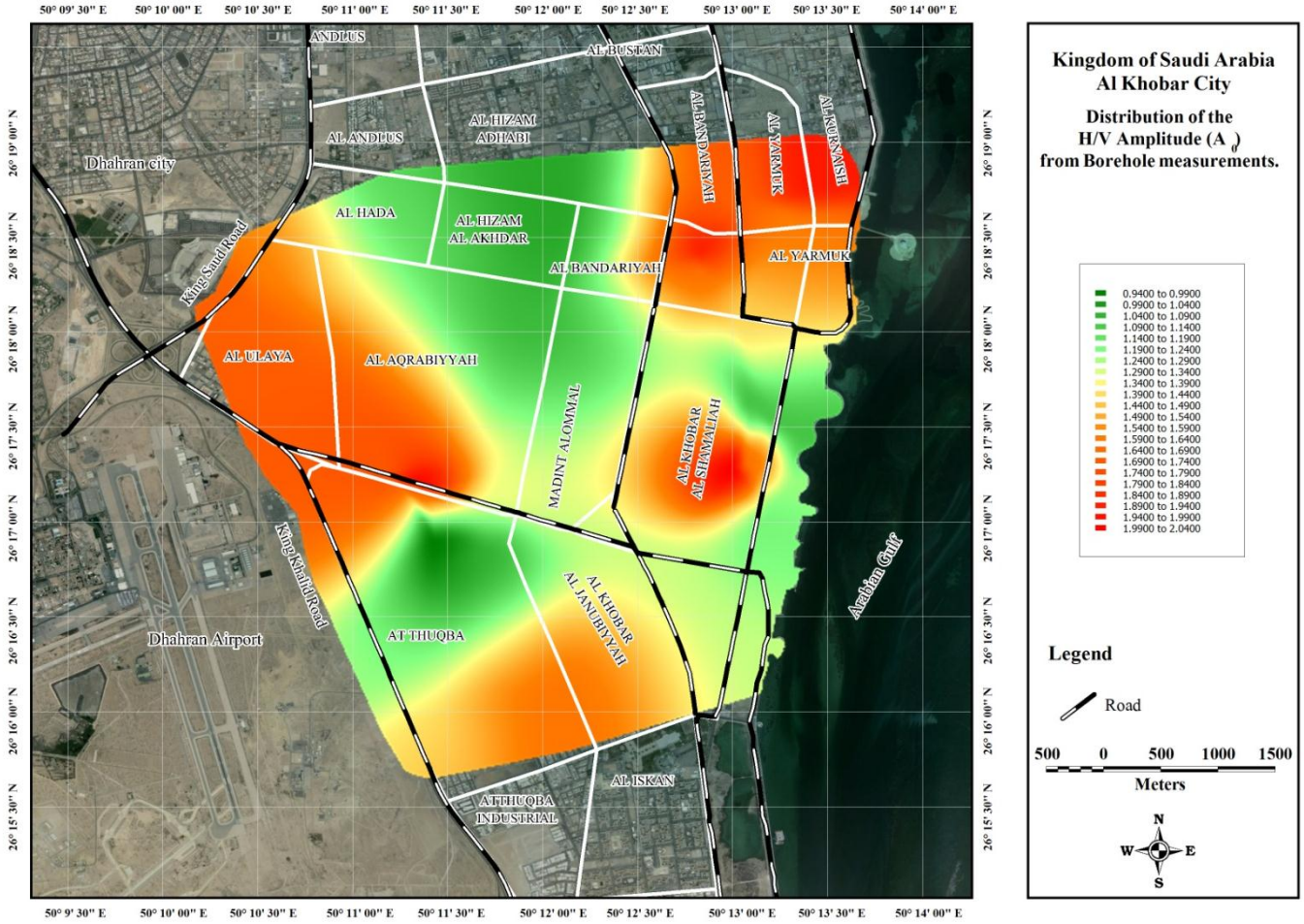

Figure 37: Distribution of (A_o) from borehole measurements in Al-Khobar City.

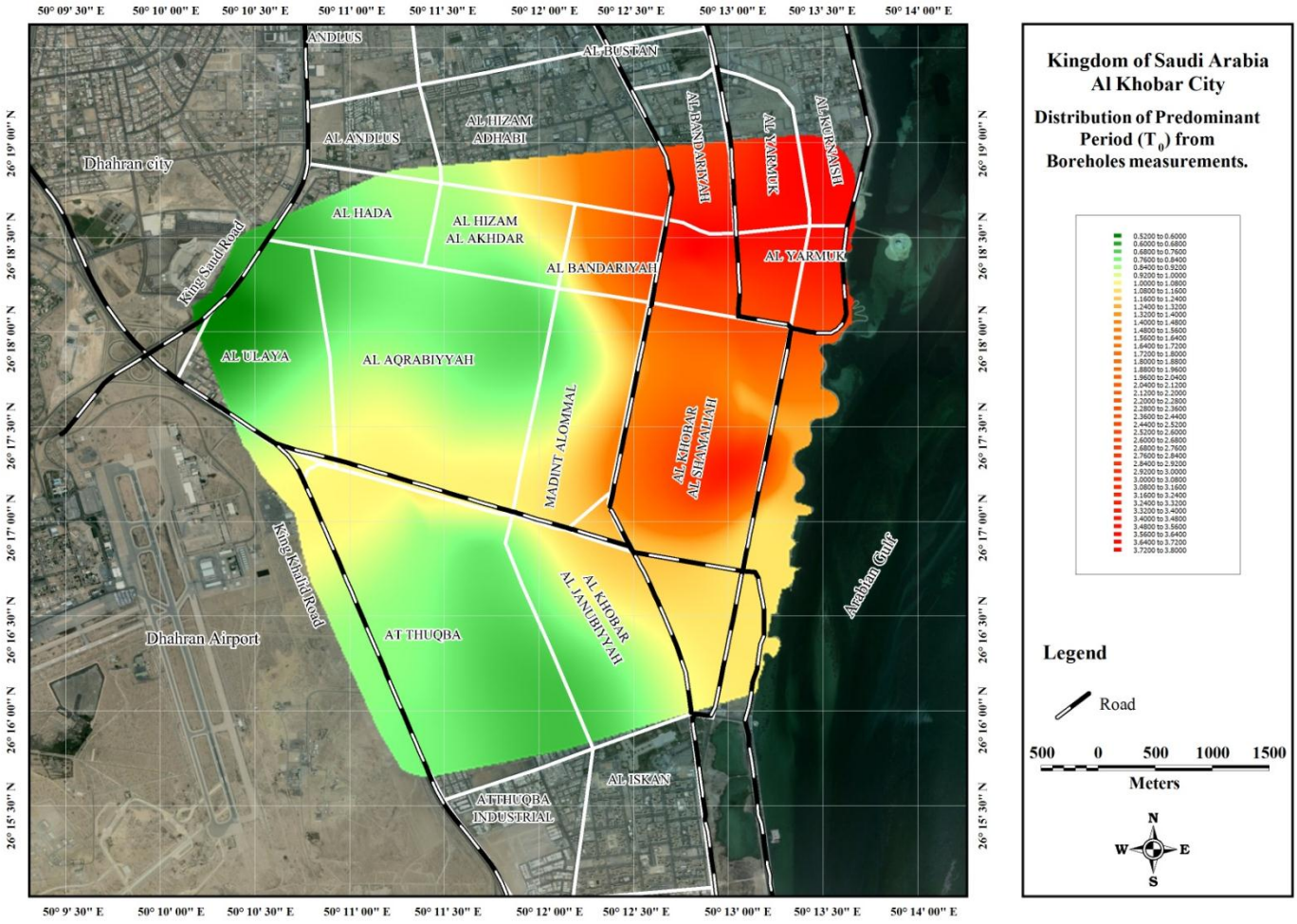

Figure 38: Distribution of the fundamental period (T_0) from borehole measurements in Al-Khobar city.

Table 19: Results of the collected bore-hole data through Al-Dammam City.

No. Borehole	Name	V_{30}	T_0 (s)	F_0 (Hz)	A_0	NEHRP-class
DB1	Al Zahour school	280	1.28	4.0	2.5	D
DB2	Al Maarif Primary School	360	0.22	4.6	1.9	C
DB3	Yazeed Al-Shibani Prim. School	363	1.60	5.0	1.9	C
DB4	Girls School	500	0.28	3.6	1.4	C
DB5	School	350	0.26	3.8	2.0	D
DB6	38 Primary School girls.	448	0.27	3.6	1.6	C
DB7	Girls School	233	0.17	5.7	3.0	D
DB8	General Girls Education	500	0.15	7.0	1.4	C
DB9	Girls School	233	0.26	3.8	3.0	D
DB10	Zaid Bin Al Khattab School	435	0.18	5.4	1.6	C
DB11	Intersection	260	0.29	3.5	2.7	D
DB12	Intersection	388	0.53	2.8	1.8	C
DB13	Civil Defence.	350	0.20	5.0	2.0	D

Where; V_{av}: Shear wave velocity;

T_0 : Natural period;

F_0: Fundamental Frequency, and

A_0: Relative Amplification

Figure 39: Distribution of the fundamental frequencies (F_0) from boreholes in Al-Dammam City.

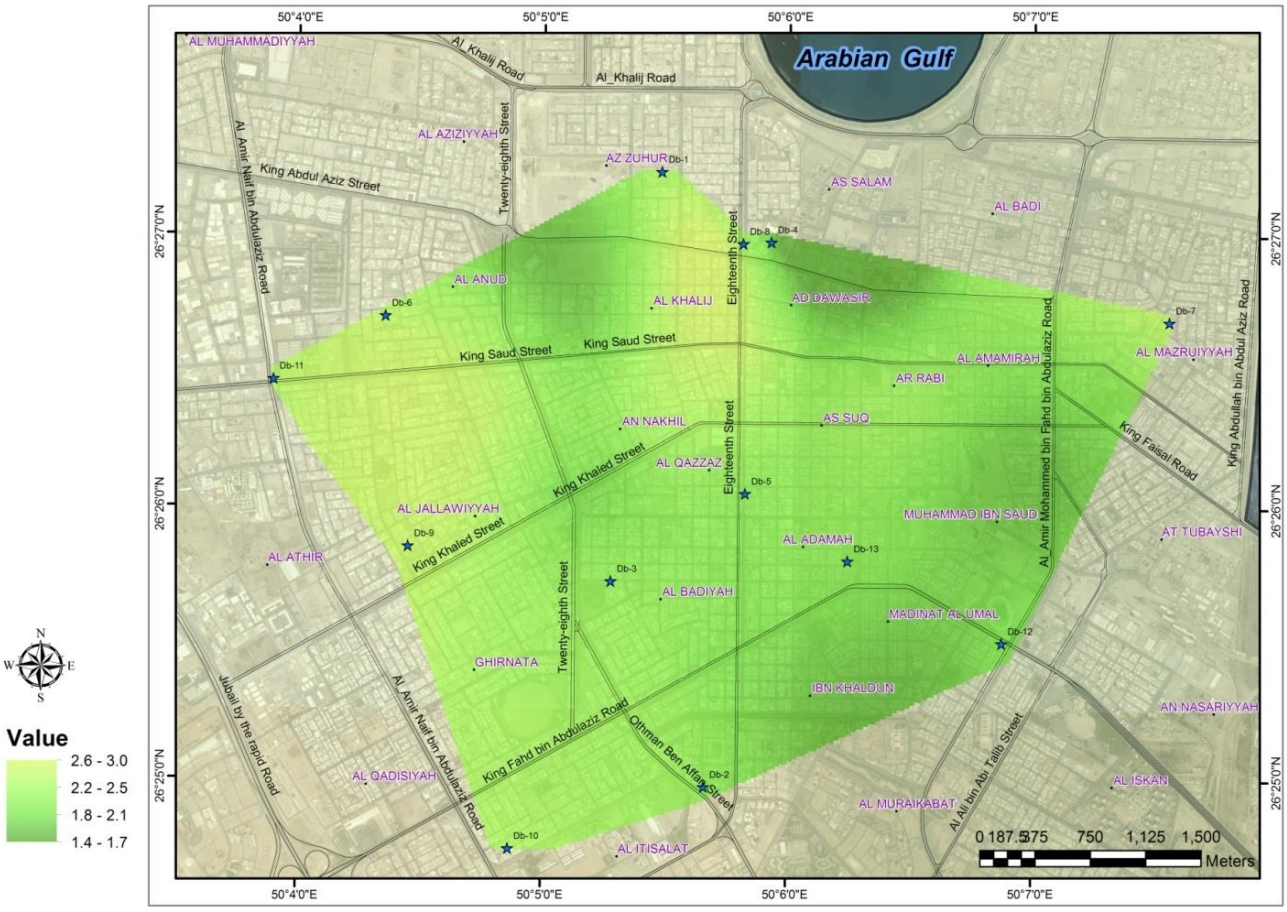

Figure 40: Amplification (A_o) from borehole measurements in Al-Dammam City.

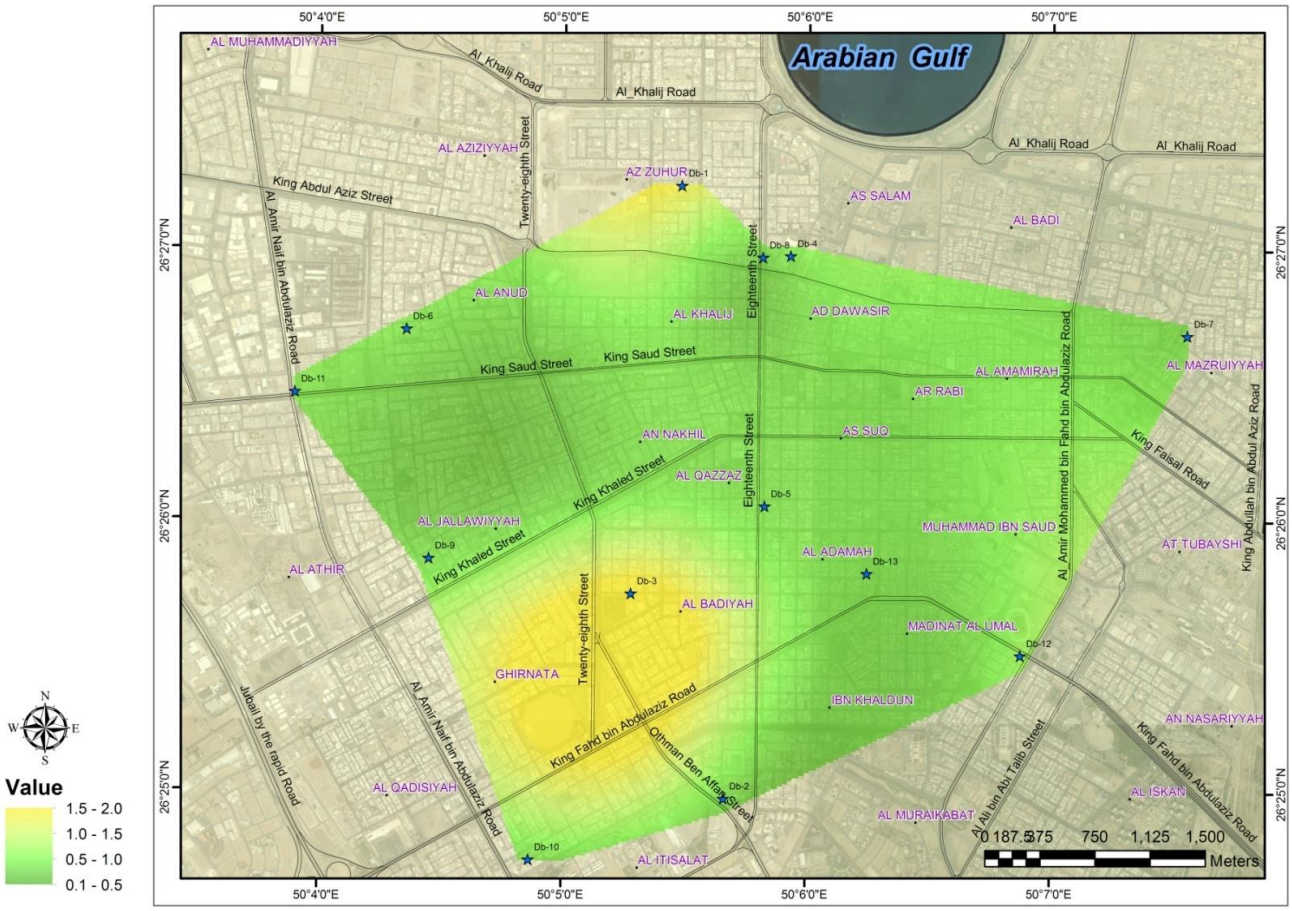

Figure 41: Fundamental period (T_0) from boreholes in Al-Dammam City.

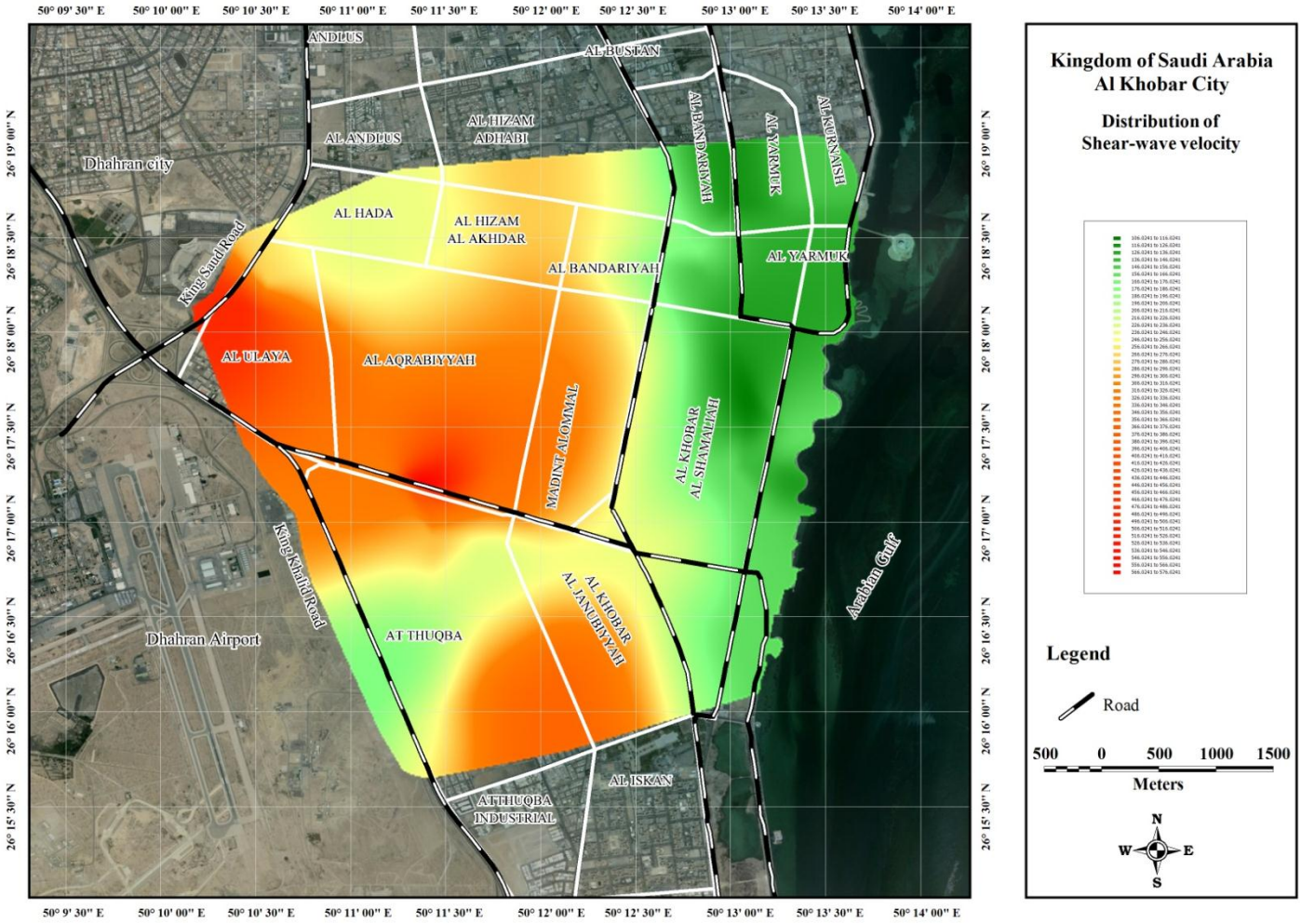

Figure 42: Shear-wave velocity through Al-Khobar City.

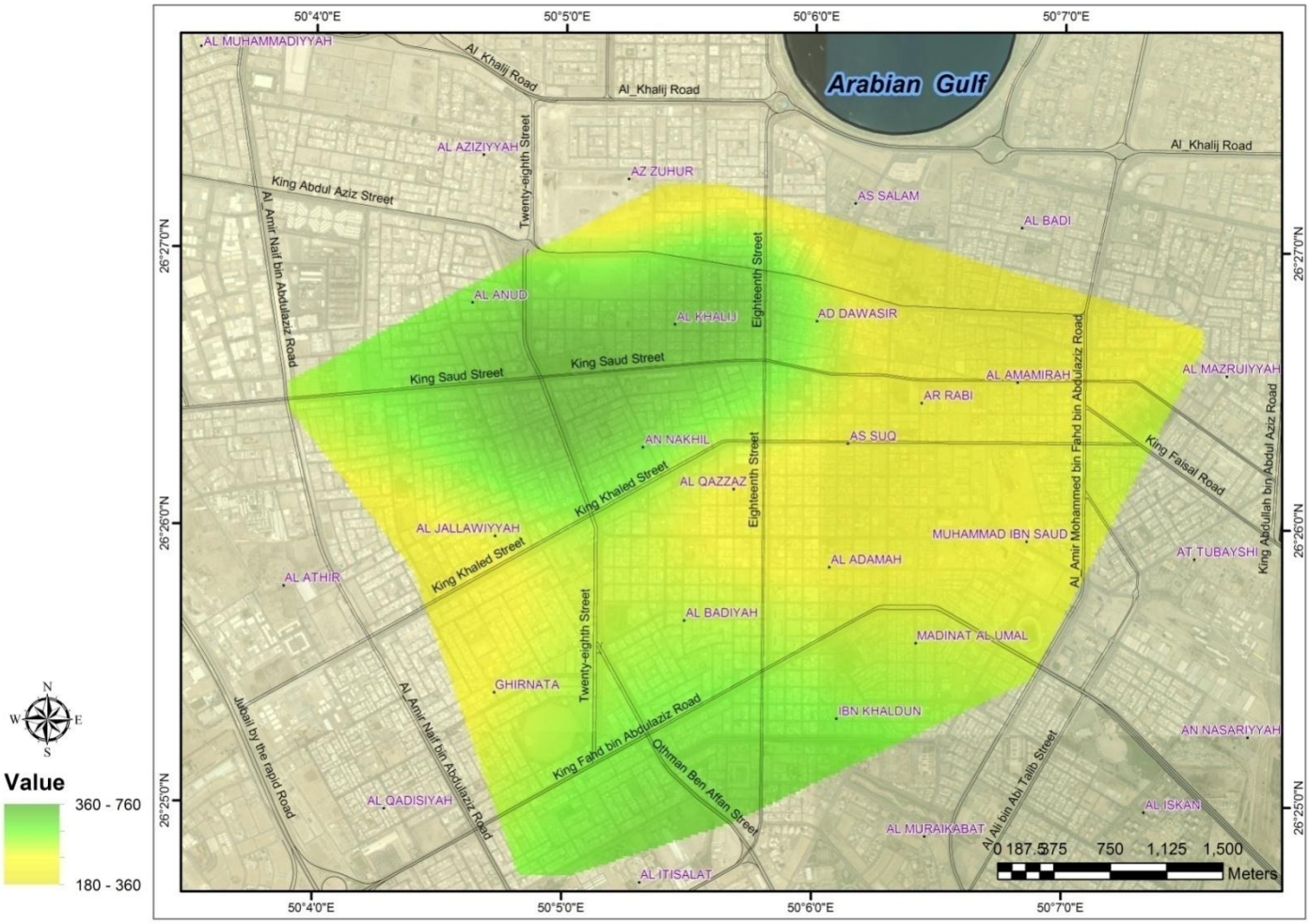

Figure 43: Shear-wave velocity through Al-Dammam City.

VII. 4 THE DEPTH TO THE BEDROCK MAPS

The depth maps of the bedrock throughout the Al-Dammam and Al-Khobar cities have been produced (Figs. 44 and 45 respectively).

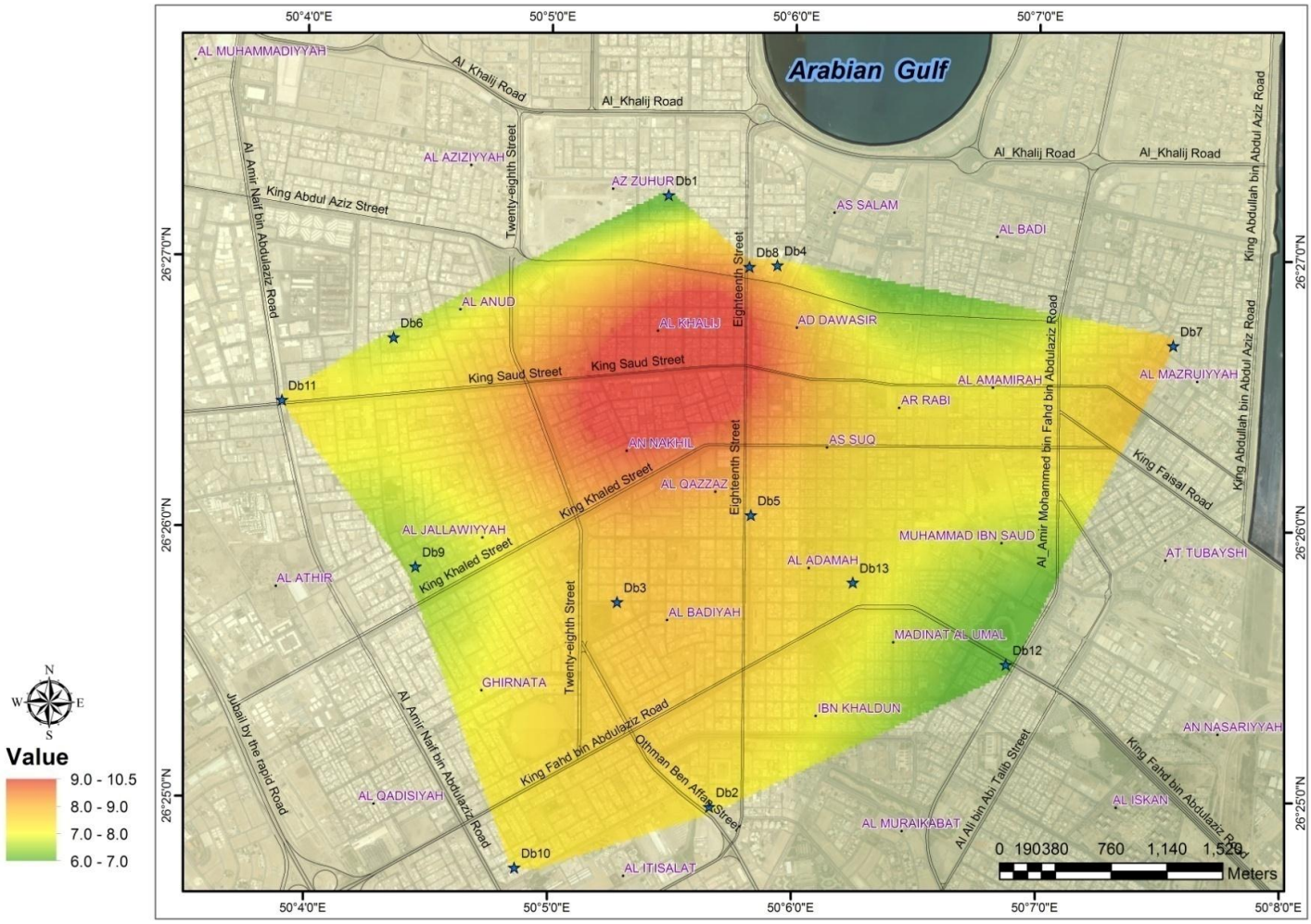

Figure 44: Depth map to the bedrock in Al-Dammam City.

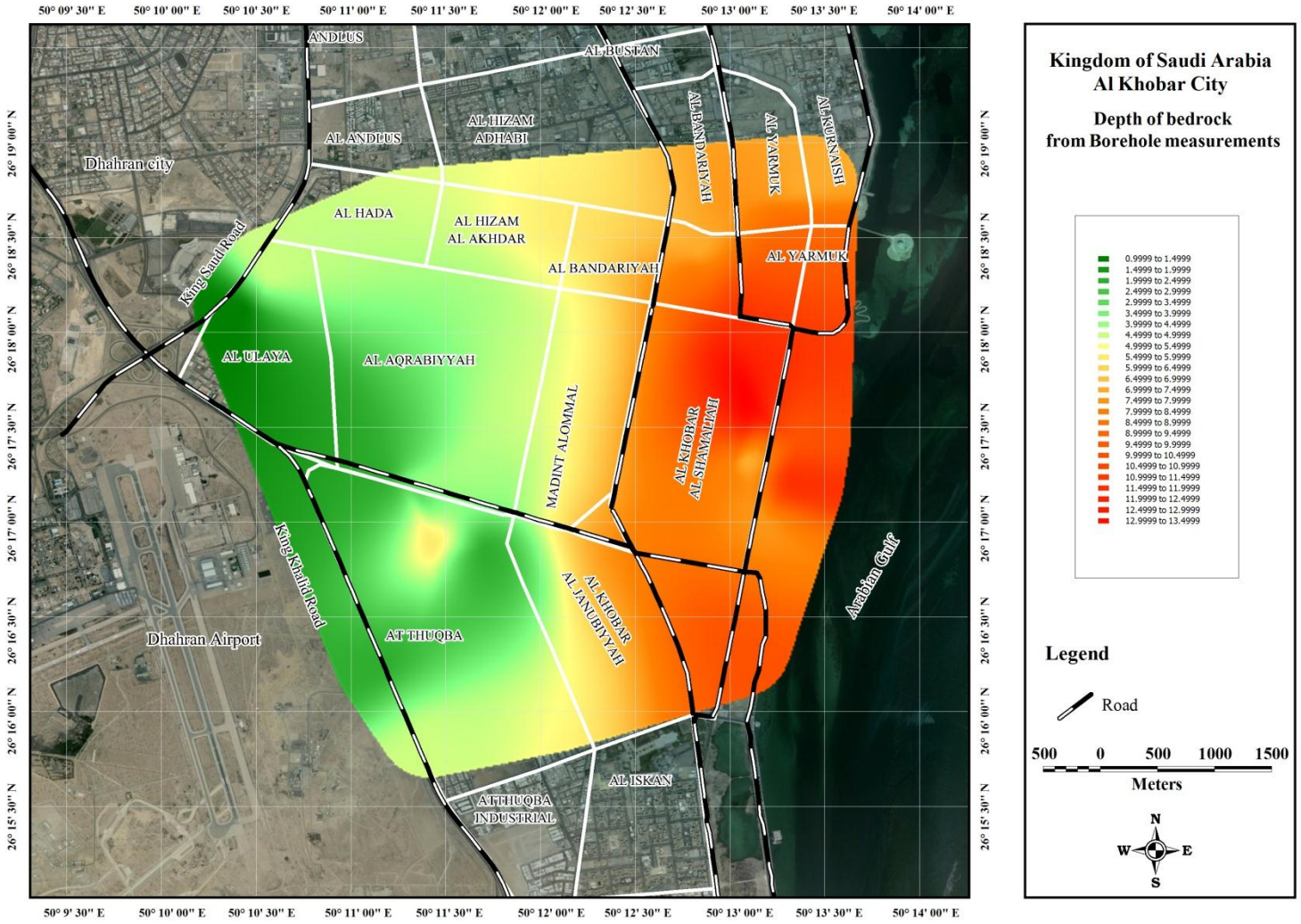

Figure 45: Depth to bedrock throughout Al-Khobar City.

VI. Seismic hazard Assessment

Seismic hazard in terms of Peak Ground Acceleration, for the eastern province of Saudi Arabia has been assessed using the estimated attenuation eq. (section III). It is noticed that, the values of PGA are not the effective parameter for damaging potentiality effect at Al-Dammam and Al-Khobar cities. But the predominant frequency and/or periods at the local site are the main effective parameters due to the small values of PGA from the distant earthquakes of Zagros seismogenic source. Hence low-rise buildings can vulnerability to seismic sources nearby, while high-rise buildings are affected ground vibrations from distant earthquakes. Therefore, we strongly recommend monitoring and analyzing the digital records of Zagros earthquakes at these cities and especially their frequency content. This will greatly support in the improvement of Saudi Building Code to mitigate the earthquake risks for the high-rise buildings in the eastern province of Saudi Arabia.

VII. DISCUSSIONS AND CONCLUSIONS

Microtremors resonance frequency and spectral amplitude ratios have been calculated and applied as an aid to perform earthquake hazard microzoning in densely populated areas of Al-Khobar City. For this purpose microtremors data at a grid pattern have been accumulated over the region of interest. Hundred and twelve measurements of microtremors were recorded to produce a distribution map for the predominant frequency of site response. The horizontal-to-vertical spectral ratios obtained from microtremors (Nakamura technique) proved to be a valuable tool to determine frequencies of great and small thickness of soft soils with multilayer distribution and linear behaviors. A good correlation has been observed between the microtremors and boreholes results both in terms of fundamental frequencies and the amplification levels.

Furthermore, the fundamental resonance frequencies determined by present study are correlated well with the thickness of the sediments in Al-Khobar City. The sediments are thick in the northern part (where site response spectra exhibit peaks at 0.33 - 1.03 Hz), while they are thin in the southern part of the city (predominant frequency of site response at 1.23 – 1.73 Hz). This behavior indicates horizontal variations both in the thickness and type of sediments.

Accordingly, Al-Khobar City can be differentiated into three zones as in Table 20, while Al-Dammam City divided into four zones as in Table 21

Table 2: Comparison between the F_0 from microtremors and boreholes in Al-Khobar City.

Zone No.	Microtremor Measurements (Hz)	Borehole Measurements (Hz)
Zone_1	0.33 –1.03	0.27 – 1.07
Zone_2	1.03 – 1.23	1.07 – 1.23
Zone_3	1.23 – 1.73	1.23 – 1.95

Table 3: Comparison between Microtremors and boreholes in Al-Dammam City.

Zone No.	Microtremor Measurements (Hz)	Borehole Measurements (Hz)
Zone_1	0.3 – 3.9	2.8 – 3.9
Zone_2	3.9 – 5.2	3.9 – 5.1
Zone_3	5.2 – 6.5	5.2 – 6.3
Zone_4	6.5 – 7.8	6.4 – 7.0

Site amplification for Al-Dammam and Al-Khobar cities indicate that soils can amplify ground motion by as much as 5.5 times its bedrock level in Al-Dammam city and 2.5 times in Al-Khobar city. This is applied for different soil classes, where, all sites with resonance frequencies of engineering interest. The relation between resonance frequency and amplification represents the alarming condition that soil

having resonance frequencies of interest can amplify earthquake ground motion as much as 5.5 times. It is indicated that, the amplification is generally decreasing with increasing frequency. The obtained values of amplification are in agreement with the surface geology of the study area. Higher H/V values occupy the northern part of Al-Khobar City due to the presence of coastal deposits and Sabkhah sediments. The lower values are encountered in the southern parts of the city. This variation in the H/V values also reflects variation in sediments thickness.

Al-Dammam urban area presents the fundamental resonance frequencies range from 0.3 to 7.8 Hz. Considering the relationship between the height of a building and its fundamental period of vibration can be expressed as T= (number of storeys)/10. It can expect that in this urban area the natural frequency of the soil maches the frequency of buildings with ≥ 1 sorey (Fig. 46). On the other hand Al-Haddad (Personal Communications) indicated that site response frequencies less than 10 Hz are of engineering concern for 1 storey reinforced concrete structures. Al-Khobar City attains fundamental frequencies in range between 0.33 and 1.73 Hz. This means that, in Al-Khobar urban area the natural frequency of the soil matches only the frequency of buildings with ≥ 5 storeys. Most of the urban area characterized by low-rise buildings and the frequency of the soil cover can be close to their fundamental frequency of vibration. According to Parolai et al., (2006), when the fundamental frequency of vibration of a building is higher than that the fundamental frequency of soil f_o it may, however be close to the frequency of higher modes.

Higher modes are expected at frequencies $f_n = (2n+1)\, fo$ where n = 1,2,3….. and f_o is the fundamental frequency. The H/V spectral ratio provides the lower frequency threshold from which ground motion amplification due to soft soil can be expected. Therefore, it cannot exclude that in Al-Dammam urban area, such soil amplification of ground motions may also occur at higher mode frequencies close to the fundamental frequency of vibration of low-rise buildings, even if it is smaller than that at the fundamental frequency of the sedimentary cover (Parolai et al., (2006).

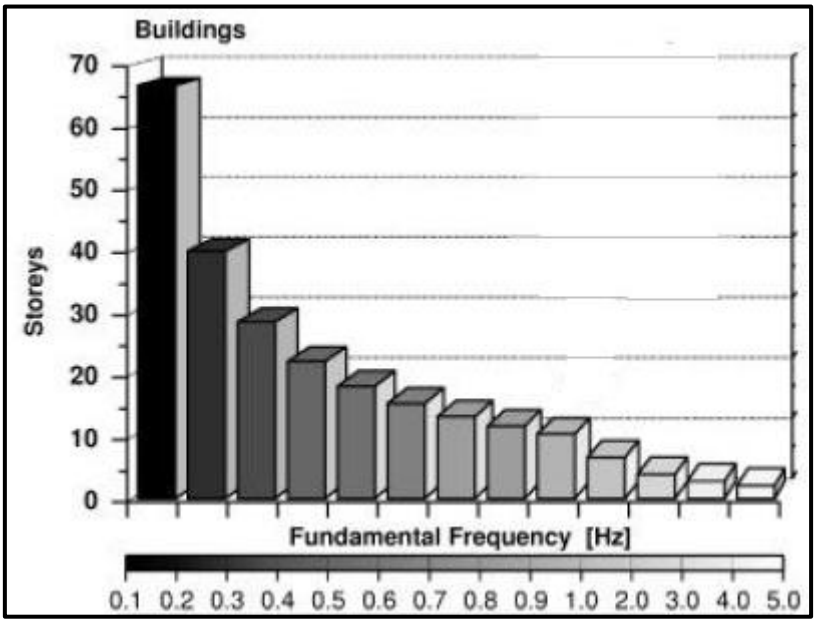

Figure 46: Fundamental frequency of vibration of the buildings versus number of storeys in Cologne area, Germany (Parolai et al., 2006)

Based on V_{s30} map of Al-Dammam city (Fig. 42), the soil profiles of Al_ Dammam city have NEHRP classes C and D characteristics. According to Table

(22), C class soil profile represented by very dense soil to soft rock with a moderate amplification of earthquake ground motion. Districts of Al-Anud, Al-Khalij; Al-Nakhil, Ibn Khaldun have soil of class C. In addition most of Al-Jallawiyyah, Al-Badiyah, and Madinat Al-Umal districts fall in class C soils. Whereas, Districts of Al-Amamirah; Ar-Rabi; As Suq; Al-Qazzaz, Al-Adamah, Muhammed Ibn Saud fall in class D in addition, the rest areas of Al-Jallawiyyah and Ghinata districts. Class D represented by stiff soil profiles that induced significant amplification of earthquake ground shaking.

Al-Khobar city (Fig. 43) illustrates classes E, D, and C soil profiles constitute the surface soil of Al-Khobar city. Class E is represented by soft soil profiles with a higher amplification of earthquake ground motion. The eastern districts of Al-Khobar as Al-Khobar Al-Shamaliah; Al-Yarmuk; Al-Kornaish; and Al-Bandariyah having class E soil profiles. The soils of districts of Al-Ulaya; Al-Aqrabiyyah; Madinat Al-Ommal; Al-Khobar Al-Janubiyyah belong to class C. While the districts of Al-Hada; and Al-Hizan Al-Akhdar districts having soils profiles of class D.

Site	Description	Site Period	Comments
A	Hard Rock	≤ 0.1 s	Hard, strong, intact rock (Vs ≥ 1500 m/s).
B	Rock	≤ 0.2 s	Most "unweathered" California rock cases (Vs ≥ 760 m/s or < 6 m of soil).
C-1	Weathered/Soft Rock	≤ 0.4 s	Weathered zone > 6 m and < 30 m (Vs ≥ 360 m/s increasing to ≥ 700 m/s).
-2	Shallow Stiff Soil	≤ 0.5 s	Soil depth > 6 m and < 30 m
-3	Intermediate Depth Stiff Soil	≤ 0.8 s	Soil depth > 30 m and < 60 m
D-1	Deep Stiff Holocene Soil, either S (Sand) or C (Clay)	≤ 1.4 s	Soil depth > 60 m and < 210 m. Sand has low fines content (< 15%) or non-plastic fines (PI < 5). Clay has high fines content (> 15%) and plastic fines (PI > 5).
-2	Deep Stiff Pleistocene Soil, S (Sand) or C (Clay)	≤ 1.4 s	Soil depth > 60 m and < 210 m. See D1 for S or C sub-categorization.
-3	Very Deep Stiff Soil	≤ 2 s	Soil depth > 210 m.
E-1	Medium Depth Soft Clay	≤ 0.7 s	Thickness of soft clay layer 3 m to 12 m.
-2	Deep Soft Clay Layer	≤ 1.4 s	Thickness of soft clay layer > 12 m.
F	Special, e.g., Potentially Liquefiable Sand or Peat	≈ 1 s	Holocene loose sand with high water table (z_w ≤ 6 m) or organic peats.

Table 22: Geotechnical Site Categories (Bray and Rodriguez-Marek, 1997)

The distribution of V_{s30} for Al-Khobar and Al-Dammam cities (Figs. 42 and 43) and the depth of bedrock (Figs. 44 and 45), indicate that, there are inverse relation between depth to pedrock and V_{s30} where increasing depth generally corresponds to lower V_{s30}. There is an almost exact direct correspondence between the V_{s30} distribution for Al-Dammam and Al-Khobar cities and the distribution of fundamental resonance frequency for these cities, where soils of low V_{s30} shows also low resonance frequency and vice versa. This is clear from figures (46 and 47) where there is a strong exponential correlation (83%) between V_{s30} and fundamental frequency for Al-Dammam city and (75%) for Al-Khobar city. These relations can be used to obtain the soil fundamental resonance frequency if V_{s30} is known. But the resonance frequency presents an inverse relation with the bedrock depth.

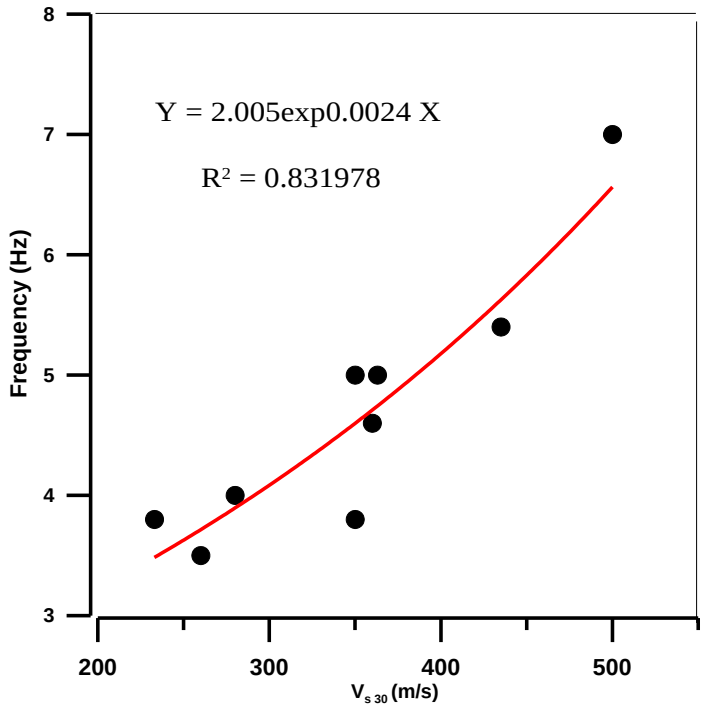

Figure 46: Relation between V_{s30} and fundamental frequency for Al-Dammam City.

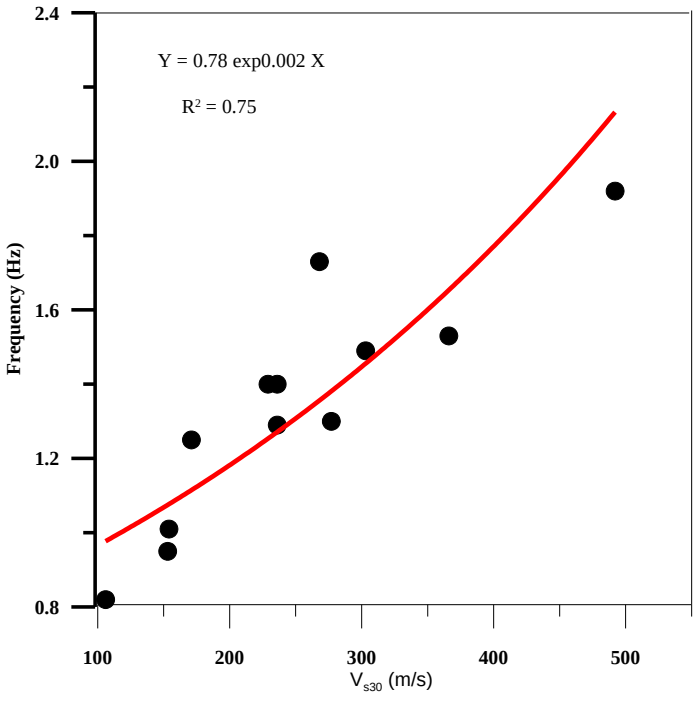

Figure 47: Relation between V_{s30} and fundamental frequency for Al-Khobar City.

CONCLUSIONS AND RECOMMENDATIONS

It has been noticed that parameters for site effects are remarkably robust. Comparison of the two neighboring points reveals that differences in the location of the fundamental frequencies and amplification levels are small and the general shapes of two horizontal components are similar. These findings significantly increase the reliability of the obtained information and emphasize the importance of a densely laid observation points in microzoning studies.

The results of both microtremor and boreholes measurements are in agreement, reflecting the ability of Nakamura method for microzoning studies, especially through the densely populated cities as Al-Dammam and Al-Khobar in Saudi Arabia. The dominant frequencies and amplification maps for Al-Khobar City can be are pre-requisite to get knowledge about future earthquake scenarios in the area. As important documents, these maps can also help the governments to set priorities in managing land uses, enforcing building codes, conducting programs for reducing the vulnerability of existing structures and planning for emergency response and long-term recovery.

The results described in this study are strongly recommending continuation of this type of microzonation investigations for seismic hazard assessment in other parts of Saudi Arabia using the microtremors data and site response functions. It is, therefore, strongly recommended that the outcome from present study should be used

as a guide to estimations the earthquake losses and related scenarios. The other functions are presented for reference and information purposes only.

Based on the experience gained from the present study, it is recommended that;

1. Microtremors measurements, in combination with Nakamura's technique, can be a powerful tool to map sedimentary cover layers. In the regions of unknown basement morphology, such a procedure may be a way to quickly obtain a general idea of the subsurface structure.
2. As demonstrated in this study, the site response variations are significant over very short distances, thus, strongly suggesting that estimation of earthquake loss scenarios should be based on the site response functions obtained over a relatively dense grid of measurement points.
3. It should be realized that the applicability of the Nakamura technique heavily depends on the amount of data. Analysis of ambient seismic noise encounters significant limitations primarily associated with the great variability of interfering sources of seismic energy. It is, therefore, essential to monitor the microtremors for a number of hours, sometimes preferably during different hours of the day, to increase the chances of selecting the appropriate time windows (of only 30 sec) that are used in the analysis. The reliable geophysical investigations it can be said that quantity is a necessity to achieve quality.

REFERENCES

Al-Amri A., Punsalan B., and Uy, E. (1998): Seismic expectancy modeling of NW Saudi Arabia, Jour. Europ. Assoc. Earthq. Engineering, 2, 16-21.

Al-Amri A., Punsalan B., and Uy, E. (1998): Spatial distribution of the seismicity parameters in the Red Sea regions. Jour. Asian Earth Sci., 16, 557-563.

Al-Amri, A. M., S. (2004): Seismic zones in the Arabian Peninsula. Seismic Studies Center, King Saud University, Riyadh, Saudi Arabia,p.215

Al-Amri, A., Rodgers, A., and Al-khalifah, T. 2008. Improving the Level of Seismic Hazard Parameter in Saudi Arabia Using Earthquake Location. Arabian J. of Geosciences, 1, DOI 10.1007/s12517-008- 0001-5, 1-15.

Abdalla, J. A & A.S. Al-Homoud (2004a). Seismic hazard assessment of United Arab Emirates and its surroundings. Journal of Earthquake Engineering, Vol. 8, No. 6, 817-837.

Abdalla, J.A. & A. Al-Homoud (2004b). "Earthquake hazard zonation of eastern Arabia", Proceedings of the 13th World Conference on Earthquake Engineering, Vancouver, Canada, August 1-6, 2004, Paper No. 1008.

Aiban, S.A., (2005): Swelling characteristics of Al-Khobar marl, eastern Saudi Arabia. Proceedings of International Conference on Problematic Soils, vol. 2. Eastern Mediterranean University, Famagusta, N. Cyprus, pp. 613–620. 25-27 May.

Aiban, S. A. (2006): Compressibility and swelling characteristics of Al-Khobar Palygorskite, eastern Saudi Arabia. Engineering Geology, 87, pp. 205-219.

Aguirre, J., and Irikura, K., 1997, Nonlinearity liquefaction, and velocity variation of soft soil layers in port island, Kobe, during the Hyogo-ken Nanbu Earthquake, Bull. Seism. Soc. Am., 87, 1244-1258.

Aki, K. and Richards, P. G., 1980. Quantitative Seismology: Theory and methods, Vol. 1, W. H. Freeman & Co., New York.

Aldama-Bustos, G., Bommer, J. J., Fenton, C. H. and Stafford, P. J. (2009): Probabilistic seismic hazard analysis for rock sites in the cities of Abu Dhabi, Dubai and Ra's Al Khaymah, United Arab Emirates. Georisk, Vol. 3, No.1, pp. 1-29.

Al-Haddad, M. Siddiqi, G. H., Al-Zaid, R., Arafa, A., Necioglu, A., and Turkelli, N., 1994, A basis for evaluation of seismic hazard and design criteria for Saudi Arabia. Earthquake Spectra 10 (2), 231-258

Al-Husseini, M. I. (1989): Tectonic and depositional model of Late Precambrian-Cambrian Arabian and adjoining plates. AAPG Bull, 73 (9), pp. 1117-1131

Al-Husseini, M. I. (2000): Origin of the Arabian Plate structures. Amar collision and Najd rift. GeoArabia, 5 (4), pp. 527-542.

Al-Mahmoud, M. J.; Khalil, M. H. and Moustafa, A. R. (2009): The Jinadriyah anticlines: a surface model for oil fields in the eastern Saudi Arabia. Arab. J. Geosciences, 2, pp. 213-234.

Al-Sayari, S. S. & Zoetl, J. G. (eds) (1978): Quaternary Period in Saudi Arabia. 1. Sedimentological, Hydrogeological Hydrochemical, Geomorphologicaland Climatological Investigations in Central and Eastern Saudi Arabia. Springer-Verlag, Vienna

Al-Shaabi, S. F. (2004): Induced seismicity at Ghawar hydrocarbon reservoir, eastern Saudi Arabia. Annals Geol. Surv. Egypt, V. XXVII, pp. 335-342.

Ambraseys A (1988): Seismicity of Saudi Arabia and adjacent areas, Report 88/11, ESEE, Imperial Coll. Sci. Tech., 88/11, London, U.K.

Ambraseys, N. N.; Melville, C. P. and Adams, R. D. (1994): The seismicity of Egypt, Arabia and the Red Sea: A historical review. Cambridge University Press, 181P.

Ambraseys, N. N. and Bommer, J. J. (1990): Uniform magnitude re-evaluation for strong motion database of Europe. European Earthquake Engineering, 4 (2), pp. 3-16.

Ambraseys, N. N. and Free, M. W. (1997): Surface-wave magnitude calibration for European region earthquakes. Journal of Earthquake Engineering, 1(1), pp. 1-22.

Ambraseys N. N. and Bommer J. J. (1991): The attenuation of ground accelerations in Europe. Earthquake Eng Struct Dyn 20:1179–1202

Ambraseys N. N., Simpson K. A. and Bommer J. J. (1996): The prediction of horizontal reponse spectra in Europe. Earthquake Eng Struct Dyn 25:371–400

Ambraseys NN, Douglas J, Sarma SK, Smit PM (2005): Equations for the estimation of strong ground motions from shallow crustal earthquakes using data

from Europe and the Middle East: horizontal peak ground acceleration and spectral acceleration. Bull Earthq Eng 3:1–53

Andrews, D. J., 1986. Objective determination of source parameters and similarity of earthquakes of different size. In: Earthquake Source Mechanics, S. Das, J. Boatwright and C. H. Scholz (editors), AGU, Washington, D. C., 259-268.

Astroza, M. and Monge, J., 1991. Regional seismic zonation in central Chile, Proceedings of the fourth international conference on Seismic Zonation, August 25-29, Stanford, California, E.E.R.I. (editor), Oakland CA,. 3, 487-494.

Atkinson G. M. and Boore, D. M. (1995): Ground-motion relations for eastern North America. Bull Seism Soc Am 85:17–30

Ayres, M. G.; Bital, M.; Jones, R. W., Slentz, L. W.; Tartir, M. and Wilson, A. O. (1982): Hydrocarbon habitat in main producing areas, Saudi Arabia. AAPG Bull, 66 (1), pp. 1-9

Bard, P. Y. and. Tucker, B. E, (1985): Underground and ridge and site effects: comparison of observation and theory, Bull. Seism. Soc. Am. 75: 905-922.

Bard, P. Y. (2000): International Training Course on: Seismology, Seismic Data Analysis, Hazard Assessment and Risk Mitigation Potsdam, Germany, 01 October to 05 November 2000.

Bard, P.-Y. and SESAME-Team (2005): Guidelines for the implementation of the H/V spectral ratio technique on ambient vibrations - measurements, processing

and interpretations. SESAME European research project EVG1-CT-2000-00026 D23.12. Available online at **http://sesame-fp5.obs.ujf-grenoble.fr**.

Bard, P. Y. (2007). International Training Course on: Seismology, Seismic data Analysis, Hazard assessment and Risk mitigation, Potsdam, Germany, 07 July to 08 September 2007, 17-22.

Bray, J. D., and Rodriguez-Marek, A. (1997): Geotechnical Site Categories. Proceedings. First PEERPG& E Workshop on Seismic Reliability of Utility Lifelines, San Francisco, CA.

Bayer, R., Chery, J., Tatar, M., Vernant, Ph., Abbassi, M., Masson, F., Nilforoushan, F., Doerflinger, E., Regard, V., and Bellier O. (2006): Active deformation in Zagros–Makran transition zone inferred from GPS measurements. Geophysical Journal International, 165, pp. 373-381.

Berberian, M., and King, G. C. P. (1981). Towards a paleogeography and tectonic evolution of Iran. Can. J. Earth Sci. **18,** 210-265.

Berberian, M. (1995): Master blind thrust faults hidden under the Zagros folds: active basement tectonics and surface morpho-tectonics. Tectonophysics, 241, 193–224.

Berberian, M. and Yeats, R. S. (1999): Patterns of historical earthquakes rupture in the Iranian Plateau. Bulletin of the Seismological Soceity of America, 89 (1), pp. 120-139.

Beresnev, I. A., Field, E. H., Van Den Abeele, K., and Johnson, P. A. (1998): Magnitude of nonlinear sediment response in Los Angeles basin during the 1994 Northridge, California, Earthquake, Bull. Seism. Soc. Am. 88, 1079-1084.

Bernreuter, D.L., Savy, J.B., Mensing, R.W., and Chen, J.C. (1989): Seismic Hazard Characterization of 69 Nuclear Power Plant Sites East of the Rocky Mountains, NUREGICR-5250, vols. 1-8, prepared by Lawrence Livermore National Laboratory for the U.S. Nuclear Regulatory Commission.

Boore, D. M. (1983): Stochastic simulation of high-frequency ground motions based on seismological models of the radiated spectra. Bull Seism Soc Am 73:1865–1894

Boore, D. M. and Boatwright, J. (1984): Average body-wave radiation coefficients. Bull Seism Soc Am 74:1615–1621

Boore, D. M, Atkinson, G.M. (1987): Stochastic prediction of ground motion in eastern North America. Bull Seism Soc Am 4:460–477

Boore, D.M.(1996): SMSIM- Fortran program for simulating ground motions from earthquakes, Version 1.0 U.S. Geol Surv, Open- File Report, pp 69–80

Boore, D. M. (2003): Simulation of ground motion using the stochastic method. Pure Appl Geophys 160:635–675

Boore, D.M. (2004b): Estimating V_{s30} (or NEHRP site Classes) from shallow velocity models (depths < 30 m). BSSA, 94, pp. 591-597.

Borcherdt, R. D. (1970): Effects of Local Geology on Ground Motion near San Francisco Bay. Bull. Seism. Soc. Am. 60, 29-61.

Borcherdt, R. D. and Gibbs, J. F., 1976. Effects of Local Geological conditions in the San Francisco bay region on Ground Motions and the intensities of the 1906 earthquake. Bull. Seismol. Soc. Am. 66, 467-500.

Borcherdt, R. D.; Wentworth, C. M.; Janssen, A.; Fumal, T. and Gibbs, J. F., 1991. Methodology for predictive GIS mapping of special study zones for strong ground shaking in the San Francisco bay region, proceedings of the Fourth International Conference on seismic zonation, August 25-29, Stanford, California. E.E.R.I. (editor), Oakland CA, III, 545-552.

Borcherdt, R., Glassmoyer, G., 1992. On the characteristics of local geology and their influence on the ground motions generated by the Loma Prieta earthquake in the San Francisco bay region, California, Bull. Seism. Soc. Am. 82, 603-641.

Bou-Rabee, F. and Abdel-Fattah, R. (2004): Seismological observations in the State of Kuwait. Kuwait Journal of Sci. and Eng., 31(1), pp. 175-192.

Bou-Rabee, F. and Nur, A. (2002): The 1993 M4.7 Kuwait earthquake: Induced by burning of the oil fields. Kuwait J..Sci. Eng., 29 (2), 10 p.

Bou-Rabee, F. (1994a): Earthquake hazard in Kuwait. Journal of Univ. Kuwait(Science), 21, pp. 253-264.

Bou-Rabee, F. (1994b): Earthquake recurrence in Kuwait induced by oil and gas extraction. Journal of Petroleum geology, 17(4), pp. 473-480.

Building Seismic Safety Council (BSSC) (2001): NEHRP recommended provisions for seismic regulations for new buildings and other structures, 2000 Edition, part I: Provisions, prepared by Building Seismic Safety Council for the

Federal Emergency Management Agency (Report FEMA 368), Washington, D.C.

Byrne, D. E. and Sykes, L. R. (1992): Great thrust earthquakes and aseismic slip along the plate boundary of the Makran subduction zone. Journal of Geophysical Research, 97 (BI), pp. 449-478.

Brune, J. (1970): Tectonic stress and the spectra of seismic shear waves from earthquakes. J. Geophys. Res. 75:4997–5009

Carbon, D. (1996): Tectonique post-obduction des montagnes d'Oman dans le cadre de la convergence Arabie-Iran. Montpellier II.

Carman, G. J. (1996): Structural elements of Onshore Kuwait. GeoArabia, 1 (2), pp. 236-266.

Carver, D. and Hartzel, S. H. (1996): Earthquake site response in Santa Cruz, California, Bull. Seism. Soc. Am. 86, 55-65.

Chen, F.H. (1988): Foundation on Expansive Soils. Elsevier Scientific Publishing Co., Amsterdam.

Chiaruttini, C. and Siro, R., 1981. The correlation of peak ground horizontal acceleration with magnitude, distance and seismic intensity for Friuli and Ancona, Italy and the Alpine belt. Bull. Seismol. Soc. Am. 71, 1993-2009.

Coppersmith, K. J., Youngs, R. R. (1986): Capturing uncertainty in probabilistic seismic hazard assessments within intraplate tectonic environments. In: Proceedings of the Third U.S. National Conference on Earthquake Engineering, vol. 1, pp. 301-312.

Coppersmith, K. J., and Youngs, R. R. (1990): Probabilistic Seismic Hazard Analysis Using Expert Opinion: An Example from the Pacific Northwest, in Krinitsky, E.L., and Slemmons, D.B., Neotectonics in Earthquake Evaluation, Geological Society of America Reviews in Engineering Geology, vol. 8, Boulder, Colorado.

Coutel, F., and Mora, P. (1998): Simulation-based comparison of four site response estimation technique, Seism. Soc. Am. 88, 30-42.

Deif A., Abed, A., kamal Abdel-Rahman; Abdel Moneim, E. (2009) Strong ground motion attenuation in Aswan Area, Egypt. Arab. Jour. Geosci. DOI 10.1007/s12517-009-0103-8.

Darragh, R. B. and Shakal, A. F., 1991. The site response of two rock and soil station pairs to strong and weak motion, Bull. Seism. Soc. Am. 81, 1885-1889.

Doherty, R.; Borcherdt, R.D.; Crouse, C.B.; Idriss, I.M.; Joyner, W.B.; Martin, G.R.; Power, M.S.; Rinne, E.E.; and Seed, R.B. (2000): New site coefficients and site classification system used in recent building seismic code provisions. Earthquake Spectra, 16, pp. 41-67.

Edgell, H. S. (1996). Salt tectonism in the Persian Gulf Basin. In "Salt Tectonics." (J. L. Alsop, D. J. lundell, and I. Davison, Eds.), pp. 129-151. Geol. Soc. Spec. Publ.

El-Enezi, A., Abdul Fatah and Safak E. (2005): Assessment of the seismic hazard for the state of Kuwait. Abstracts of the Gulf Seismic Forum, UAE University, Al-Ain, U. A. E.

El-Enezi, A., Petrat, L., and Abdel-Fattah, R. (2008): Induced seismicity and surface deformation within Kuwait's oil fields. 2nd IASME/WSEAS International conference on geology and seismology (GES'08), Cambridge, UK, February 23-25.

El-Naggar, Z. (1988): Foundation problems in sabkha deposits. Short Course on Foundation Engineering for Practicing Engineers, CE Department, KFUPM, pp. SD1–SD54.

El-Shahat, A. M., 2003. Estimating earthquake ground motions at the northwestern part of the Gulf of Suez, Egypt. PhD. In Geophysics, Ain Shams University 2003. Pp. 145-147.

Evernden, J. F. and Thomson, J. M., 1985. Predicting seismic intensities, U.S.G.S. Professional paper 1360, 151-202.

Faccioli, E., 1991. Seismic amplification in the presence of geological and topographic irregularities. In: Proceedings of the Second International Conferences on Recent Advances in Geotechnical Earthquake Engineering and Soil Dynamics, March 11-15, St Louis, Missouri, S. Prakash (editor), Univ. of Missouri-Rolle, 2, 1779-1797.

Faeh, D.; Subhadolc, P. and Panza, G.F., 1990. A new method for the realistic estimation of seismic ground motion in megacities: the case of Rome. Earthquake Spectra, 9, 643-668.

Faeh, D.; Iodice, C.; Subhadolc, P. and Panza, G. F., 1993. Estimation of strong ground motion in laterally heterogeneous media: model summation-finite

differences, Proceedings of the 9th European Conference of Earthquake Engineering, Sept. 11-16, 1993, Moscow, 4A, 100-109.

Faeh, D.; Subhadolc, P.; Mueller, St. and Panza, G. F., 1994. A hybrid method for the estimation of ground motion in sedimentary basins: Quantitative modeling for Mexico City. Bull. Seismol. Soc. Am. 84, 383-399.

Falcon, N.L. (1974): Southern Iran: Zagros Mountains. In Mesozoic–Cenozoic Orogenic Belts; Spencer, A.M., Ed.; Scottish Academic Press: Edinburgh, UK, pp. 199–211.

Farhoudi, G. and Karig, D. E. (1977): Makran of Iran and Pakistan as an active arc system. Geology, 5, pp. 664-668.

Faure-Muret, A., and Choubert, G. (1971): Aperçu de l'évolution structurale de l'Iran. In "Tectonique de l'Afrique." pp. 141-151. Sciences de la Terre, 6. Unesco.

Field, E. H.; Hough, S. E. and Jacob, K. H., 1990, Using microtremors to assess potential earthquake site response: A case study in flushing Meadows, New York city, Bull. Seismol. Soc. Am., 80, 1456-1480.

Field, E. H., and Jacob, K. H. (1995): A comparison and test of various site-response estimation techniques, including three that are not reference-site dependent, Bull. Seism. Soc. Am. 85, 1127-1143.

Field, E. H., Jacob, K. H., and Hough, S. E. (1992): Earthquake site response estimation: a weak-motion case study, Bull. Seism. Soc. Am. 82, 2283-2306.

Field, E. N. (1996): Spectral amplification in sediment-filled valley exhibiting clear basin-edge-induced waves. Bull. Seism. Soc. Am. 86, 991-1005.

Field, E., Jacob, K. H. (1993): The theoretical response of sedimentary layers to ambient seismic noise. Geophysical research letters, vol. 20, No 24, 2925-2928.

Finn, W. and Liam, D., 1991. Geotechnical engineering aspects of seismic microzonation. In: Proceedings of the Fourth International Conference on Seismic Zonation, August 25-29, Stanford, California, E.E.R.I. (editor), Oakland CA, I 199-250**.**

Fnais, M. S.; kamal Abdel-Rahman and Al-Amri, A. M. (2010): Microtremor measurements in Yanbu City of western Saudi Arabia: A tool of seismic microzonation. Journal of King Saud University- Science (ElSEVIER), DOI: 10.1016/j.jksus.2010.02.006.

Gardner, J. K. and Knopoff, L. (1974): Is the Sequence of Earthquakes in Southern California, with Aftershocks Removed, Poissonian?, Bulletin of the Seismological Society of America, Vol. 64, No 5, pp 1363-1367.

Géli, L.; Bard, P.-Y. and Jullien, B., 1988. The effect of topography on earthquake ground motion: a review and new results. Bull. Seismol. Soc. Am. 78, 42-63.

Gitterman, Y., Zaslavsky, Y., Shapira, A. and Shtivelman, V. (1996): Empirical site response evaluations: case studies in Israel, Soil Dynamics Earthquake Engineering 15, 447-463.

Gutierrez, C. and Singh, S. K. (1992): A site effect study in Acapulco, Guerrero, Mexico: Comparison of results from strong-motion and microtremor data, Bull. Seism. Soc. Am. 82, 642-659.

Hariri, M. M. and Abdullatif, O. (2001): Use of the GIS to delineate lineaments from Landsat images, Dammam dome, eastern Saudi Arabia. GeoArabia, V 16 Number 1, p.59

Hariri, M. M. and Abdul latif, O. M. (1994): Characterization of fractures within Dammam dome, Saudi Arabia. GeoArabia, V 9 Number 1, p.76

Harms, J. C., Cappel, H. N., and Francis, D. C. (1984): The Makran coast of Pakistan: its stratigraphy and hydrocarbon potential. In "Marine Geology and Oceanography of Arabian Sea and Coastal Pakistan." (B. U. Haq, and J. D. Milliman, Eds.), pp. 3-26. Van Nosrand Reinhold, Co., New-York.

Hartzell, S. H., Leeds, A., Frankel, A. and Michael, J. (1996): Site response for urban Los Angeles using aftershocks of the Northridge earthquake, Bull. Seism. Soc. Am. 86, 168-192.

Hartzell, S. (1998): Variability in nonlinear sediments response during the 1994 Northridge, California, earthquake, Bull, Seism. Soc. Am. 88, 1426-1437.

Hessami, K., Koyi, H. A., and Talbot, C. J. (2001): The significance of strike-slip faulting in the basement of the Zagros fold and thrust belt. Journal Of Petroleum Geology **24,** 5- 28.

Hwang, H., Huo, J. R. (1997): Attenuation relations of ground motion for rock and soil sites in eastern United States. J. Soil. Dynam. Earthquake Eng 16:363–372

Muhammad Irfan; Magdi El-Emam; Zahid Khan; and Jamal Abdalla (2012): Local Site Effects on Seismic Ground Response of Dubai-Sharjah Metropolitan Area. http://dx.doi.org/10.1061/9780784412121.192.

Iyengar R. N. and Raghukanth, STG (2004): Attenuation of strong ground motion in Peninsular India. Seismol Res Lett 75:530–540

Jackson, J., and T. Fitch (1981): Basement faulting and the focal depths of the larger earthquakes in the Zagros Mountains (Iran), Geophys. J. R. Astron. Soc., 64, 561-586.

Jacob, K. H., and Quittmeyer, R. L. (1979): The Makran region of Pakistan and Iran: Trencharc system with active plate subduction. In "Geodynamics of Pakistan." (A. Farah, and K. A. de Jong, Eds.), pp. 305-317. Geological Survey of Pakistan, Quetta.

James, G. A., and Wynd, J. G. (1965): Stratigraphic nomenclature of Iranian oil consortium agreement area. AAPG Bull. **49,** 2162-2245.

Jarpe, S. P., Cramer, C. H., Tucker, B. E. and Shakal, A. F. (1988): A comparison of observations of ground response to weak and strong motion at Coalinga, California, Bull, Seism. Soc. Am. 78, 421-435.

Joyner, W. B. and Fumal, T. 1984. Use of measured shear wave-velocity for predicting site effects on strong motion. Proceedings of the eighth world conference on earthquake engineering, San Francisco, 2, 777-783.

Jongmans, D. and Campillo, M. (1993): The response of the Ubaye valley (France) for incident SH and SV waves: comparison between measurements and modeling, Bull. Seism. Soc. Am. 83, 907-924.

Johnson, D.H., (1978): Gulf coastal region and 1st Hinterland: general geology. In: Al-Sayari, Zotl (Eds.), Quaternary Period in Saudi Arabia. Springer–Verlag, Wien, Austria, pp. 45–50.

Joyner, W. B. and Boore, D. M. (1981): Peak horizontal acceleration and velocity from strong motion records including records from the 1979, Imperial valley, California earthquake. Bull Seism Soc Am 71:2011–2038

Kagami, H., Duke C.M., Liang, G.C., and Ohta, Y. (1982): Observation of 1- to 5-second microtremors and their application to earthquake engineering. Part II. Evaluation of site effect upon seismic wave amplification deep soil deposits, Bull. Seism. Soc. Am. 72, 987-998.

Kagami, H.; Okada, S. and Ohta, Y., 1988. Versatile application of dense and precision seismic intensity data by an advanced questionnaire survey. In: Proceedings of the Ninth World Conference on earthquake engineering, Tokyo-Kyoto, Ed.: Maruzen, 8, 937-942.

Kanai, K., 1952. Relation between the nature of surface layer and the Amplitude of Earthquake motion, Tokyo Univ. Earthquake Research Int. Bull. 30, Pt 1, 31-37.

Katz, L. J. (1976): Microtremor analysis of local geological conditions, Bull. Seism. Soc. Am. 66: 45-60.

Katz, L. J., and Bellon, R.S., (1978): Microtremor site analysis study at Beatty, Nevada,Bull. Seism. Soc. Am. 68: 757-565.

Kanamori, H. (1986): Rupture process of subduction-zone earthquakes. Ann. Rev. Earth. Planet. Sci., 14, pp. 293-322.

Konno, K. and Ohmachi, T. (1998): Ground-motion characteristics estimated from spectral ratio between horizontal and vertical components of microtremors, Bull. Seism. Soc. Am. 88, 228-241.

Kopp, C., Fruehn, J., Flueh, E. R., Reichert, C., Kukowski, N., Bialas, J., and Klaeschen, D. (2000): Structure of the Makran Subduction zone from wide angle and reflection seismic data. Tectonophysics **329,** 171-191.

Kramer, S. L., 1996. Geotechnical Earthquake Engineering (Prentice Hall, Upper Saddle River, New Jersey).

Lachet, C., and Bard P.Y. (1994): Numerical and theoretical investigations on the possibilities and limitations of the Nakamura's technique, J. Phys. Earth, 42, 377-397.

Lermo, J., and Chavez-Garcia, F. J. (1993): Site effect evaluation using spectral ratios with only one station, Bull. Seism. Soc. Am. 83, 1574-1594.

Lermo, J. and Chavez-Garcia, F. J. (1994): Are microtremors useful in site response evaluation?, Bull. Seism. Soc. Am. 84, 1350-1364.

Liu, H. -P., Warrick, R. E., Westerlund, R. E., Sembera, E. D., and Wennerberg, L. (1992): Observation of local site effects at a downhole-and-surface station in the marina district of San Francisco, Bull. Seism. Soc. Am. 82, 1563-1591.

Malagnini, L., Tricarico, P., Rovelli, A., Herrmann, R. B., Opice, S., Biella G., and de Franco, R. (1996): Explosion, earthquake, and ambient noise recording

in a Pliocene sediment-filled valley: inferences on seismic response properties by reference- and non-reference-site techniques, Bull. Seism. Soc. Am. 86, 670-682.

McCall, G. J. H. (1997): The geotectonic history of the Makran and adjacent areas of southern Iran. J. Asian Sci. **15,** 517-531.

McCall, G. J. H., Morgan, K. H., Campe, G. C., Child, R., Porter, D. J., Wyatt, J. D., Bailey, P. B. H., Craik, D. I., Dalaei, H., Jones, D., McCormick, C. D., Motamedi, S., Nunn, G. A. G., Pooyai, N., Power, P., Smith, G. H., Swain, C. R., Simonian, K., Deighton, I., Mallett, C. W., Huber, H., Peterson, L. W., Rudzinskas, K. K., Samimi Namin, M., and Hadji Zad-Kabir, Y. (1985): Minab quadrangle map 1:250,000 and explanatory text, pp. 534. Geological Survey of Iran.

McGarr, A., Celebi, M., Sembera, E., Noce, T. and Mueller, C. (1991): Ground motion at the San Francisco international airport from the Loma Prieta earthquake, sequence, Bull. Seism. Soc. Am. 81, 1923-1944.

Medvedev, J., 1962. Engineering seismology, Science Academy Press, Moscow.

Midorikawa, S., 1987. Prediction of isoseismal map in the Kanto plain due to hypothetical earthquake, Journal of structural engineering, 33B, 43-48.

Minakami, T. and Sakuma, S., 1948. The earthquake motions on various formations of the earths' surface observations at Koti City, Tokyo Univ. Earthquakes Res. Inst. Bull., V. 26, 61-66.

Mokhtar, T. A., C. J. Ammon, R. B. Herrman, and Ghalib, H. A. A. (2001): Surface-wave velocities across Arabia, Pure Appl. Geophys., 158, 1425–1444.

Mucciarelli M. (1998): Reliability and applicability of Nakamura's technique using microtremors: an experimental approach, Journal of Earthquake Engineering, 4, 625-638.

Mucciarelli, M.; Contri, P.; Monachesi, G. and Calvano, G. (1998): Towards an empirical method to instrumentally assess the seismic vulnerability of existing buildings, Proceedings of Conference on Disaster Mitigation and Information Technology, London.

Mueller, C. S.; Boore, D. M. and Porcella, R. L., 1982. Detailed study of site amplification at El Centro strong motion array station No. 6, Proceedings of the Third International Earthquake Micro-Zonation Conference, Seattle, Washington, V. 1, 413-424.

Nakamura, Y. (1989): A method for dynamic characteristics estimation of subsurface using microtremor on the ground surface. QR of RTRI, Vol. 30, No.1, 25-33.

Nakamura, Y. (1996): Real-time information systems for hazards mitigation. Proceedings of the 11th World Conference on Earthquake Engineering, Acapulco, Mexico.

Ohsaki, Y., 1981. On subdivision of layers in response analysis of soil deposit as a discrete system, Research Report 81-03, Dept. of Architecture, Faculty of Eng. Univ. of Tokyo.

Ohmachi, T., Nakamura, Y., Toshinawa, T. (1991): Ground motion characteristics of the San Francisco bay area detected by microtremor measurements. Second

International conference on recent advances in geotechnical earthquake engineering and soil dynamics, St. Louis, Missouri, 1643-1648.

Ohta, Y., Kagami, H., Goto, N., and Kudo, K. (1978): Observation of 1- to 5-second microtremors and their application to earthquake engineering. Part I: Comparison with long period accelerations at the Tokachi-Oki earthquake of 1968, Bull. Seism. Soc. Am. 68: 767-779.

Okada H. (2003): The microtremor survey method. In: Geophysical Mono-graph Series No. 12, Society of Exploration Geophysicists, Tulsa, OK, USA.

Ooba, S., 1957. Study of the relation between subsoil conditions and the distribution of damage percentage of wooden dwelling hoses in the province of Totomi in the case of the Tonankai Earthquake of December, 7th, 1994, Tokyo Univ. Earthquakes Res. Inst. Bull., V. 36, 201-295.

Panza, G. F.; Vaccari, F.; Costa, G.; Suhadole, P. and Fäh, D., 1996. Seismic input modeling for zoning and microzoning. Earthquake Spectra. 12, 529-566.

Parolai, S; Bormann, P.; and Milkereit, C. (2006): Measurements of the fundamental resonance frequency of the sedimentary cover in thje Cologne area: contribution to the seismic microzonation. Ergebnisse aus dem Deutschen Forschungesnetz Naturkatastrophen, pp. 301-305.

Peiris, N.; Free, M.; Lubkowski; Z. and Hussein, A.T. (2006): Seismic hazard and seismic design requirements for the Arabian Gulf region. Proceedings of the 1st European Conference on Earthquake Engineering and Seismology, Geneva, September 2006, Paper No. 1121.

Platt, J. P., Leggett, J. K., and Alam, S. (1988): Slip vectors and fault mechanics in the Makran accretionary wedge, southwest Pakistan. J. Geophys. Res., **93,** 7955-7973.

Platt, J. P., Leggett, J. K., Young, J., Raza, H., and Alam, S. (1985): Large-scale underplating in the Makran accretionary prism, southwest Pakistan. Geology **13,** 507-511.

Powers, L.F., Ramirez, L.F., Redmond, C.D., Elberg, E.L., (1963): Geology of the Arabian Peninsula - sedimentary geology of Saudi Arabia. ARAMCO-USGS (147 pp.).

Powers, R. W., Ramires, L. F., Redmond, C. D., and Elberg, E. L. (1966): Geology of the Arabian Peninsula: Sedimentary Geology of Saudi Arabia, U.S. Geological Survey Professional Paper 560-D.

Punsalan, B. and Al-Amri, A. (2003): Scaling relations of earthquake parameters in the Red Sea region. Journal of King Saud Univ. (Sci.2), V. 15, pp. 942-946.

Pascucci, V., Free, M.W., and Lubkowski, Z.A. (2008): Seismic hazard and seismic design requirements for the Arabian Peninsula. The 14th World Conference on earthquake engineering, October 12-17, Beijing, China.

Quittmeyer, R. C. (1979): Seismicity variations in the Makran region of Pakistan and Iran: Relation to great earthquakes. Pure and Applied Geophysics, 117 (6), pp. 1212-1228.

Quittmeyer, R. C. and Jacob, K. H. (1979): Historical and modern seismicity of Pakistan, Afghanistan, northwestern India, and southeastern Iran. Bulletin of the Seismological Society of America, 69 (3), pp. 773-823.

Reinoso, E., and Ordaz, M. (1999): Spectral amplification for Mexico City from free-field recordings, Earthquake Spectra, Vol. 15 No. 2, 273-295.

Reuter, H.I.; Nelson, A.; and Jarvis, A. (2007): An evaluation of void filling interpolation methods for STRM data. Int. Geographic Information Science, 21, 9, pp. 983-1008.

Rogers, A. M., Borcherdt, R. D., Covington, P. A. and Perkins, D.M. (1984): A comparative ground response study near Los Angeles using recordings of Nevada nuclear tests and the 1971 San Fernando earthquake, Bull. Seism. Soc. Am. 74, 1925-1949.

Sadek, A. W. (2004): Seismic map for the state of Kuwait. Emirates Journal for Engineering Research, 9 (2), pp. 53-58.

Safak, E. (1997): Models and methods to characterize site amplification from apair of records, Earthquake spectra, 13, 97-129.

Satoh, T., Sato, T., and Kawase H. (1995): Nonlinear behavior of soil sediments identified by using borehole records observed at the Ashigara valley, Japan, Bull. Seism. Soc. Am. 85, 1821-1834.

Saner, S., Al-Hinai, Kh., Perincek, D. (2005): Surface expressions of the Ghawar structure, Saudi Arabia. Marine and Petroleum Geology, V. 22, pp. 657–670

Saragoni, G. R. and Hart, G. C. (1974): Simulation of artificial earthquakes. Earthquake Eng Structural Dyn. 2:249–267

Schmidt, D.L., Hadley D. G., and Stoeser, D. B. (1979): Late Proterozoic crustal history of the Arabian Shield, southern Najd province, Kingdom of Saudi Arabia, evolution and mineralization of the Arabian-Nubian Shield, I.A.G. Bull., 3, 41-58.

Schluter, H. U., Prexl, A., Gaedicke, C., Roeser, H., Reichert, C., Meyer, H., and von Daniels, C. (2002). The Makran accretionary wedge: sediment thicknesses and ages and the origin of mud volcanoes. Marine Geology **185,** 219.

Sharland, P. R.; Archer, R.; Casey, D. M.; Daves, R. B.; Hall, S. H.; Heward, A. P.; Horbury, A. D. and Simmons, M. D. (2001): Arabian p0late sequence stratigraphy. GeoArabia, Special Publication,2.

Shadfan, H.; Mashhady, A. S.; Dixon, J. B. and Hussen A. A. (1985): Palygorskite from Tertiary formations of eastern Saudi Arabia. Clays and Clay Minerals, Vol. 33, No. 5, 451-457.

Shima, E., 1978. Seismic microzoning map of Tokyo, proceedings of the second international conference on seismic zonation, I, 519-530.

Seekins, L. C., Wennerberg, L., Margheriti, L. and Liu, Hsi-Ping (1996): Site amplification at fife locations in San Francisco, California: a comparison of S waves, codas and microtremors, Bull. Seism. Soc. Am. 86, 627-635.

Singh, S. K., Mena E., and Castro, R. (1988): Some aspects of source characteristics of the 19 September 1985 Michoacan earthquakes and ground

motion amplification in and near Mexico City from strong motion data, Bull. Seism. Soc. Am. 78, 451-477.

Steineke, M., Bramkamp, R., and Sander, N. (1958): Stratigraphic relations of Arabian Jurassic oil, American Association of Petroleum Geologists Symposium, Tulsa, U.S.A., pp. 1294–1329.

Stocklin, J. (1984): Orogen and tethys evolution in the Middle East—an appraisal of current concept; In Report for the 27th International Geological Congress, Suezach, Switzerland, August, 1984; p. 1391.

Su, F., Anderson, J. G., and Zeng, Y. (1998): Study of week and strong ground motion including nonlinearity from the Northridge, California, Earthquake Sequence, Bull. Seism. Soc. Am., 1998, 88, 1411-1425.

Szabo, F., and Kheradpir, A. (1978): Permian and Triassic stratigraphy, Zagros Basin, southwest iran. J. Petrol. Geol. **1,** 57-82.

Talebian, M. and Jackson, G. (2004): A reappraisal of earthquake Focal mechanisms and active shortening in Zagros mountain of Iran. Geophys. J. Int., 156, 506–526.

Tavakoli B. (1996): Major Seismotectonic Provinces of Iran. International Institute of Earthquake Engineering and Seismology, Internal Document, Tehran, Iran.

Teves-Costa, Matias, P., L. and Bard, P.-Y. (1996): Seismic behavior estimation of thin alluvium layers using microtremor recordings, Soil Dynamics and Earthquake Engineering 15, 201-209.

Theodulidis, N., Bard, P.Y., Archuleta, R. and Bouchon, M. (1996): Horizontal-to-vertical spectral ratio and geological conditions: the case of Garner valley downhole in Southern California, Bull. Seism. Sos. Am. 68, 767-779.

Toro, G., Abrahamson, N. and Schneider, J. (1997): Model of strong ground motion in eastern and central North America: best estimates and uncertainties. Seismol. Res Lett. 68:41–57

Trifunac, M. D. and Novikova, E. I., 1994. State of the art review on strong motion duration. In: Proceedings of the Tenth European Conference on Earthquake Engineering. Vienna, Austria, G. Duma (editor), Balkema, Rotterdam, I, 131-140.

Tucker, B. E. and King, J. L. (1984): Dependence of sediment-filled valley response on input amplitude and valley properties, Bull. Seism. Soc. Am. 74, 153-165.

Vaslet, D., Al Muallem, M., Maddah, S., Brosse, J., Fourniguet, J., Breton, J., and Le Nindre, Y. (1991): Geologic map of the Ar Riyad quadrangle, sheet 241, scale 1: 250,000 (including report), Saudi Arabian Directorate General of Mineral Resources, Geoscience map GM-121 C.

Wakamatsu, K. and Yasui, Y. (1996): Possibility of estimation for amplification characteristics of soil deposits based on ratio of horizontal to vertical spectra of microtremors. Proceedings of the 11th World Conference on Earthquake Engineering Acapulco. Mexico. Geophysical prospecting, 30: pp. 55-70.

White, R. S. (1982): Deformation of the Makran accretionary sediment prism in the Gulf of Oman (north-west Indian Ocean). In "Trench and Fore-Arc Geology: Sedimentation and Tectonics on Modern and Ancient Active Plate Margins." (J. K. Leggett, Ed.). Blackwell Scientific Publications, Oxford.

Zahradnik, J. and Jech, J. and Bartak, V., 1991. Predicting ground motion variations at the Turkey-Flat test site, California. PAGEOPH, 137, 63-84.

Zahradnik, J.; Moczo, P. and Hron, F., 1994. Blind Prediction of the site effects at Ashigara valley, Japan, and its comparison with reality. Natural Hazards. 10, 149-170.

Zaslavsky, Y. (1987): Analysis of microseisms at the Dushanbe seismological observatory, Instruments and methods of earthquake registration, ISS 19, 152-157, Moscow.

Zaslavsky, Y., Gitterman, Y. and Shapira, A. (1995): Site response estimations in Israel using weak motion measurements. The fifth International conference on Seismic Zonation, Nice, France, 1713-1722.

Zaslavsky, Y., Shapira, A., Arzi A. A. (1998): Site response study in the Dead Sea area using earthquake end microtremors data, Proceeding of XXVI General assembly of the European seismological commission (ESC), Tel Aviv, Israel, August 23-28, 258-262.

Zaslavsky, Y., Karryev, B., Gitterman, Y., Esenov, E., Kanel, E. and Shapira, A. (1998): Microzonation studies of Ashgabat, Turkmenistan, using

microtremor measurements, XXVI General Assembly, European Seismological Commission (ESC), Tel Aviv.

Zaslavsky, Y., Sapira, A., Arzi A. (2000): Amplification effects from earthquakes and ambient noise in the Dead Sea rift (Israel), Soil Dinamics and Earthquake Engineering 20, 187-207.

Zaslavsky, Y., Shapira, A., and Leonov Y. (2000): Measurements of site effects at strong motion accelerograph stations in Israel, XXVII General Assembly of the European seismological commission (ESC), Lisbon, Portugal, September10-15, p 97.

Zaslavsky, Y., Shapira, A., Gorstein, M., Kalmanovich, M., Giller, V., Ion Livshits, I., Alexander Shvartsburg, A., Ataev, G., Aksienko, T., Dagmara Giller, D., Ilana Dan, I. and Perelman, N. (2003): Local site effect of Hashefela and Hasharon regions based on ambient vibration measurements. Progress report, July, 2003, GII Report No. 569/313/03.